CHAR
BASE

CHARACTERIZATION OF AMORPHOUS POROUS CARBONS BASED UPON STRUCTURAL ENHANCEMENT OF SORPTION POTENTIALS

By

Robert J. Dombrowski

A DISSERTATION

Submitted to
Michigan State University
in partial fulfillment of the requirements
for the degree of

DOCTOR OF PHILOSOPHY

Department of Chemical Engineering

2001

CHA
UPO

Analysis
heteroge
reaction
simulati
structure
Molecul
for a giv
been use
77K for b
generall
Although
as the pro
and has n
that the tw
functional
Sorption a
potential fu
characteris
susceptibil

Abstract

CHARACTERIZATION OF AMORPHOUS POROUS CARBONS BASED UPON STRUCTURAL ENHANCEMENT OF SORPTION POTENTIALS

By

Robert J. Dombrowski

Analysis of gas sorption isotherms may yield information about structural heterogeneity that can be used to control selectivity of separations processes, catalytic reactions, and gas storage. Disordered porous materials may be analyzed via simulation of sorption isotherms using methods that rely on simple geometric structures with a single source of heterogeneity to render the problem more tractable. Molecular simulations (MS) and density functional theory (DFT) are considered exact for a given simple pore structure and chemical makeup. DFT model isotherms have been used to analyze experimental isotherms for several amorphous porous carbons at 77K for both argon and nitrogen. The pore size distributions (PSD) of the two gases generally agreed within 8% for both the total volume and mode of the distribution. Although both probe gases yielded similar results the argon is recommended for use as the probe gas of choice, as it is smaller than nitrogen, is a monatomic molecule, and has no permanent multipole moment. Elemental analysis of the carbons indicates that the two probe gases are in better agreement when the carbons do not contain functional groups.

Sorption analysis is very dependant upon the model parameters used to describe the potential functions. The potential parameters may be determined from bulk physical characteristics of a molecule such as the polarizability and the magnetic susceptibility, or may be fitted to isotherm data. The monolayer filling pressure of

carbon po

choosing

with that

An alterna

distribution

single-wa

determine

comparison

parameters

Similar to

superpositi

micropores.

structure.

one hundre

DFT or MS

MS and DF

original HK

completely

pressures lo

size as com

has the adv

to a nonporo

carbon pores larger than 10 molecular diameters approaches the maximum therefore choosing the parameters to match the monolayer filling pressure of a large slit pore with that of a nonporous carbon is an excellent way to fit the potential parameters. An alternate means to accomplish the same goal is to fit an isotherm to a known distribution of pore sizes. Transmission electron microscope pictures may be taken of single-walled carbon nanotubes to determine their PSD, which can be used to determine the potential parameters. The technique has be verified through comparison PSD of isotherms generated with the use of nonporous carbon fitted parameters with the TEM data resulting in an error of less than 3% .

Similar to the DFT and MS methods the Horvath-Kawazoe (HK) method relies on the superposition of the adsorbent-adsorbate potential to enhance adsorption in micropores, and may be used to determine isotherms for a pore of a given size and structure. The HK method with a generalized potential function requires less than one hundredth of the time required to generate a series of isotherms using either the DFT or MS methods, while remaining remarkably accurate for its simplicity. Both MS and DFT predict pore wall wetting prior to condensation in the pore, whereas the original HK method predicted that the pores are either completely empty or completely full. The HK method was modified to approximate pore wall wetting at pressures lower than the filling pressure, yielding closer agreement of predicted pore size as compared to DFT. The addition of the monolayer filling in the HK method has the advantage of rendering it possible to fit the potential parameters of the system to a nonporous reference, in addition to improved accuracy for the mesopore range.

I thank m
were inva
I learned
throughou
to my fel
must also
working w
Special th
became a
Miller, Dr
through cl
My utmos
Prince, wh
Through Jar
and I will
Dombrowsk

Acknowledgements

I thank my advisor Dr. Christian Lastoskie. Our conversations discussing research were invaluable to my progress and growth as a researcher. Through our discussions I learned several techniques and approaches to problems that I foresee using throughout my career in matters concerning research and daily life. I am also grateful to my fellow graduate students each of whom touched my life in a unique way. I must also thank the many undergraduate researchers whom I have had the pleasure of working with, and hope that their experience was as beneficial as it was to me. Special thanks are due to Dan Hyduke who intelligently aided my research and became a friend. Additionally, I would like to thank my committee members Dr. Miller, Dr. Boyd, and Dr. Teppen, for the knowledge that they imparted to me through classes and personal discussions.

My utmost praise and thanks are extended to my fellow graduate student Jamaica Prince, who aided my progress in innumerable ways and became my closest friend. Through Jamaica I learned several lessons about professionalism and life in general and I will always be grateful. I also thank my parents Richard and Judith Dombrowski who always encouraged me to excel and gave me my core beliefs.

Table of Contents

List of Tables

List of Figures

1.1 Ratio

Characte

propertie

selective

based sole

Several te

mass tran

selectively

excluded

conversely

area, leav

smaller sp

separate g

the minor

narrower

properties

angstrom

magnitud

function

affinities

swing ads

Chapter 1.

Introduction to Adsorption

1.1 Rationale

Characterization methods for porous materials are required to effectively utilize their properties such as pore size and adsorptive capacities for a variety of purposes. Size selective adsorbents may be used for a variety of catalytic reactions as well as separations based solely on the physical size and potential interactions of the bulk fluid molecules. Several techniques based upon the size variations are employed, such as restriction of the mass transfer of the larger compounds. In a reactive system it may be desirable to selectively control the species that have access to the catalyst. Larger species can be excluded from the catalyst, allowing the smaller species to selectively react. [1] Or conversely smaller species may be allowed to preferentially diffuse out of the reactive area, leaving the larger species to react further and possibly increase the yield of the smaller species, as in the production of xylene. [2] The pore size may also be used to separate gases based upon there diffusivity. Uranium isotopes may be enriched through the minor decrease in the Knudsen diffusion of the heavier isotopes in pores that are narrower than the mean free path of the gaseous compound. In addition to diffusion properties, it has been demonstrated that altering the size of a pore by less than one angstrom may increase the selectivity of one compound over another by several orders of magnitude. [3] Alternately, the storage of hydrogen in carbon nanotubes is a strong function of their size and tube separation. [4] Therefore a means to predict the relative affinities is required to optimally utilize any sorbent used in temperature or pressure swing adsorption.

1.2 Intro

Several

solid. Al

or matte

electron

to "see" i

pore size

determine

probes su

layers w

preventi

principle

Sorption

heteroge

variation

regarde

material

to the s

of a por

$$\Gamma(P) =$$

Where

is the p

characte

1.2 Introduction to Sorption Theories

Several techniques exist to determine information about the surface characteristics of a solid; all require a probe, an interaction, and a response. [5] Probes may be either waves or matter, each with various limitations and strengths. Wave probes such as electromagnetic radiation or electrons suffer from the lack of depth which they allow one to "see" into the surface therefore can only be used with materials that contain a regular pore size throughout. X-ray diffraction [6,7] and electron microscopy [7] may be used to determine the pore size of regular materials such as carbon nanotubes or zeolites. Matter probes such as an adsorbing gas have the ability to penetrate into the material beyond the layers where wave probes are absorbed, however they may experience size exclusion preventing them from entering narrow or bottlenecked pores. Gas adsorption is still the principle technique [8] used to determine the structure of amorphous porous media.

Sorption measurements are based upon the heterogeneity of the sorbent, the cause of the heterogeneity may come from the surface chemistry, surface charges, or structural variations. The heterogeneity displayed in the filling pressures of an isotherm may be regarded to be derived from the range of pore widths in chemically homogeneous materials. An integral equation can be written which relates the measured isotherm $\Gamma(P)$ to the source of the heterogeneity, which is expressed in equation (1.1) solely as the size of a pore H.

$$\Gamma(P) = \int_{H_{min}}^{H_{max}} \Gamma(P,H) F(H) dH \qquad (1.1)$$

Where $\Gamma(P,H)$ is the thermodynamic model isotherm, at pressure P, and size H, and $F(H)$ is the pore size distribution. Although the adsorption integral is a convenient way to characterize a solid it is based upon assumptions to render the problem tractable while

sacrifici

model as

to repres

chemical

1.2.1 Sorb

While th

integral t

molecular

pore matr

based upo

representa

they are u

to control

irregularly

micropore

of an iso

alternative

radial dis

determine

over meso

that of th

range. Th

sacrificing some degree of realism. Some typical assumptions chosen to simplify the model are, independent noninteracting pores, a particular geometric structure is assumed to represent the pore width such as a slit or cylinder, and the surfaces are assumed to be chemically homogeneous.

1.2.1 Sorbent Structural Modeling

While the previously mentioned assumptions do simplify inversion of the adsorption integral to determine the pore size distribution (PSD), they are less accurate than a molecular simulation of an exact representation of the solid. However, since the exact pore matrix within an amorphous carbon is unknown the nearest representations are based upon either physical data gathered from the system studied or an amorphous representation. The representations of the adsorbent require statistical data of the systems they are used to study, for instance pore glasses may be used [9] at various quench times to control the pore size and connectivity. These models have the advantage of realistic irregularly shaped and interconnected pores, thus attaining some degree of realism for micropores, however the model fails to yield accurate results for the high pressure range of an isotherm which is usually attributed to filling of meso and macropores. An alternative to the controlled pore glass is the reverse Monte Carlo method where the radial distribution function (RDF) of carbon plates are chosen to match the RDF determined by X-rays or neutron diffraction which are incapable of measuring the effect over mesopores. Like the pore glass method the experimentally measured isotherm and that of the disordered solid determined via simulation agree only in the low-pressure range. The meso and macropores that are generally considered to be responsible for the

filling at

negligib

1.2.2 Cla

The simp

and the a

methods

isotherm

selecting

classical

approac

equation

otherwi

$$\ln\left(\frac{P_2}{P_1}\right)$$

In the

adsor

const

respe

Wetti

press

thick

accu

adso

filling at higher pressures cannot be determined from the diffraction patterns due to their negligible influence on the opposing pore wall.

1.2.2 Classical Methods

The simple geometric models have the advantage of requiring less computational time and the ability to account for pores of any size range. There are a variety of established methods based upon simple geometric models that predict the thermodynamic model isotherm used to invert the adsorption integral (equation 1.1), reducing the problem to selecting the model which most appropriately describes the system of interest. The classical methods are based upon measured bulk fluid properties and fail as pores approach molecular size, where continuum approximations no longer apply. The Kelvin equation or modified versions may be used for pores that are larger than 75 Å [10] otherwise the pore size will tend to be underestimated.

$$\ln\left(\frac{P_C}{P_0}\right)=\frac{-2\gamma_l}{RT\rho_l(r_k-t)} \qquad (1.2)$$

In the modified Kelvin Equation γ_l is the surface tension, ρ_l is the liquid density of the adsorbate, t is the adsorbate film thickness, r_k is the radius of the meniscus, R is the gas constant, T is the temperature, P_C and P_0 are the filling pressure and saturation pressures respectively. Equation 1.2 is a form of the modified Kelvin equation for a perfectly wetting fluid with constant molar volume, which relates the change in mechanical pressure to the change in molar free energy. The addition of a term accounting for the thickness of the film that occurs due to wetting prior to condensation increases the accuracy and range of the model. Micropores are known to have coarse structure in the adsorbed liquid phase, as well as enhanced adsorption due to fluid wall interactions. The

Kelvin equa

interface is a

strongly inte

predict hys

retreating in

smaller pore

modified Ke

condensation

side of equa

is based so

calculate su

The Kelvin

layering a

Assuming t

adsorption

Prigogene

condition f

$$\frac{d(\Delta G)}{dN} = 0$$

$$= \int$$

where $d(\Delta G$

respective

Kelvin equation is derived to describe the equilibrium mechanical pressure where the interface is a continuum, therefore cannot be applied to pores with structured fluids which strongly interact with the pore walls. The simplicity of the model and its ability to predict hysteresis based upon changes in the radius of curvature for advancing and retreating interfaces, has lead many to attempt modifications that render it applicable to smaller pores. Recent studies of MCM-41 adsorbents [11,12,13] it was found that the modified Kelvin equation could be brought to closer agreement to measured capillary condensation pressures by subtracting a constant from the $(r_k\text{-}t)$ term of the right hand side of equation 1.2. The value of this constant was found to vary for different gases and is based solely upon empirical observations, therefore there is no means presented to calculate such a parameter for different gas solid systems.

The Kelvin equation has been further modified to account for the effects of surface layering and adsorbent-adsorbate interactions for a cylindrical pores. [14,15,16] Assuming that the vapor-liquid interface is represented by a cylindrical meniscus during adsorption and by a hemispherical meniscus during desorption, and invoking the Defay-Prigogene expression for a curvature-dependent surface tension [17], the equilibrium condition for capillary coexistence in a cylindrical pore is obtained as

$$\begin{aligned}\frac{d(\Delta G)}{dN} = 0 &= \int_{P_g}^{P_0} v_g dP + \tilde{\phi}(t,R) - \frac{v_l \gamma_\infty (R-t)}{(R-t-\lambda/2)^2} \\ &= \int_{P_g}^{P_0} v_g dP + \tilde{\phi}(R,R) - \frac{2 v_l \gamma_\infty (R-t)^2}{\left[(R-t)(R-t-\lambda) + \lambda\sigma_{ff}/4\right](R-t-\lambda)}\end{aligned} \tag{1.3}$$

where $d(\Delta G)/dN$ is the Gibbs free energy change per mole adsorbed; v_g and v_l are the respective gas and liquid molar volumes at the saturation pressure P_0; γ is the surface

tension of

pore radius

interaction

condensate

adsorbent

for an adso

The adsorb

field by sol

then be cor

the known

good agree

DFT for a

materials.

below the

predicting

vapor to por

1.2.3 Semi-e

Semi-empir

adsorption

Horvath-Ka

enthalpy an

that the ent

approaches

tension of the vapor-condensate interface; σ_{ff} is the adsorbate molecular diameter; R is the pore radius; and $\lambda = (2/3)^{1/2}\sigma_{ff}$. [14] The potential field $\tilde{\phi}(r,R)$ represents the net interaction of an adsorbate molecule at radial coordinate r with the surrounding condensate and solid. This field is given as the difference between the adsorbate-adsorbent and adsorbate-adsorbate potentials, and it is represented using the 9-3 potential for an adsorbate confined within a cylindrical pore of a structureless Lennard-Jones solid. The adsorbed layer thickness t can be determined for a given pore radius and potential field by solving the equality given by equation (1.3). The capillary coexistence curve can then be constructed by calculating the condensation pressure P_g from equation (1.3) using the known values of film thickness and pore radius. This method was shown to give good agreement with the capillary coexistence curve and pore criticality predicted by DFT for adsorption of nitrogen [14,15,16] and other probe gases [15] on MCM-41 materials. The method also qualitatively predicts some wetting features of the isotherm below the capillary condensation pressure. [14,15] This model is therefore capable of predicting continuous filling of micropores with a transition to condensation of pore vapor to pore liquid.

1.2.3 Semi-empirical Methods

Semi-empirical methods have also been developed to account for the enhanced adsorption in micropores due to the superposition of the potential of the pore walls. The Horvath-Kawazoe method HK relates the change in the free energy of the system to the enthalpy and entropy change that occurs due to adsorption. [18] With the assumption that the entropy change of the system is small the change in free energy of the system approaches the change in enthalpy of the system. The original HK was based upon the

Lennard-J

iamiliar 19

Hill theory

Unfortunate

However, t

was specifi

to the pot

developme

for cylindr

attempts

function

realistic.

alone tec

density

density

condens

presente

1.2.4 St

Statisti

[25,26,

rivals

metho

cylind

Lennard-Jones 12-6 potential for a plane of graphite, and was integrated to yield the familiar 10-4 potential. The potential well depth was calculated using the Frenkel Halsey Hill theory and utilized the Kirkwood-Muller expression for the adsorption potential. Unfortunately, these were erroneously applied, as will be discussed in Chapters 4 and 5. However, the HK method was a milestone in the advancement of adsorptive studies, as it was specifically designed for use with micropores and the enhancement of adsorption due to the potential between the adsorbent and adsorbate. The HK method led to the development of similar models with different geometries such as the Saito-Foley method for cylindrical pores [19] or the Yang method for spherical pores [20,21]. Further attempts to improve the HK method have involved improvements to the potential function [20,22] and modifications to make the density profile within the pore more realistic. [20,23,24] In addition to the work done to improve the HK method as a stand alone technique it has been modified to the better correlate with the results obtained via density functional theory DFT, such alterations include modification of the average density profile and addition of a step to account for pore wall wetting prior to pore condensation. A more detailed discussion of the modifications to the HK method will be presented in Chapters 4 and 5.

1.2.4 Statistical Thermodynamic Models

Statistical thermodynamic models such as the density functional theory DFT [25,26,27,28] produce model isotherms and predict the density profile within a pore that rivals the predictions of molecular simulation MS for simple geometries. [10] The DFT method is only applicable to pores that are of a simple geometry such as a sphere, slit, or cylinder, and do not contain much chemical heterogeneity of the surface atoms, however

for simple

required

assumed

details of

will be pr

density pr

Ω_{L^2}

where Ω

fluid de

spatially

temper

profile

across

chem

profi

isoth

equa

1.3

The

upon

mesh

Whe

com

for simple systems it provides accurate results in less than one hundredth of the time required for MS. When utilizing the DFT method all pores in a particular carbon are assumed to have a common shape with size being the only source of heterogeneity. The details of DFT will be discussed in Chapters 2 and 3, therefore only a brief description will be provided here. The grand potential of the pore is written as a function of the density profile within a pore

$$\Omega[\rho(r)] = F[\rho(r)] - \int \rho(r)[\mu - V_{ext}(r)]dr \qquad (1.4)$$

where Ω is the grand potential, F is the Helmholtz free energy functional, $\rho(r)$ is the local fluid density, r is the position in the pore, μ is the chemical potential and V_{ext} is the is a spatially varying potential. The grand potential is then minimized for a specific temperature, chemical potential, and pore size with respect to the smoothed density profile. Once the density profile is obtained the volume average of the density is taken across the entire pore volume and used to represent the density at a particular bulk chemical potential and pore size. Although local minima may exist for several density profiles, the lowest grand potential indicates the equilibrium profile. A series of isotherms are generated over the pressure range of interest and used in conjunction with equation (1.1) to determine the pore size distribution.

1.3 Choice of Method

The choice of method used to determine the PSD of a particular material is dependant upon the known physical characteristics of the system of interest. The most accurate method is a MS based upon assumptions about the materials that are being studied. When the simplistic pore models are chosen the DFT method predicts results that are comparable to the MS while requiring one hundredth of the time, additionally the density

profiles ir

methods i

Methods

used app

macropor

range it is

and modi

range. how

advantage

or MS iso

Chapter 5

profiles in the pores are also predicted. The advantage of using either the DFT or MS methods is that they may are capable of predicting the behavior of pores of any size. Methods such as the HK and Kelvin equation are limited in the ranges where they can be used appropriately. The Kelvin equation is capable of producing accurate results for macropores, while modified versions appear to extend the applicability to the mesoporous range it is doubtful however that this may be applied to the micropore range. The HK and modified versions are capable of predicting the PSD in the micro and mesopore range, however is less accurate than either the DFT or MS methods, however is advantageous in the efficiency of determining the model isotherms. Therefore when DFT or MS isotherms are not in existence the modified two-stage HK method described in Chapter 5 is recommended.

1.4 Refer

1. Cher

2. Last

for the

1994.

3. Madd

Bucky

4. Wan

5. Adar

New

6. Inou

Mol

468

7. Ri

F.

R

c

6

8. C

I

9. C

1.4 References

1. Chemical engineering progress Jan 2001 p 18.
2. Lastoskie, C.M. A Statistical Mechanics Interpretation of the Adsorption Isotherm for the Characterization of porous Sorbents PhD. Dissertation Cornell university 1994.
3. Maddox M.W, and Gubbins KE. Molecular Simulation of Fluid Adsorption in Buckytubes. Langmuir 1995; 11 3988.
4. Wang, Q.; Johnson, K. Journal of Chemical Physics 1999, 110, 577.
5. Adamson A.Physical Chemistry of Surfaces 5th ed. John Wiley and Sons Inc, New York 1990.
6. Inoue S, Ichikuni N, Suzuki T, Kaneko K. Capillary Condensation of N2 on Multiwall Carbon Nanotubes The Journal of Physical Chemistry B 1998; 102 (24) 4689.
7. Rinzler, A.G.; Liu, J.; Dai, H.; Nikolaev, P.; Huffman, C. B.; Rodriguez-Macias, F.J.; Boul ,P.J.; Lu, A.H.; Heymann, D.; Colbert, D. T.; Lee, R. S., Fischer, J. E., Rao, A.M. Eklund, P.C. Smalley R. E. Large Scale purification of single-wall carbon nanotubes: process, product, and characterization. Appl. Phys. A.. 1998, 67, 29.
8. Gregg SJ, Sing KSW. Adsorption, Surface Area and Porosity. Academic Press, London 1982.
9. Gelb, L.D. and K.E. Gubbins, *Langmuir* **15** (1999) 305.

10. Lastoskie, C
Molecular
Engineerin
11. M. Kruk a
12. M. Kruk, M
13. M. Kruk, M
14. C.G. Sonw
15. C.G. Sonw
16. S.K. Bhat
17. R. Defay a
and Co., B
18. Horvath G
Distributio
Japan 16 (
19. Saito A. an
Adsorption
20. Rege, S an
Distributio
21. Cheng, L. a
Spherical P
Enigineerin
22. Dombrow
Model for P

10. Lastoskie, C. and Gubbins, K. Characterization of Porous Materials Using Molecular Theory and Simulation. Submitted to Advances in Chemical Engineering 2001.

11. M. Kruk and M. Jaroniec, *Chem. Mater.* **12** (2000) 222.

12. M. Kruk, M. Jaroniec, J.M. Kim and A. R. Ryoo, *Langmuir* **15** (1999) 5279.

13. M. Kruk, M. Jaroniec and A. Sayari, *Langmuir* **13** (1997) 6267.

14. C.G. Sonwane and S.K. Bhatia, *Chem. Eng. Sci.* **53** (1998) 3143.

15. C.G. Sonwane, S.K. Bhatia and N. Calos, *Ind. Eng. Chem. Res.* **37** (1998) 2271.

16. S.K. Bhatia and C.G. Sonwane, *Langmuir* **14** (1998) 1521.

17. R. Defay and I. Prigogine, *Surface Tension and Adsorption*: Longmans, Green and Co., Bristol (1966).

18. Horvath G. and Kawazoe, K. Method for the Calculation of Effective Pore Size Distribution in Molecular Sieve Carbon. Journal of Chemical Engineering of Japan 16 (1983), 470.

19. Saito A. and Foley, H. Curvature and Parametric Sensitivity in Models for Adsorption in Micropores. AIChE Journal 37 (1991) 3, 429.

20. Rege, S and Yang, R. Corrected Horvath-Kawazoe Equations for Pore-Size Distribution. AICHE Journal 46 (2000) 4, 734.

21. Cheng, L. and Yang, R. Improved Horvath-Kawazoe Equations Icluding Spherical Pore Models for Calculating Micropore Size Distributions Chemical Enigineering Science 49 (1994) 16, 2599.

22. Dombrowski, R. and Lastoskie, C. A Two-Stage Horvath-Kawazoe Pore Filling Model for Pore Size Distribution Analysis. Submitted to the Journal of AIChE.

23. Lastoskie, C.
Studies in Sur
24. Dombrowski, F
Revisited. Col
25. Lastoskie, C.; (
Slit Pore: A De
26. Seaton, N.; Wa
27. Ravikovitch, P.
28. Nilson, R and G

23. Lastoskie, C. A modified Horvath-Kawazoe Method for Micropore Size Analysis. Studies in Surface Science and Catalysis 128 (2000) 475.

24. Dombrowski, R.; Lastoskie, C.; and Hyduke, D. The Horvath-Kawazoe Method Revisited. Colloids and Surfaces A in press 2001

25. Lastoskie, C.; Gubbins, K.; Quirke, N. Pore size Heterogeneity and the Carbon Slit Pore: A Density Functional Theory Model.Lamgmuir 9 (1993) 2693.

26. Seaton, N.; Walton, J.; Quirke, N. Carbon 27 (1989) 853.

27. Ravikovitch, P.; Haller, G.; Neimark, A. Adv. Coll. Int. Sci. 76 (1998) 203

28. Nilson, R and Griffith, S. J Chem Phys. 111 (1999) 4281.

Dombrowski RJ. Hyd
from argon and nitrog
16(11): 5041-5050 N

Chapter 2.

Dombrowski RJ, Hyduke DR, Lastoskie CM .Pore size analysis of activated carbons from argon and nitrogen porosimetry using density functional theory. LANGMUIR 16 (11): 5041-5050 MAY 30 2000.

Pore
and Nitr

2.1. Introduction

Activated car
and as selective a
mixtures. The t
activated carbon
Characterization
involving the u

Comme
various feedst
The carbonize
dioxide to dev
of manufactu
Although suc
"typical" acti
along their e
of two hundr
connectivity

Chapter 2.

Pore Size Analysis of Activated Carbons from Argon and Nitrogen Porosimetry Using Density Functional Theory

2.1. Introduction

Activated carbons are used in the chemical process industries as gas storage media and as selective adsorbents for the separation and purification of vapor- and liquid-phase mixtures. The thermodynamic behavior of a fluid, or a fluid mixture, adsorbed on an activated carbon depends principally on the pore size distribution (PSD) of the adsorbent. Characterization of the PSD is therefore an important problem in industrial applications involving the use of activated carbons.

Commercial activated carbons are manufactured by thermolytic decomposition of various feedstock materials, including cellulosic matter and synthetic polymer resins. The carbonized thermolysis products are "activated" via exposure to steam or carbon dioxide to develop the accessible internal pore volume of the adsorbent [1]. This method of manufacture yields activated carbons that have semiamorphous microstructures. Although such materials defy a simple topological description, we might envision a "typical" activated carbon as a contiguous network of graphitic microcrystals, joined along their edges by surface functional groups, with each crystal containing on the order of two hundred atoms, stacked into two or three graphite layers [2]. The size, shape and connectivity of the pores in an activated carbon depend in a complex manner on the

feedstock materi

of steam- or CO_2-

conditions and the

Unlike crystalline

MCM-41 mesopo

by X-ray diffract

determined indire

Extracting PSD in

make several ass

solution of the P

carbon is com

homogeneous. g

activated carbon

presented as equ

In order to

must be emplo

side of equat

adsorption on

Comparisons

DFT model a

with simple

model adso

computation

feedstock material used, the temperature and duration of the carbonization, and the extent of steam- or CO_2-activation. At the present time, the relationship between the processing conditions and the resultant carbon structure is poorly understood.

Unlike crystalline adsorbents such as zeolites, or templated porous materials such as MCM-41 mesoporous molecular sieves, activated carbons are not readily characterized by X-ray diffraction or by neutron scattering. Rather, the PSD of a carbon is generally determined indirectly through interpretation of gas adsorption measurements [3]. Extracting PSD information from the experimental adsorption isotherm requires that we make several assumptions regarding the structure of the adsorbent, thus rendering the solution of the PSD numerically tractable. Usually, it is assumed that the activated carbon is composed of noninterconnected, slit-shaped pores with chemically homogeneous, graphitic surfaces. By invoking these assumptions, the PSD of an activated carbon, $f(H)$, can be determined by solving the adsorption integral equation presented as equation 1.1.

In order to obtain accurate results for the adsorbent PSD, a realistic pore filling model must be employed to construct the model isotherms $\Gamma(P,H)$ that appear on the right-hand side of equation (1.1). Lastoskie reported a thermodynamic model for nitrogen adsorption on graphitic slit pores at 77K based upon density functional theory (DFT) [4]. Comparisons of DFT results to Monte Carlo molecular simulations have shown that the DFT model accurately describes the density profile of the inhomogeneous adsorbed fluid with simple pore structures such as carbon slit pores [5]. DFT thus provides correct model adsorption isotherms for use in equation (1.1), at a small fraction of the computational time needed to obtain the same isotherms from molecular dynamics or

Monte Carlo mo

Kelvin equation

frequently used

that these classi

in micropores.

[8,9]. Moreove

the Kelvin equ

pore filling mo

Nitrogen

inexpensive,

experimental

normal liqui

temperature

choice, sinc

maintained

situations i

carbons th

interaction

(e.g. carbo

does not

for any e

nitrogen

errors in

Monte Carlo molecular simulation. Other, simpler methods that predate DFT, such as the Kelvin equation [6] or the Horvath-Kawazoe (HK) equation [7], have also been frequently used as pore filling models. However, it has been convincingly demonstrated that these classical pore filling models do not provide a realistic description of adsorption in micropores, and therefore they are not suitable for micropore size characterization [8,9]. Moreover, the classical models are limited in the scope of their applicability, e.g. the Kelvin equation for mesopores and the HK method for micropores, whereas the DFT pore filling model describes adsorption over the entire range of carbon pore sizes.

Nitrogen is the probe gas most commonly used for PSD analysis because it is inexpensive, readily obtained, inert, and well-studied in the adsorption literature. The experimental isotherm on the left-hand side of equation (1.1) is usually measured at the normal liquid nitrogen boiling point of 77 K, which is sufficiently below the critical temperature so that a large uptake of the adsorbate is realized. This is again a convenient choice, since liquid nitrogen is inexpensive and isothermal conditions can easily be maintained using liquid nitrogen as a cryostat. Despite these merits, there may arise situations in which a probe gas species other than nitrogen is desirable. On activated carbons that have substantial chemical heterogeneity, there may be significant interactions between the quadrupolar nitrogen molecule and various functional groups (e.g. carboxylic acids) on the carbon surface. The DFT model for nitrogen adsorption does not account for the nonspherical shape of the nitrogen molecule, nor does it allow for any electrostatic interactions other than dipole and induced dipole interactions, of nitrogen molecules with the carbon surface. The neglect of these features may result in errors in the calculation of the carbon PSD.

Argon is

heterogeneous ad

moments, and it

extensively for P

oxides [3,10]. D

normal boiling po

argon as the ter

more expensive

out the argon ad

Therefore, in t

pores at 77 K

reported in Se

obtained for

interpret exp

2.2. Theor

A d

literature [

the local d

determine

functional

Ω

Argon is nearly an ideal probe gas for characterizing the pore structure of heterogeneous adsorbents, since it is a monatomic, spherical molecule with no multipolar moments, and it is similar in size to nitrogen. Argon porosimetry has been used extensively for PSD analysis of activated carbons, silicas, aluminas and mesoporous oxides [3,10]. DFT model isotherms have been computed for argon adsorption at its normal boiling point of 87 K [11]. This temperature is readily maintained by using liquid argon as the temperature bath for the sorption measurement. Because liquid argon is more expensive than liquid nitrogen, however, it is convenient and economical to carry out the argon adsorption measurement at the normal liquid nitrogen boiling point of 77 K. Therefore, in this work we present a DFT model for argon adsorption in graphitic slit pores at 77 K. This model is described in Section 2.2 and the model isotherms are reported in Section 2.3. We then compare and analyze, in Section 2.4, the PSD results obtained for several activated carbons, using the argon and nitrogen DFT models to interpret experimental argon and nitrogen isotherms measured on the carbon adsorbents.

2.2. Theoretical Section: Density Functional Theory

A detailed description of the DFT method has been presented extensively in the literature [4], and so we will provide a short summary of the theory. In the DFT method, the local density profile $\rho(\mathbf{r})$ of the inhomogeneous adsorbed fluid at phase equilibrium is determined by solving for the density profile that minimizes the grand potential functional Ω of the confined fluid. The grand potential functional is given as

$$\Omega[\rho(\mathbf{r})] = F[\rho(\mathbf{r})] - \int d\mathbf{r}\,\rho(\mathbf{r})[\mu - V_{ext}(\mathbf{r})] \qquad (2.1)$$

where F is the H

the adsorbate-sol

taken over the en

H, located betwe

directions (Figur

coordinate, the d

$$V_{ss}(z) = \phi_{ij}(z$$

In equation (2.2),

and H is the sepa

of the opposing po

spacing $\Delta = 3.35$

potential [12]

$$\phi_{ij} = 2\pi\varepsilon_{ij}\rho\sigma$$

where σ_{ij} and ε_{ij} a

with a carbon ato

graphite layers ha

(assuming a spati

slab. This approx

a one-dimensiona

The Helmhol

sum of the hard

adsorbate interac

where F is the Helmholtz free energy functional; μ is the chemical potential; and V_{ext} is the adsorbate-solid potential at spatial coordinate **r**. The integration in equation (2.1) is taken over the entire pore volume of the adsorbent. In a slit pore of physical pore width H, located between two homogeneous graphitic slabs that are unbounded in the lateral directions (Figure 2.1), the external potential V_{ext} depends only upon one spatial coordinate, the distance z of the adsorbate center-of-mass from the adsorbent surface:

$$V_{ext}(z) = \phi_{sf}(z) + \phi_{sf}(H - z) \tag{2.2}$$

In equation (2.2), ϕ_{sf} is the adsorbate interaction potential with one of the bounding slabs, and H is the separation distance between the carbon nuclei in the surface graphite layers of the opposing pore walls. For a solid density $\rho_s = 0.114$ Å^{-3} and a graphite lattice plane spacing $\Delta = 3.35$ Å, the adsorbate-solid potential is well-represented by the 10-4-3 potential [12]

$$\phi_{sf} = 2\pi\varepsilon_{sf}\rho_s\sigma_{sf}^2\Delta\left[\frac{2}{5}\left(\frac{\sigma_{sf}}{z}\right)^{10} - \left(\frac{\sigma_{sf}}{z}\right)^{4} - \frac{\sigma_{sf}^4}{3\Delta(z+0.61\Delta)^3}\right] \tag{2.3}$$

where σ_{sf} and ε_{sf} are the Lennard-Jones parameters for the adsorbate molecule interaction with a carbon atom in the porous solid. In equation (2.3), the lateral structure of the graphite layers has been replaced with an integration over the lattice plane surface area (assuming a spatially uniform carbon atom density) and a summation of the layers in each slab. This approximation conveniently reduces the DFT grand potential minimization to a one-dimensional solution of the adsorbate density profile $\rho(z)$.

The Helmholtz free energy functional is computed from perturbation theory as the sum of the hard sphere Helmholtz free energy functional F_h (for the repulsive adsorbate-adsorbate interactions), and a mean field contribution for the dispersion interactions:

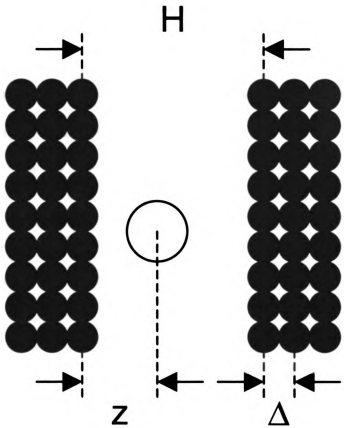

Figure 2.1: Schematic of graphitic slit pore model showing definition of physical pore width *H*.

$F[\rho(\mathbf{r})] = F_c[\rho(\mathbf{r}$

The first term in

attractive fluid-f

Chandler-Anders

$\phi_{ff}(|\mathbf{r}-\mathbf{r}'$

where $r_m = 2^{1/6}\sigma$

whose centers of

$\phi_{fs}(r) = 4$

(2.6)

The parameters σ

the adsorbate-ads

The hard-sphe

ideal and an exce

$F_c[\rho(\mathbf{r})]d$

(2.7)

In equation (2.7

contribution to

wavelength, T is

Planck and Boltz

f_{ex} that appears in

$$F[\rho(\mathbf{r})] = F_h[\rho(\mathbf{r});d] + \frac{1}{2}\iint d\mathbf{r}d\mathbf{r}'\,\rho(\mathbf{r})\rho(\mathbf{r}')\phi_{att}(|\mathbf{r}-\mathbf{r}'|) \qquad (2.4)$$

The first term in equation (2.4) is calculated for hard spheres of diameter d, and the attractive fluid-fluid potential ϕ_{att} in the second term is obtained from the Weeks-Chandler-Anderson representation [13]

$$\begin{aligned} \phi_{att}(|\mathbf{r}-\mathbf{r}'|) &= \phi_{ff}(|\mathbf{r}-\mathbf{r}'|), \qquad |\mathbf{r}-\mathbf{r}'| > r_m \\ &= -\varepsilon_{ff}, \qquad |\mathbf{r}-\mathbf{r}'| < r_m \end{aligned} \qquad (2.5)$$

where $r_m = 2^{1/6}\,\sigma_{ff}$ and ϕ_{ff} is the Lennard-Jones potential for a pair of adsorbate molecules whose centers of mass are separated by a distance r:

$$\phi_{ff}(r) = 4\varepsilon_{ff}\left[\left(\frac{\sigma_{ff}}{r}\right)^{12} - \left(\frac{\sigma_{ff}}{r}\right)^{6}\right] \qquad (2.6)$$

The parameters σ_{ff} and ε_{ff} are the Lennard-Jones molecular diameter and well depth for the adsorbate-adsorbate pair potential.

The hard-sphere Helmholtz free energy functional in equation (2.4) is divided into an ideal and an excess component

$$F_h[\rho(\mathbf{r});d] = kT\int d\mathbf{r}\rho(\mathbf{r})[\ln(\Lambda^3\rho(\mathbf{r})) - 1] + kT\int d\mathbf{r}\rho(\mathbf{r})f_{ex}[\bar{\rho}(\mathbf{r});d] \qquad (2.7)$$

In equation (2.7), the first term on the right-hand side represents the ideal gas contribution to the hard-sphere free energy; $\Lambda = h/(2\pi mkT)^{1/2}$ is the thermal wavelength, T is the temperature, m is the adsorbate molecular mass, and h and k are the Planck and Boltzmann constants, respectively. The excess molar Helmholtz free energy, f_{ex}, that appears in the second term on the right-hand side of equation (2.7), is calculated

using a *nonlocal*

density profile ρ

adsorbed within

effects [14]. Th

oscillatory densit

profiles have als

micropores [5].

minimization of

calculation of th

is obtained in t

and molecular

To pro

(2.7), the dens

account for th

density profile

$$\bar{\rho}(\mathbf{r}) =$$

Various presc

work, we ado

this nonlocal

energy is obt

[17], with an

[18].

using a *nonlocal* or "smoothed" density profile $\bar{\rho}(\mathbf{r})$ instead of the local adsorbed fluid density profile $\rho(\mathbf{r})$. It is known from surface force microscopy measurements that fluids adsorbed within micropores have highly structured density profiles due to confinement effects [14]. The high degree of fluid ordering at the pore wall surface results in an oscillatory density profile that dampens toward the center of the pore. Similar density profiles have also been observed in molecular simulation studies of fluids confined in micropores [5]. The DFT model does not yield an oscillatory density profile from the minimization of the grand potential functional, if the local density profile is used in the calculation of the excess Helmholtz free energy. A relatively unstructured density profile is obtained in the local version of DFT; such a profile is inconsistent with experimental and molecular simulation results.

To properly represent the excess free energy of the adsorbed fluid in equation (2.7), the density profile that is input to the f_{ex} functional must be weighted so as to account for the sharp spatial gradients in the confined fluid density. A smoothed input density profile is therefore calculated as

$$\bar{\rho}(\mathbf{r}) = \int d\mathbf{r}' \, \rho(\mathbf{r}')w[|\mathbf{r} - \mathbf{r}'|; \bar{\rho}(\mathbf{r})] \tag{2.8}$$

Various prescriptions for the weighting function w have been proposed [15]. In this work, we adopt the weighting function suggested by Tarazona; a detailed description of this nonlocal version of DFT can be found elsewhere [16]. The excess Helmholtz free energy is obtained from the Carnahan-Starling equation of state for a hard sphere fluid [17], with an equivalent hard sphere diameter d given by the Barker-Henderson diameter [18].

Adsorption is

adsorbate densit

adsorbed fluid

adsorption $\Gamma P.H$

width of the pore

$$\Gamma(P.H) = \frac{1}{H}$$

where $\rho(z)$, ρ_b an

potential μ. The

of mean-field equ

$$\mu(\rho_b) = \mu$$

$$P(\rho_b) =$$

where μ_b and P_b

[17], respectivel

$$a = 4\pi \int$$

In the argon an

adsorption is u

then used to c

product of th

adsorption. N

used in calc

experimental

Adsorption isotherms for pores of different width H are constructed by solving for the adsorbate density profiles $\rho(z)$ that minimize the grand potential functional of the adsorbed fluid over a range of chemical potential values μ. The specific excess adsorption $\Gamma(P,H)$ is then obtained from the line average of the density profile across the width of the pore

$$\Gamma(P,H) = \frac{1}{H}\int_0^H [\rho(z) - \rho_b]dz \tag{2.9}$$

where $\rho(z)$, ρ_b and P are the density profile, bulk gas density and pressure at chemical potential μ. The bulk fluid equations of state that relate ρ_b, P and μ are given by the set of mean-field equations

$$\mu(\rho_b) = \mu_h(\rho_b, d) + a\rho_b \tag{2.10}$$

$$P(\rho_b) = P_h(\rho_b, d) + \tfrac{1}{2}a\rho_b^2 \tag{2.11}$$

where μ_h and P_h are the Carnahan-Starling hard sphere chemical potential and pressure [17], respectively, and a is the van der Waals attractive parameter

$$a = 4\pi\int_0^\infty r^2 \phi_{att}(r)dr \tag{2.12}$$

In the argon and nitrogen adsorption experiments (reported in the next section), helium adsorption is used to calibrate the pore volume. This helium-calibrated pore volume is then used to convert the absolute adsorption to an excess adsorption, by subtracting the product of the bulk gas density and the calibrated pore volume from the absolute adsorption. Neimark and Ravikovitch have noted that the same convention should be used in calculating excess adsorption isotherms from DFT for comparison with experimental results [19]. They used DFT to compute a helium-calibrated pore volume,

and found that

carbon slit por

In the case o

calibrated por

width smaller

thus inaccess

use equation

specific exce

2.3. Experi

Arg

The select

activated c

An argon

order to

graphitic

hours; in

transferr

Isotherm

and nit

automa

the bul

obtain

using

and found that the excess isotherms calculated for supercritical methane adsorption in carbon slit pores decrease by 4 to 5% when the correction for the pore volume is applied. In the case of argon or nitrogen adsorption at 77 K, the correction for the helium-calibrated pore volume is negligibly small (less than 2%), except in slit pores of physical width smaller than 6 Å. Pores that are this narrow exclude argon and nitrogen, and are thus inaccessible to PSD analysis using argon or nitrogen porosimetry. We may therefore use equation (10), rather than the helium-calibrated DFT pore volume, in calculating the specific excess adsorption with minimal error.

2.3. Experimental Section: Argon and Nitrogen Porosimetry

Argon and nitrogen isotherms were measured on four porous carbons at 77 K. The selected carbons were Aldrich powdered activated carbon 16155-1, granular activated carbon 4021-s, a 100-200 mesh Saran char, and a 50-200 mesh coconut char. An argon isotherm was also measured on Sterling FT, a nonporous graphitized carbon, in order to obtain the solid-fluid potential parameters for argon adsorption in the model graphitic slit pores. All samples were outgassed at 350 °C for a period of at least 20 hours; in all cases, ultimate pressures below 10^{-5} torr were achieved. Samples were then transferred to an insulated Dewar containing a temperature bath of liquid nitrogen. Isothermal conditions at 77.3 ± 0.1 K were maintained during all experiments. Argon and nitrogen adsorption isotherms were measured using a Coulter Omnisorp 100 automated system, over a pressure range from approximately $10^{-5}P_0$ to $0.8P_0$, where P_0 is the bulk saturation pressure of the adsorbate. The specific excess adsorption isotherm is obtained from the absolute amount of gas adsorbed by correcting for the bulk gas density using helium calibration of the pore volume. All isotherms are reported in terms of

relative pressure P/P

the experimental va

pressure of solid ar

2.4. Fitting of the

The Lennar

fitted[5] to match th

boiling point of 7

temperature of bu

Lennard-Jones p

supercooled liqui

In this work, we

supercooled liqu

(2.10) and (2.1

solid phase coe

supercooled liq

agree well wi

saturated liquid

that DFT is in

density profil

supercooled li

theoretical m

condenses in t

relative pressure P/P_0. For liquid nitrogen at 77 K, $P_0 = 762 \pm 2$ torr; for argon at 77 K, the experimental value of P_0 was found to be 204 $\pm$ 4 torr, which is the saturation pressure of solid argon.

2.4. Fitting of the DFT Model Parameters

The Lennard-Jones parameters σ_{ff} and ε_{ff} for bulk nitrogen have been previously fitted[5] to match the saturated liquid nitrogen density of 0.02887 mol/cm^3 at its normal boiling point of 77.347 K. The fitted parameters are listed in Table 2.1. The triple point temperature of bulk argon is 83.8 K; hence, at 77 K, one may elect to fit the bulk argon Lennard-Jones parameters to either the solid argon (0.0411 mol/cm^3; 205 torr) or the supercooled liquid argon (0.0365 mol/cm^3; 229 torr) density and saturation pressure [20]. In this work, we have chosen to fit the model parameters using the physical properties of supercooled liquid argon; this yields the fitted values listed in Table 2.1. Equations (2.10) and (2.11) describe only vapor-liquid coexistence, and cannot predict the vapor-solid phase coexistence of bulk argon at 77 K. However, the saturation pressure of supercooled liquid argon calculated from equations (2.10) and (2.11) has been found to agree well with the experimental saturation pressure obtained by extrapolating the saturated liquid coexistence line below the argon triple point [21]. It should also be noted that DFT is incapable of predicting solid-phase transitions; hence, the condensed-phase density profiles computed from DFT for argon adsorption at 77 K correspond to supercooled liquid argon, not solid argon. In principle, this mismatch between the theoretical model and the experimental isotherms (which indicate that solid argon condenses in the carbon pores) may cause errors in the PSD analysis. As we shall later

demonstrate, however

of the condensed arg

minimal.

Table 2.1: Lennard-J

model.

Parameter	Ar
	Superc
σ_{ff}(Å)	3.3
ε_{ff}/k(K)	11
σ_{ss}(Å)	3.3
ε_{ss}/k(K)	58

The Lennard

with carbon atoms

adsorption isother

values listed in Ta

the argon-carbon

diameter is set e

molecular diamet

is then determine

between the expe

isotherm for argo

mesopore is suffi

the slit pore have

DFT isotherm in

(nonporous) grap

demonstrate, however, the computed DFT isotherms are largely unaffected by the choice of the condensed argon phase, and so the effect of this choice on the PSD analysis will be minimal.

Table 2.1: Lennard-Jones potential parameters for nitrogen [5] and argon used in DFT model.

Parameter	Argon		Nitrogen
	Supercooled liquid	Solid	
σ_{ff} (Å)	3.375	3.27	3.572
ε_{ff}/k (K)	110.2	113.	93.98
σ_{sf} (Å)	3.362	3.31	3.494
ε_{sf}/k (K)	58.02	61.5	53.22

The Lennard-Jones parameters σ_{sf} and ε_{sf} for the interaction of adsorbed nitrogen with carbon atoms in a graphite surface have been previously fitted [5] to the nitrogen adsorption isotherm on the nonporous graphitized carbon Vulcan at 77 K (parameter values listed in Table 2.1). We follow a similar procedure for fitting the parameters of the argon-carbon interaction potential. The argon-carbon effective intermolecular diameter is set equal to the arithmetic mean of the argon-argon and carbon-carbon molecular diameters. The Lennard-Jones well depth ε_{sf} for the argon-carbon interaction is then determined by selecting the value that provides the best quantitative agreement between the experimental argon isotherm of the nonporous reference carbon and the DFT isotherm for argon adsorption in a model graphitic slit pore of width H = 67.5 Å. This mesopore is sufficiently large so that the adsorbed films on the two opposing surfaces of the slit pore have no significant potential interactions; i.e. at low relative pressures, the DFT isotherm in this slit pore can be regarded as the adsorption isotherm on two isolated (nonporous) graphite surfaces. To directly compare the experimental and DFT model

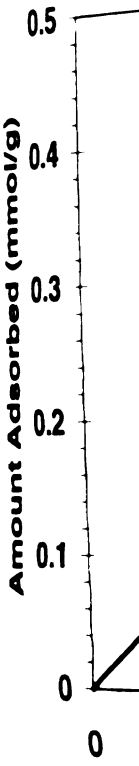

Figure 2.2: E

comparison t

isotherm: the

this fitted lin

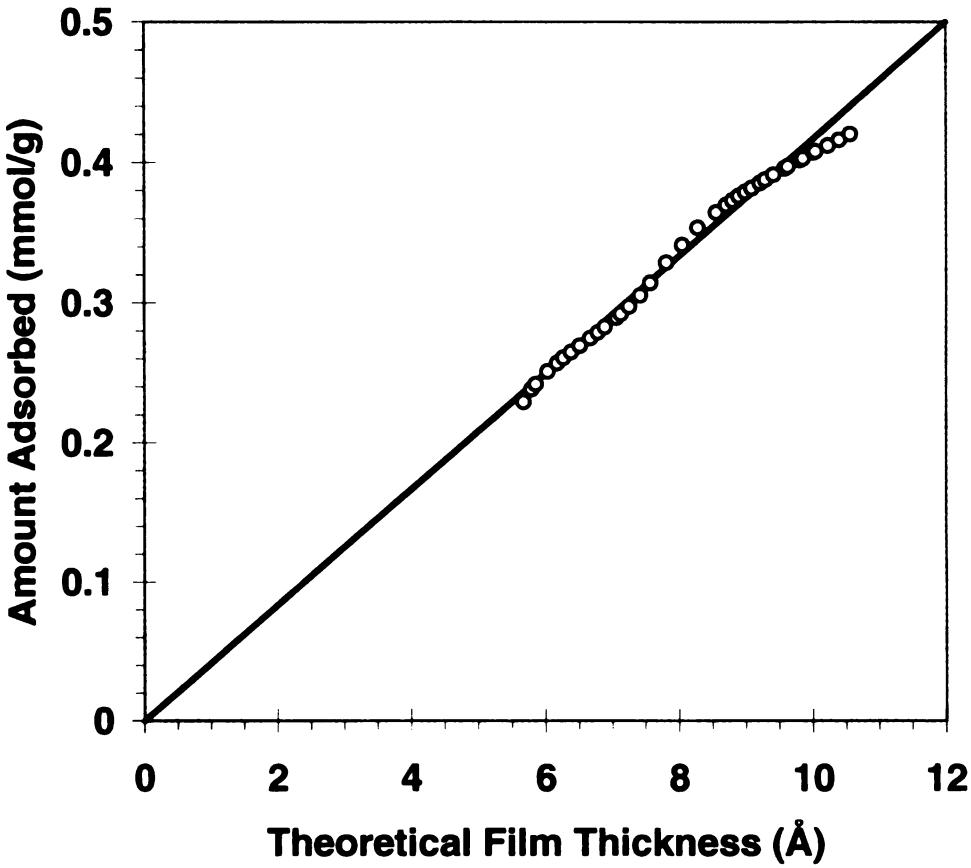

Figure 2.2: Evaluation of the specific surface area of Sterling nonporous carbon from comparison to the universal film thickness curve. The circles are the experimental isotherm; the solid line shows the linear fit of the data through the origin. The slope of this fitted line yields the specific surface area.

isotherms, we must

which in the case of

de Boer *et al.* [22], t

the argon uptake ve

area of 11.3 m^2/g w

convert the DFT-cal

a pore volume basis

The well-depth paran

the experimental ar

experimental isother

value of ε_{ff} was con

the DFT isotherm.

closely matched th

isotherm.

It has been f

this inflection point

DFT isotherm is b

whereas the Sterling

degree of surface h

graphitized. Surfac

distribution of the

shallower slope tha

should also be note

isotherms, we must first determine the specific surface area of the reference carbon, which in the case of argon is a Sterling FT graphitized carbon. Following the method of de Boer *et al.* [22], the specific surface area is obtained by fitting a line through a plot of the argon uptake versus the theoretical film thickness (Figure 2.2). A specific surface area of 11.3 m^2/g was measured for the Sterling carbon; this value was then used to convert the DFT-calculated specific excess argon adsorption in the 67.5 Å-slit pore from a pore volume basis to an adsorbent mass basis, as described in our previous work [5]. The well-depth parameter ε_{sf} that yielded the best agreement between the DFT model and the experimental argon isotherm is reported in Table 2.1, and a comparison of the experimental isotherm and the fitted DFT isotherm is shown in Figure 2.3. The best-fit value of ε_{sf} was considered to be the one for which the low-pressure inflection point in the DFT isotherm, corresponding to the formation of an adsorbed monolayer, most closely matched the inflection point in the monolayer region of the experimental isotherm.

It has been found that the DFT isotherm always exhibits a greater slope around this inflection point than the experimental isotherm. This is to be expected, since the DFT isotherm is based upon adsorption on a homogeneous model graphitic surface, whereas the Sterling reference carbon, and any other nonporous carbon, will retain some degree of surface heterogeneity, no matter what the extent to which the adsorbent was graphitized. Surface physical and/or chemical heterogeneities broaden the site energy distribution of the adsorbent surface, and cause the measured isotherm to have a shallower slope than it would if the surface were energetically homogeneous [23]. It should also be noted that we have deliberately chosen to fit the solid-fluid potential

Figure 2.3: Argo

experimental iso

DFT-fitted isoth

the Lennard-Jon

endpoints) and s

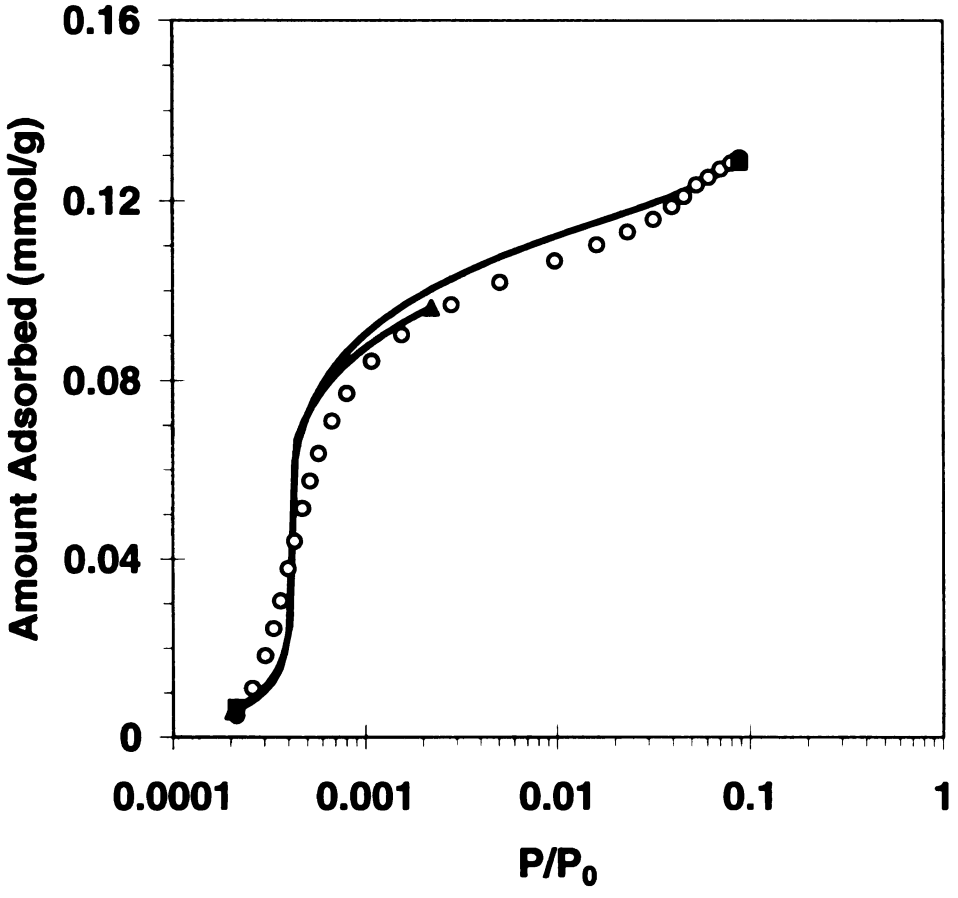

Figure 2.3: Argon adsorption on nonporous carbon surface at 77 K. The circles are the experimental isotherm measured on Sterling FT graphitized carbon. The lines are the DFT-fitted isotherms in a model graphitic slit pore of width H = 67.5 Å, obtained using the Lennard-Jones potential parameters calculated from the supercooled liquid (square endpoints) and solid (triangle endpoints) argon bulk physical properties.

parameters to the m

attempted to obta

experimental isothe

10^{-3}), the principal p

carbon atoms: wh

substantial as the

multilayer/condens

the DFT model, be

at a relative pressu

inconsequential to

can be accomplish

reference isotherm

25. DFT Model I

In Figure

graphitic slit pore

Table 2.1. For co

over the same size

nitrogen isotherms

in the mesopores,

larger slit pores, w

notable differences

adsorption model, t

parameters to the monolayer region of the nonporous reference isotherm, and have not attempted to obtain quantitative agreement between the DFT isotherm and the experimental isotherm at higher relative pressures. At low relative pressures (i.e. $P/P_0 < 10^{-3}$), the principal potential interactions are between the argon molecules and the surface carbon atoms; whereas at higher pressures, argon-argon interactions become more substantial as the adsorbed films thicken. It is generally not possible to fit the multilayer/condensation region of the nonporous (BET-type) isotherm at $P/P_0 > 0.4$ using the DFT model, because the model isotherm will exhibit a condensation phase transition at a relative pressure specific to the pore slit width. This lack of agreement, however, is inconsequential to the fitting of the Lennard-Jones solid-fluid potential parameters, which can be accomplished very satisfactorily using only the low-pressure portion of the reference isotherm.

2.5. DFT Model Isotherms for Carbon Slit Pores

In Figure 2.4, the model DFT isotherms are shown for argon adsorption in graphitic slit pores at 77 K, calculated using the potential parameters summarized in Table 2.1. For comparison, the DFT isotherms for nitrogen adsorption at 77 K in pores over the same size range are presented in Figure 2.5. The overall shape of the argon and nitrogen isotherms are similar: in the micropores, the pores fill in a single step; whereas in the mesopores, condensation is preceded by the formation of a monolayer, and, in the larger slit pores, wetting of one or more additional adsorbed layers. There are some notable differences between the argon and nitrogen DFT isotherms. In the nitrogen adsorption model, the isotherms of the micropores smaller than 10 Å are continuous;

Figure 2.4: Argo

calculated from

reading from left

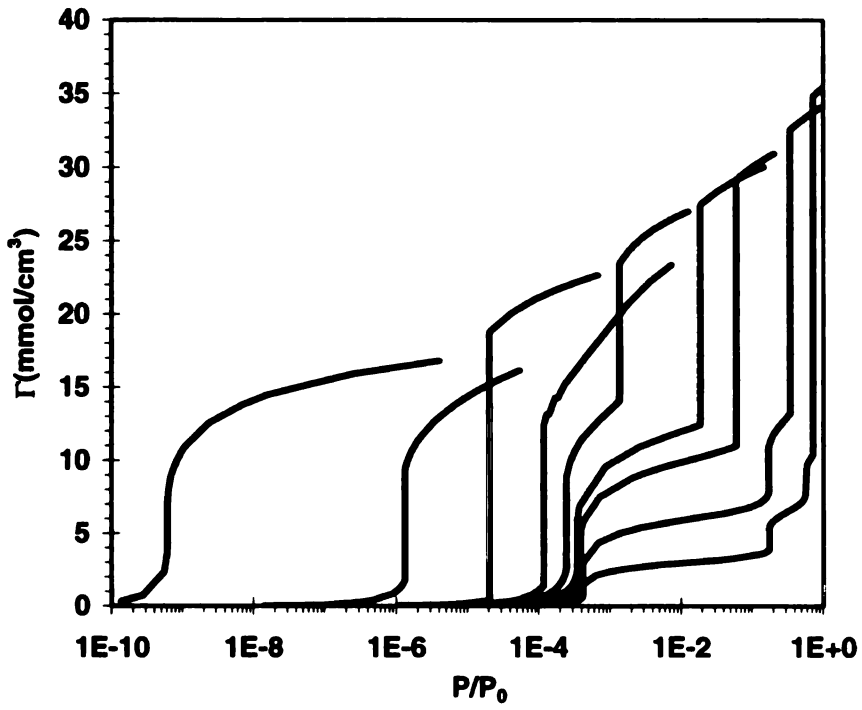

Figure 2.4: Argon specific excess adsorption in model graphitic slit pores at 77 K, calculated from DFT. Isotherms are shown for slits having a physical pore width *H* (reading from left to right) of 6.8, 8.4, 10.5, 11.8, 13.5, 16.9, 20.2, 33.8, and 67.5 Å.

I (mmol/cm³)

Figu

calc

freq

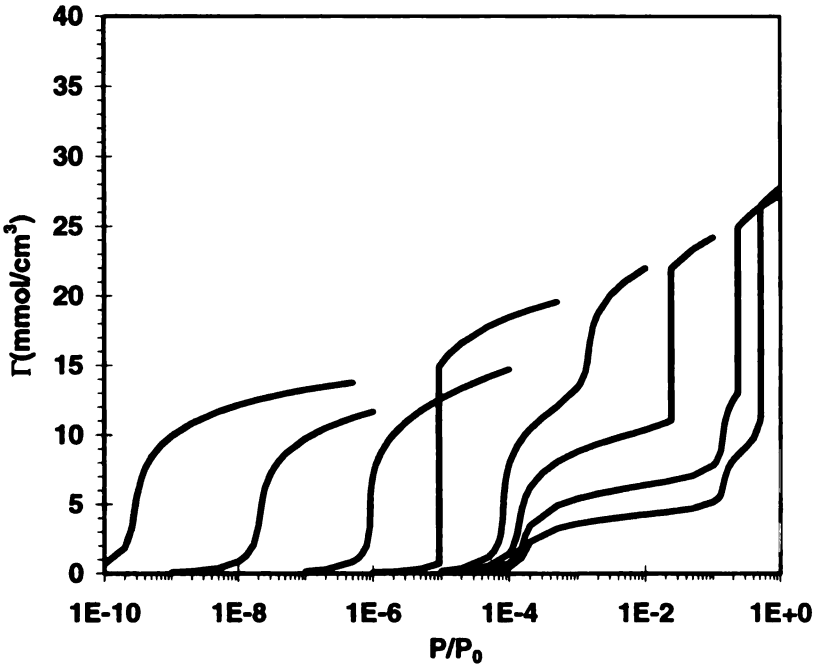

Figure 2.5: Nitrogen specific excess adsorption in model graphitic slit pores at 77 K, calculated from DFT[5]. Isotherms are shown for slits having a physical pore width *H* (reading from left to right) of 7.1, 8.0, 8.9, 10.7, 13.4, 17.9, 28.6, and 42.9 Å.

whereas for the argon model, a phase transition is predicted in these pores. In the pores larger than 14 Å, the nitrogen model predicts continuous pore filling during growth of the adsorbed film, followed by a single phase transition at the capillary condensation pressure. The argon DFT isotherms, in contrast, exhibit multiple phase transitions at the monolayer and multilayer filling pressures, in addition to the capillary condensation pressure. The more step like structure of the argon DFT isotherms is not unexpected, since these isotherms are calculated at a lower reduced temperature T/T_c than the nitrogen isotherms. (The critical temperature T_c of argon, obtained from mean-field theory using equations (2.11) and (2.12), is 164.7 K; for nitrogen, it is 140.5 K. Both of these values, it should be noted, are approximately 14 K higher than the actual critical temperatures of the gases, since mean-field theory does not correctly predict the curvature of the liquid-vapor coexistence curve near the critical point.)

The pore filling pressures are shown as a function of slit pore width in Figure 2.6 for argon and nitrogen adsorption at 77 K. It can be seen that for a given pore width, argon and nitrogen condense at nearly the same pressure. The adsorbed argon density, however, is greater than the adsorbed nitrogen density when complete pore filling has occurred. (This can be seen by comparing Figures 2.4 and 2.5.) A higher adsorbed-fluid density is achieved for argon because it has a smaller molecular diameter than nitrogen, and it is adsorbed at a lower reduced temperature than nitrogen.

2.6. PSD Analysis of Porous Carbons

Experimental argon and nitrogen adsorption isotherms at 77 K are reported in Figures 2.7-2.10 for four porous carbons. The total excess adsorption of argon exceeds

Filling Pressure P_o/P_o

1E

1E

1E

1E

1E

Figure

nitrogen

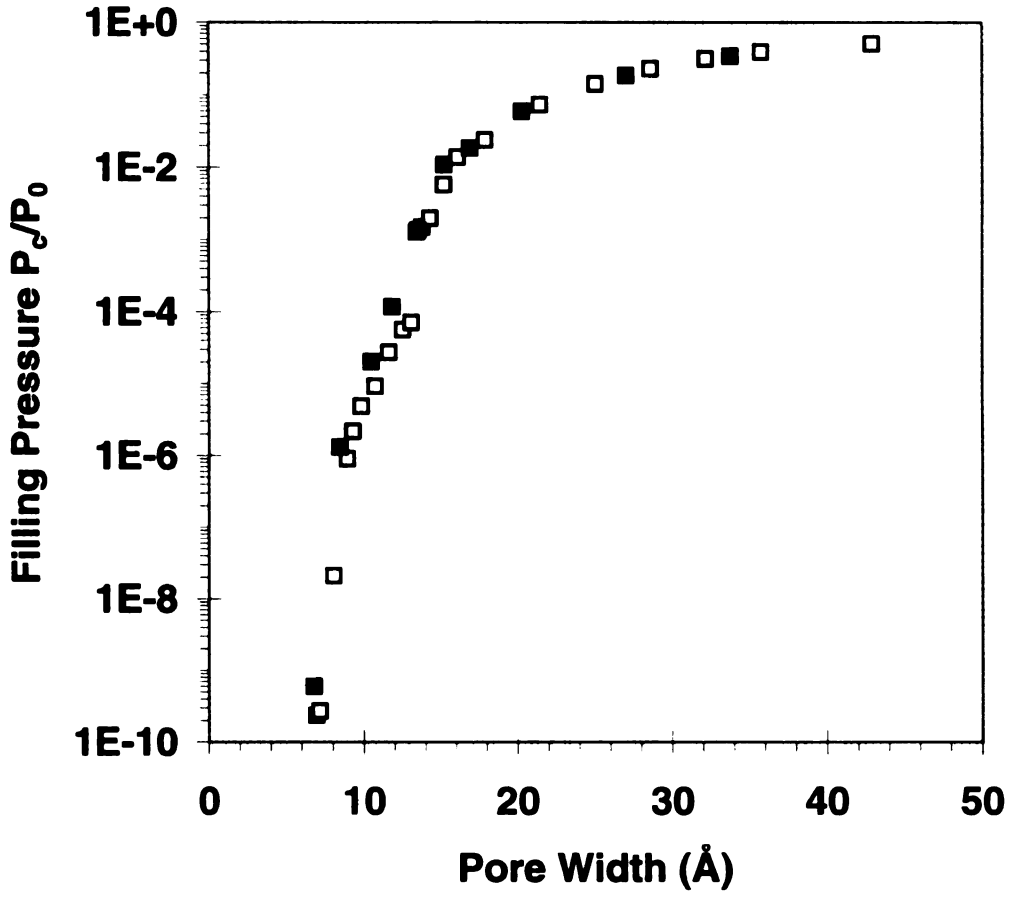

Figure 2.6: Pore filling correlation to slit pore width for DFT models of argon and nitrogen adsorption at 77 K. Filled squares: argon; open squares: nitrogen.

Figure 2.7:

open square

argon and

isotherm of

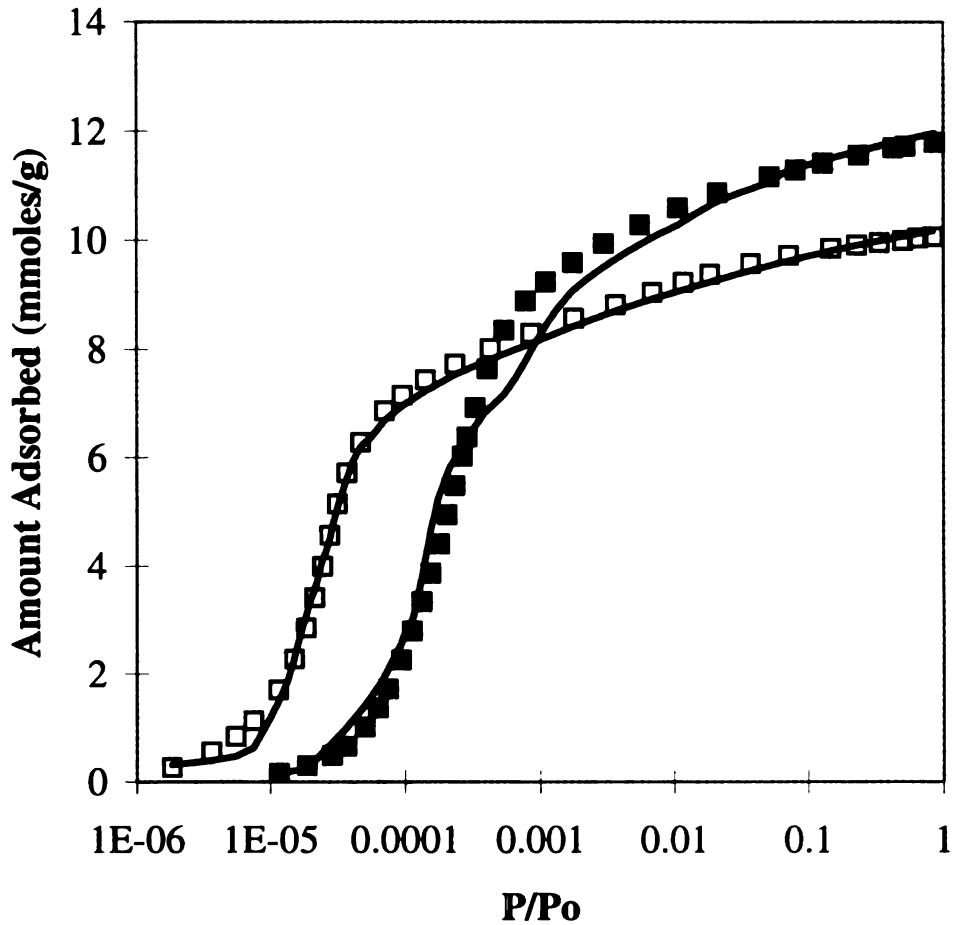

Figure 2.7: Adsorption isotherms on Saran char at 77 K. Filled squares: argon uptake; open squares: nitrogen uptake. The lines show the respective DFT isotherms obtained for argon and nitrogen using the PSD that best fits the DFT model to the experimental isotherm of each probe gas. The PSDs for argon and nitrogen are fitted separately.

Amount Adsorbed (mmole/g)

Figure 2

same as

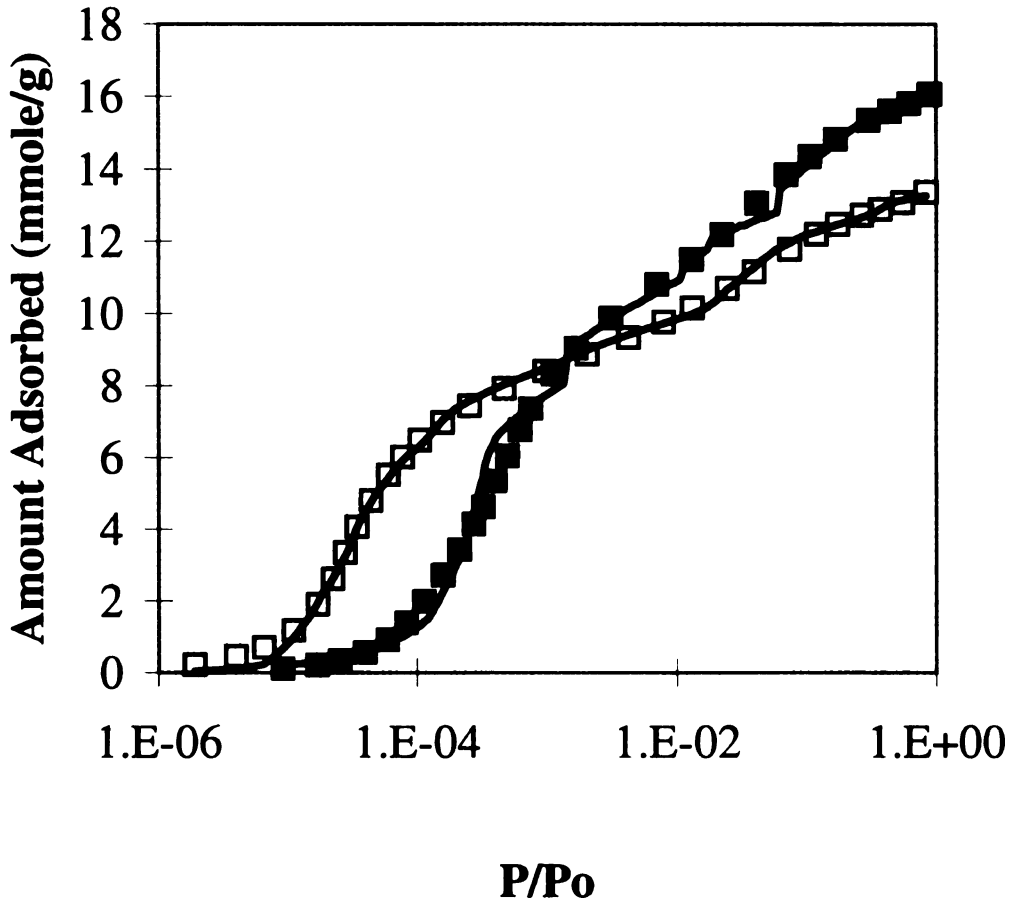

Figure 2.8: Argon and nitrogen isotherms on coconut char at 77 K. The notation is the same as in Figure 7.

Figure 2.9

notation is

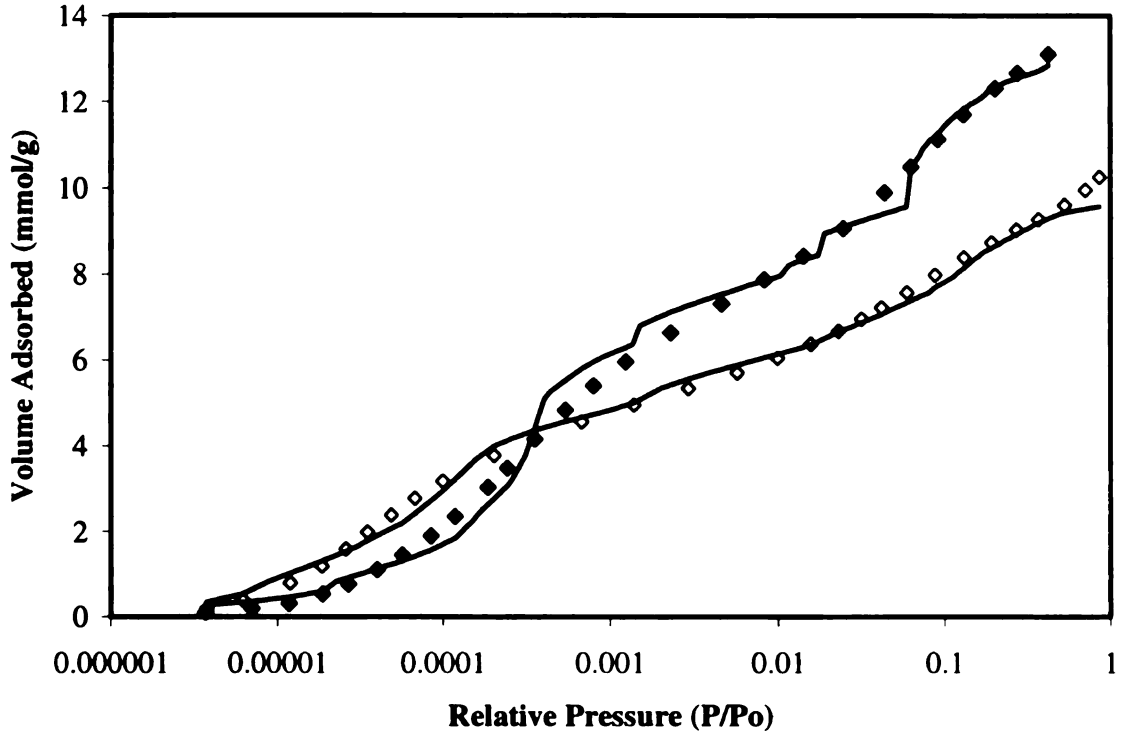

Figure 2.9: Argon and nitrogen isotherms on granular activated carbon at 77 K. The notation is the same as in Figure 7.

Figure 2.1

notation is

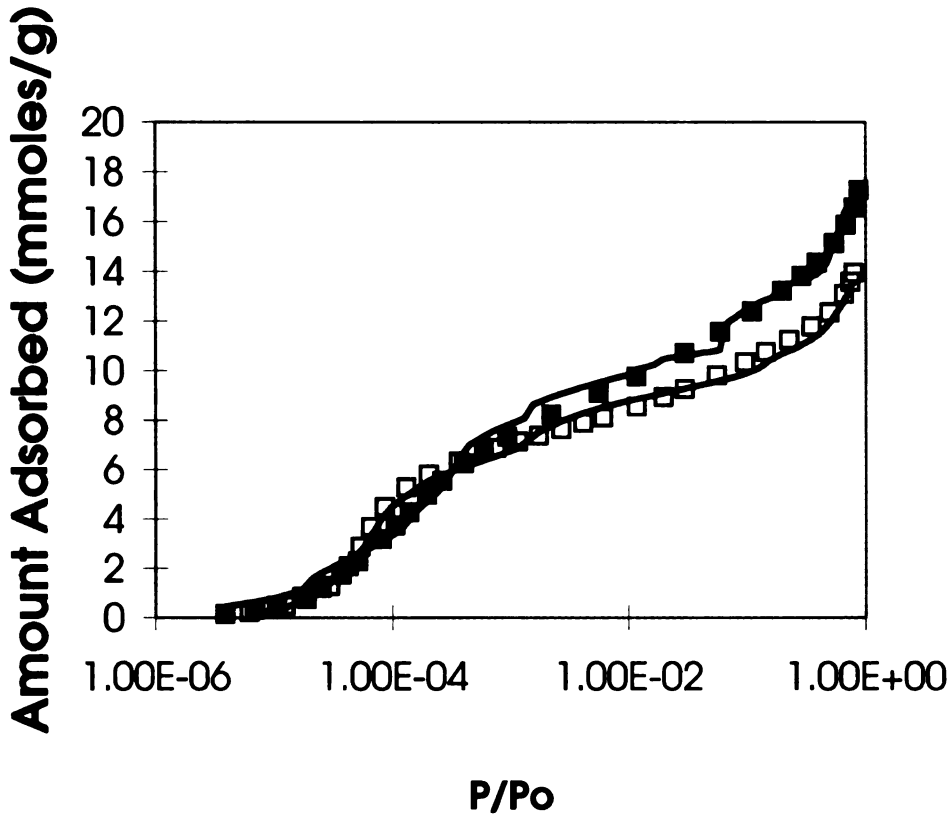

Figure 2.10: Argon and nitrogen isotherms on powdered activated carbon at 77 K. The notation is the same as in Figure 7.

that of nitrogen in all four cases; this is consistent with the predictions of the DFT models shown in Figures 2.4 and 2.5.

The adsorption isotherm of each carbon is fitted using the appropriate DFT pore filling model in equation (1.1), to obtain the PSD of the adsorbent. For convenience, we have elected to fit the PSD of each carbon to a trimodal gamma distribution ($m = 3$)

$$f(H) = \sum_{i=1}^{m} \frac{\alpha_i (\gamma_i H)^{\beta_i}}{\Gamma(\beta_i) H} \exp(-\gamma_i H) \tag{2.13}$$

which has nine adjustable parameters: the amplitude α_i, mean β_i, and variance γ_i of each mode i of the distribution. In equation (14), Γ refers to the gamma function. It is important to note that this choice of a fitting function is completely arbitrary, and that there is no physical basis for assuming that the PSD of an adsorbent is uniquely described by the gamma distribution, or any other sum of mathematical distributions. There is in fact no need whatsoever to use a distribution function to fit the PSD; an equally valid approach is to subdivide the PSD into several dozen or more pore width increments, and assign an independently adjustable amplitude coefficent α_j to each pore width increment j. The only mathematical constraint on the PSD function is that it must be nonnegative for all pore widths H. If the PSD function contains too few adjustable parameters (e.g. a unimodal distribution), the choice of the fitting function may unduly constrain the PSD results. It has been our experience, however, that a trimodal distribution provides ample flexibility for determining the PSDs of activated carbons. We have previously demonstrated, for example, that the nitrogen adsorption isotherm of a porous carbon can be fit very accurately with the DFT model using either a trimodal gamma distribution or a

Figure

porosim

per gra

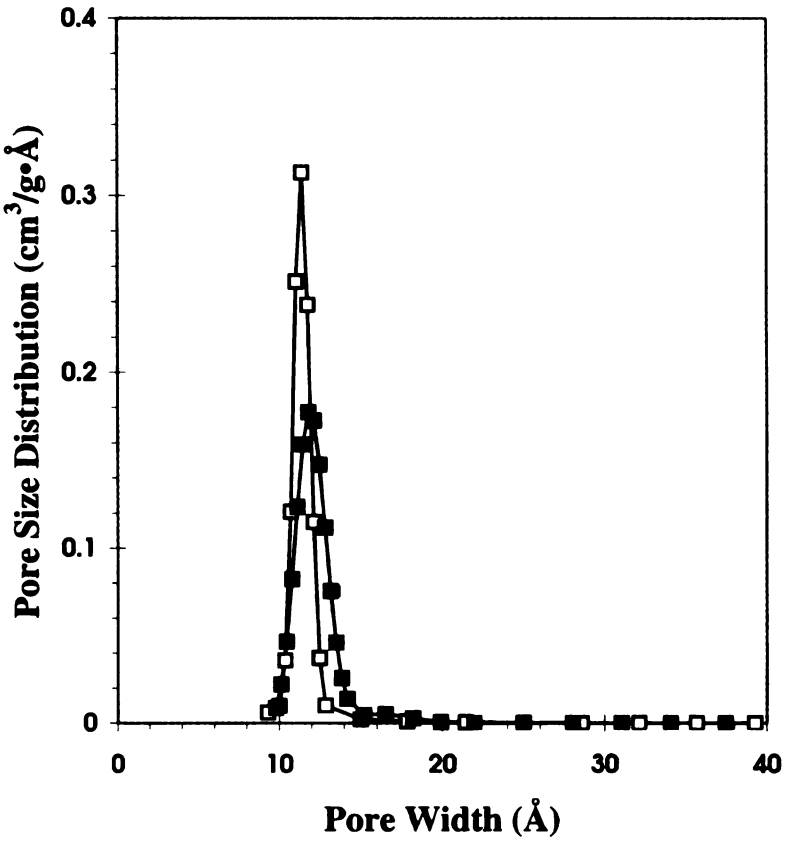

Figure 2.11: PSDs obtained from argon (filled squares) and nitrogen (open squares) porosimetry for Saran char using DFT method. The PSD is reported as cm^3 pore volume per gram of adsorbent per Å of pore width interval.

Figure 2.12

DFT metho

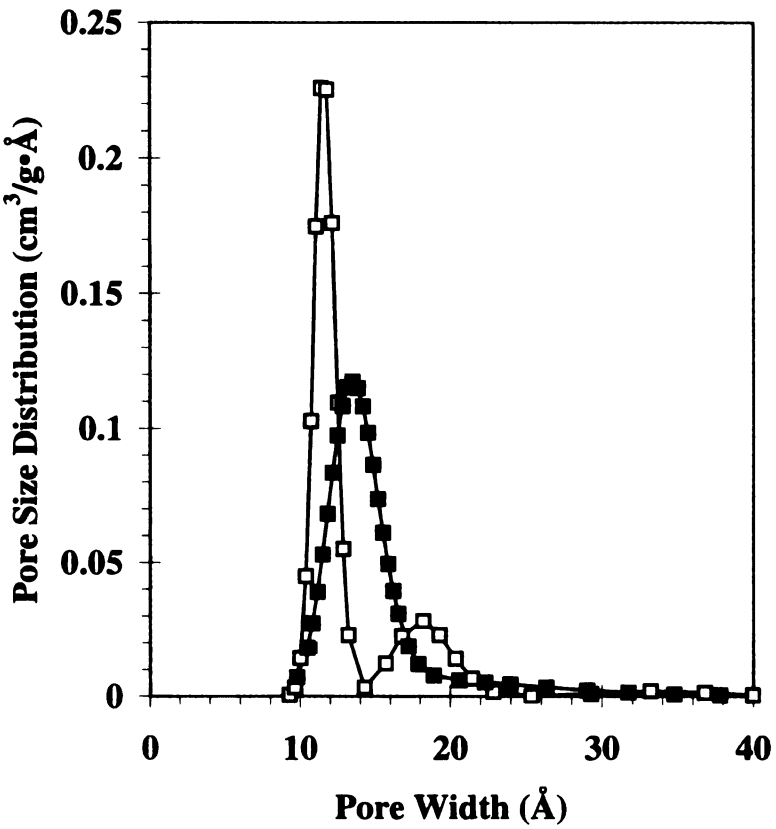

Figure 2.12: PSDs obtained from argon and nitrogen porosimetry for coconut char using DFT method. The notation is the same is in Figure 11.

Figure 2

carbon

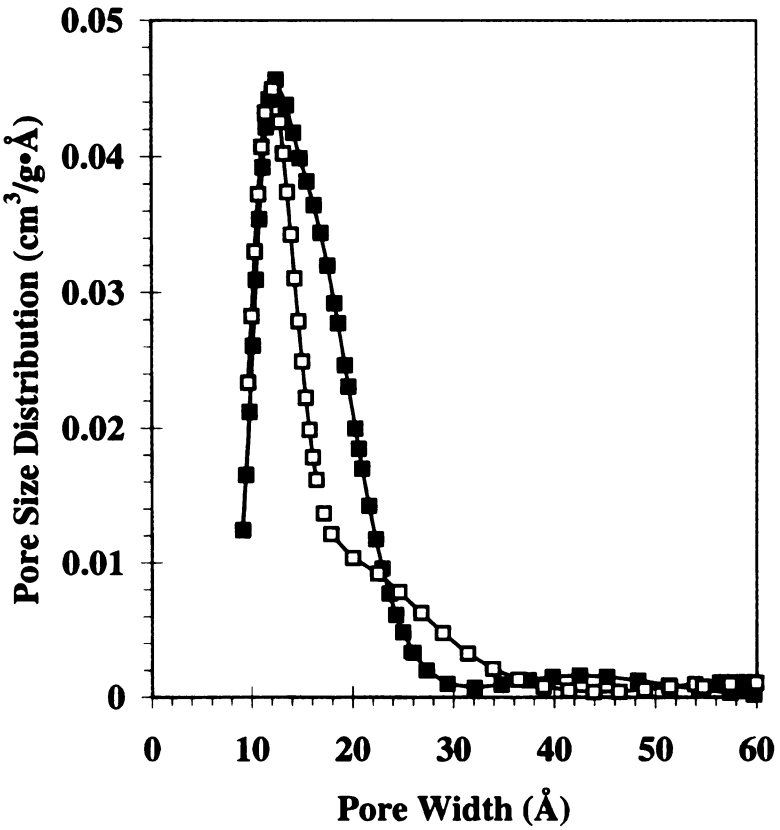

Figure 2.13: PSDs obtained from argon and nitrogen porosimetry for granular activated carbon using DFT method. The notation is the same is in Figure 11.

Figure 2

carbon u

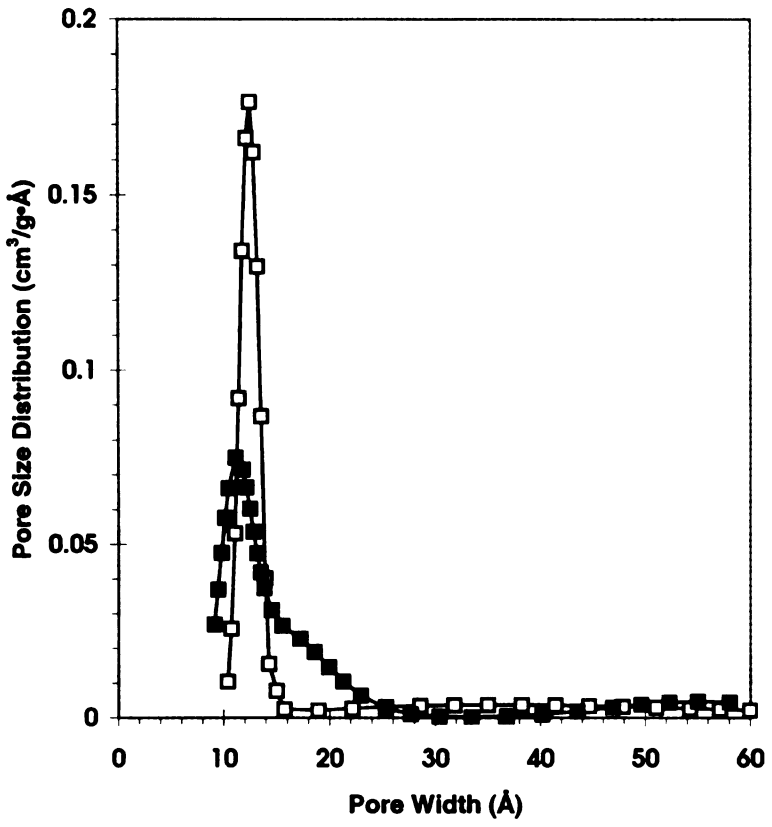

Figure 2.14: PSDs obtained from argon and nitrogen porosimetry for powdered activated carbon using DFT method. The notation is the same is in Figure 11.

trimodal lognormal distribution to represent $f(H)$ [4]. The PSDs obtained using these two distributions are essentially indistinguishable from one another, underscoring that it is the *numerical values* of the PSD itself that are unique, not the function that is arbitrarily chosen to represent the PSD.

The adsorption integral, equation (1.1), is evaluated for each probe gas/adsorbent pair using numerical integration. A least-squares error minimization criterion is used to determine the best-fit PSD parameters for each carbon. The best-fit model isotherm for each experimental isotherm is shown as a solid line in Figures 2.7-2.10. A comparison of the PSDs that yield the best-fit argon and nitrogen DFT isotherms is shown for each porous carbon in Figures 2.11-2.14. We note that a good fit of the DFT model to the experimental data is obtained for all eight measured isotherms. The cases where there are observable differences between the DFT model and the experimental isotherm can be attributed to the model isotherm being more structured than the measured isotherm. This is due to the assumption of physical and chemical homogeneity in the graphitic slit pore model, and to the effects of heterogeneity in smoothing the structure of the experimental isotherms. The differences between the DFT and experimental results are slightly more pronounced for the set of argon isotherms, because of the phase transitions predicted by DFT for this adsorbate at 77 K, as noted earlier. Overall, however, an acceptable fit of each experimental isotherm is obtained using a trimodal gamma distribution for the PSD.

The PSD for each adsorbate/adsorbent pair (Figures 2.11-2.14) is truncated at a lower bound corresponding to the width of the slit pore that condenses at the lowest pressure measured in the experimental isotherm. This lower pore size bound is determined from interpolation of the DFT pore filling correlations shown in Figure 2.6. Our justification

for truncating the PSD is that all the pores that are narrower than the lower bound pore width are already filled with condensate at the start of the experimental isotherm measurement. Consequently, no phase transition will be observed in these pores over the course of the experiment, and no information regarding the PSD of these micropores may reliably be obtained. (A slight increase in the condensate density does occur in pores of all size as the pressure increases, due to compression of the adsorbed fluid; however, this compression effect alone is insufficient to unambiguously determine the PSD of micropores smaller than the lower bound pore width.

All four porous carbons have a large micropore volume, as can be seen from the PSD peak exhibited by each adsorbent in the 11 to 13 Å range. Some mesopore volume also appears to be present in the granular and powdered activated carbons, as evidenced by the broad secondary peak in the PSDs of these samples in the 40 to 60 Å range. In each of the four samples, the PSD interpreted from the argon porosimetry data has a somewhat broader distribution of pore sizes than the PSD obtained from the nitrogen data. A comparison of the pore volume and the maximum in the PSD of each adsorbent is presented in Table 2.2. The percentage difference in the values of the PSD maxima for argon and nitrogen, calculated as

$$100\% \times (\text{absolute difference in Ar and } N_2 \text{ PSD maxima})/(\text{Ar PSD maximum})$$

ranges between 3 and 16%, with an average differential of 8.7% for the four samples tested. A larger difference was found in the pore volumes calculated from the argon and nitrogen PSDs, than for maxima in the PSD. The pore volumes reported in Table 2.2 are obtained by integrating the PSD over all pore widths. The pore volume predicted from argon porosimetry consistently exceeds the value derived from nitrogen porosimetry; the

ifferential. ag

with an averag

Table 2.2: PSD

DFT interpret

Carb
Saran cha
coconut c
granular
powdere

27. Discu

Wi

of a porou

PSD max

DFT cons

probe ga

to error r

Isotherm

soundne

to obtain

differential, again computed relative to the argon results, ranges between 16 and 31%, with an average difference of 25%.

Table 2.2: PSD maxima and pore volumes of the four carbon samples as determined from DFT interpretation of argon and nitrogen porosimetry data.

Carbon	Adsorbate	PSD Maximum (Å)	Pore Volume (cm^3/g)
Saran char	Ar	11.8	6.54
	N_2	11.4	4.99
	% difference	*3.4*	*23.7*
coconut char	Ar	13.5	5.77
	N_2	11.4	4.85
	% difference	*15.6*	*15.9*
granular AC	Ar	12.5	4.66
	N_2	12.9	3.20
	% difference	*3.2*	*31.3*
powdered AC	Ar	11.1	9.15
	N_2	12.5	6.28
	% difference	*12.6*	*31.4*

2.7. Discussion of Argon and Nitrogen Porosimetry Methods

With regard to fluid separation applications, the most important physical property of a porous carbon is the maximum in its PSD. The average differential of 8.7% in the PSD maxima calculated from the argon and nitrogen porosimetry measurements using DFT constitutes may be regarded as reasonably good agreement between the two separate probe gas analyses. This is particularly so given that the calculation of the PSD is subject to error resulting from any of three separate inputs: (1) the precision of the experimental isotherm measurement; (2) the accuracy of the DFT pore filling model; and (3) the soundness of the numerical method used to invert the Fredholm integral of equation (1.1) to obtain the PSD. Of these three contributing factors, the second is most likely to be

sponsible for t

rogen adsorp

the solution

gard to the s

size, surfac

pproximatio

is to be ev

and nitroge

the assump

adsorbent.

between t

highly-or

adsorbent

DFT to in

type adso

cylindrical

On

from nitrog

There is re

factors: the

and steric

volume of t

responsible for the observed differences in the PSDs computed from the argon and nitrogen adsorption measurements. The construction of the DFT isotherms $\Gamma(P,H)$ used in the solution of $f(H)$ in equation (1.1) requires that we invoke major simplifications in regard to the structure of the model carbon adsorbent. The assumptions of a slit pore shape, surface homogeneity, neglect of connectivity, and so forth are at best a crude approximation of the actual structures of the porous carbons studied in this work. Hence, it is to be expected that some inconsistencies will arise in the PSDs calculated from argon and nitrogen porosimetry as a result of the DFT model assumptions (or, for that matter, the assumptions made in any other pore filling model). In the case of a more ordered adsorbent, such as a mesoporous molecular sieve, we might anticipate better agreement between the argon- and nitrogen-derived PSDs, since our pore model construct for a highly-ordered porous material will more closely match the actual pore structure of the adsorbent. For example, excellent agreement was found in PSD results obtained by using DFT to interpret argon and nitrogen adsorption isotherms at 77 K and 87 K on MCM-41 type adsorbents, a class of mesoporous molecular sieves that have one-dimensional, cylindrical oxide channels with pore diameters between 32 and 45 Å [21].

One might then ask the question: which of the PSDs obtained, from argon and from nitrogen porosimetry, is the more reliable representation of the actual carbon PSD? There is reason to favor the PSD interpreted from argon porosimetry, on the basis of two factors: the interaction of the nitrogen quadrupole with carbon surface functional groups, and steric exclusion of the larger nitrogen molecule from portions of the internal pore volume of the adsorbent. As we shall now discuss, these two effects collectively provide

a plausible explanation of the differences in the PSDs and pore volumes obtained from the argon and nitrogen isotherm measurements.

A comparison of Figures 2.4 and 2.5 indicates that the argon and nitrogen DFT models both predict that an adsorbed monolayer will form at $P/P_0 \cong 10^{-4}$ in pores larger than 13 Å. In the experimental isotherms of the activated carbons (Figures 2.9 and 2.10), the monolayer filling pressures for argon and nitrogen were indeed observed to be the same. In the case of the char samples (Figures 2.7 and 2.8), however, the nitrogen monolayer formed at a pressure nearly a full order-of-magnitude lower than the argon monolayer. We speculate that the lower nitrogen monolayer filling pressure is the result of quadrupolar interactions of the nitrogen adsorbate with functional groups on the surface of the chars. Argon, which has no permanent multipole, is largely unaffected by the presence of these functional groups, whereas nitrogen adsorbs at a lower pressure on the chemically heterogeneous carbon surface on account of its quadrupole. Unlike the granular and powdered activated carbons, the Saran and coconut chars were not subjected to activation during their synthesis. We therefore hypothesize that activation of the thermolyzed carbon source material eliminates functional groups from the adsorbent surface. This would explain the consistency in the monolayer filling pressures for argon and nitrogen on the activated carbon samples.

The quadrupole moment of nitrogen has been invoked to explain differences in the site energy distributions of controlled pore glasses calculated from argon and nitrogen adsorption at 77 K [24], and the PSDs of microporous carbons determined from supercritical methane adsorption and subcritical nitrogen adsorption [25]. Electrostatic interactions are not explicitly accounted for in the DFT pore filling model presented in

this work, which assumes that the adsorbate molecules are spherically symmetric and interact only via van der Waals (i.e. dispersion/repulsion) forces. If the neglected quadrupolar interactions are substantial, then DFT analysis of the nitrogen isotherm will yield PSD estimates that are skewed toward pore widths that are too small. This might explain some of the observed differences in the PSDs obtained for the chars. It is therefore our recommendation that argon porosimetry be used to interpret the PSDs of porous carbons if there is reason to believe that the adsorbent is chemically heterogeneous. While this procedure will not eliminate the effects of other heterogeneities (e.g. surface defect sites, pore junctions) that may be present, and that equally impact argon and nitrogen adsorption, it will at a minimum avoid the potentially confounding effects of the nitrogen quadrupole on the analysis of the PSD.

For all of the carbon samples, the total pore volume, per unit mass of adsorbent, calculated from argon porosimetry is substantially larger than the pore volume obtained from nitrogen porosimetry (Table 2.2). One possible explanation, that would reconcile the average pore volume differential of 25%, is that the internal pore volume of each adsorbent is partitioned into an array of void spaces, connected to one another by way of narrow pore linkages or bottlenecks. The nitrogen molecular diameter is approximately 0.2 Å larger than the argon diameter (Table 2.1). Therefore, if some of the bottlenecks have a pore width smaller than the nitrogen diameter, but larger than the argon diameter, nitrogen diffusion will be kinetically limited, or perhaps excluded altogether, in these linkages, whereas argon may be able to diffuse unhindered through the bottlenecks. If this were the case, nitrogen as an adsorbate would be unable to probe the void volume accessible only through the narrow pore linkages, whereas the argon adsorbate would

penetrate a greater extent of the internal pore volume of the adsorbent. (The additional volume sampled by argon may also account for some of the observed differences in the argon and nitrogen PSDs.)

It is conceivable that polar surface functional groups, spanning the edge planes of adjacent graphitic microcrystals, might act as pore bottlenecks in the microstructures of the porous carbons. If this were so, then the aforementioned quadrupolar interactions of the nitrogen molecules with the polar functional groups would "corral" the nitrogen adsorbate at these sites of heterogeneity and inhibit further penetration of nitrogen into the carbon internal pore volume. The concept of adsorbate size exclusion in micropores has been recently proposed as a means of probing the connectivity of a porous adsorbent, by using percolation theory to interpret the adsorption isotherms of different-sized adsorbate molecules [26]. In the DFT pore filling model, the connectivity of the pore volume is altogether neglected, and is substituted with a conceptual model of isolated slit pores of infinite aspect ratio. If there is evidence that the network of voids in the adsorbent contains many narrow pore junctions, a more accurate sampling of the internal pore volume will probably be obtained using the smaller argon, rather than nitrogen, molecule as the probe gas.

It has been noted that the Lennard-Jones parameters for the argon-argon pair interaction potential can be fit to physical properties of either solid argon or supercooled liquid argon at 77 K. The argon DFT isotherms and PSD results reported in this work were obtained using the supercooled liquid argon properties to fit the model parameters. The saturation pressure measured in the argon adsorption experiments, on the other hand, indicates that solid argon condenses in the porous carbons. In order to assess the possible

errors caused by the mismatch of the condensed argon phase in the theory and experiments, the potential parameters for the argon-argon and argon-carbon interactions were recalculated using the solid argon physical properties, following the same procedure outlined in Section 2.4. The best-fit Lennard-Jones parameters using the solid argon properties as the basis for fitting are summarized in Table 2.2, and a comparison of the DFT model isotherms, fitted to the Sterling reference isotherm, is shown in Figure 2.3 for the two different sets of argon potential parameters. It is found that using the solid argon physical properties increases the argon-argon potential well-depth by 3% and decreases the argon molecular diameter by the same amount. Using the arithmetic mean for the argon-carbon effective diameter, and a recalculated specific surface area of 10.1 m^2/g from the thickness curve plot, it is found that the Sterling isotherm is best fit with an argon-carbon well depth that is 6% larger than the well depth fitted from the supercooled liquid data. As can be seen from inspection of Figure 2.3, however, either set of potential parameters will yield a set of DFT isotherms that reproduces the experimental monolayer filling pressure of $\sim 10^{-4} P_0$. The only observable difference in the fitted isotherms is in the adsorbed phase density. Thus, the two sets of model parameters will yield different predictions of pore volume, but the location of the PSD maxima (as determined from the pore filling pressure correlation) will be nearly the same for the two argon models. Based upon the rather small value of σ_{ff} obtained by fitting the parameters to the solid data, and other considerations discussed in Section 2.4, it is our recommendation that the supercooled liquid properties be used to model argon adsorption at 77 K. An alternative, to avoid uncertainty in the parameter fitting, is to conduct the argon experiments and

modeling at the normal liquid argon boiling point of 87 K, using liquid argon instead of liquid nitrogen as the temperature bath.

Finally, it should be noted that the PSD results reported in Figures 2.11-2.14 are obtained without the use of regularization methods. Regularization refers to a numerical technique whereby additional constraints are specified in order to convert a mathematically ill-posed problem – the solution of the PSD function $f(H)$ in equation (1) – into a well-posed problem [27]. The effect of regularization is to "smooth" the PSD by suppressing perturbations caused by experimental error in the isotherm data [28]. Given that we have not used any regularization in solving the adsorption integral equation for the best-fit PSD, the general agreement between the argon and nitrogen results for the PSD maxima is quite good. If regularization were to be utilized, we would expect to find even closer agreement between the argon- and nitrogen-derived PSDs. For example, a large value of the regularization "smoothing" parameter would convert the bimodal PSD fits obtained for some of the carbons into unimodal PSDs. The relatively good agreement between the argon and nitrogen porosimetry results, even in the absence of regularization, may be taken as evidence of the fundamental soundness of the DFT pore filling model.

2.8. Conclusion

In this work, we have shown that a DFT model of argon adsorption at 77 K in slit-shaped carbon pores yields PSD results from argon porosimetry that are comparable those obtained by interpreting nitrogen adsorption at 77 K using a similar DFT model. The maximum in the PSD of an adsorbent can be bracketed to within nine percent, on average, by comparing the PSDs determined from the two separate probe gas

meas

volu

incr

diver

inter

func

in co

the a

measurements. Larger differences are observed in the calculation of the internal pore volume of the adsorbent using argon and nitrogen porosimetry. The DFT model does not incorporate pore connectivity effects or nitrogen quadrupolar interactions. Thus, divergent PSD results can be expected if the argon and nitrogen DFT models are used to interpret the isotherms of porous carbons with narrow bottleneck pores or polar surface functional groups. In such instances, it is recommended that argon porosimetry be used in conjunction with the argon DFT model to determine the PSD and the pore volume of the adsorbent.

2.10 References

1. Yang, R.T. *Gas Separation by Adsorption Processes*; Butterworths: Boston, 1985.
2. Bonsal, R.; Donnet, J.; Stoeckli, F. *Active Carbon*; Marcel Dekker: New York, 1988.
3. Gregg, S.J.; Sing, K.S.W. *Adsorption, Surface Area and Porosity*; Academic Press: New York, 1982.
4. Lastoskie, C.; Gubbins, K.E.; Quirke, N. *J. Phys. Chem.* **1993**, *97*, 4786.
5. Lastoskie, C.; Gubbins, K.E.; Quirke, N. *Langmuir* **1993**, *9*, 2693.
6. Barrett, E.P.; Joyner, L.G.; Hallenda, P.P. *J. Am. Chem. Soc.* **1951**, *73*, 373.
7. Horvath, G.; Kawazoe, K. *J. Chem. Eng. Japan* **1983**, *16*, 474.
8. Lastoskie, C.; Quirke, N.; Gubbins, K.E. In *Equilibria and Dynamics of Gas Adsorption on Heterogeneous Solid Surfaces*; Rudzinski, W.; Steele, W.A.; Zgrablich, G., Eds.; Elsevier: Amsterdam, 1997; Vol. 104, p. 745.
9. Ravikovitch, P.I.; Haller, G.L.; Neimark, A.V. *Adv. Coll. Int. Sci.* **1998**, *76*, 203.
10. Ravikovitch, P.I.; Haller, G.L.; Neimark, A.V. In *Mesoporous Molecular Sieves*; Rudzinski, Bonneviot, L.; Beland, F.; Danumah, C.; Giasson, S.; Kaliaguine, S., Eds.; Elsevier: Amsterdam, 1998; Vol. 117, p. 77.
11. Olivier, J.P. *Carbon* **1998**, *36*, 1469.
12. Steele, W.A. *Surf. Sci.* **1973**, *36*, 317.
13. Weeks, J.D.; Chandler, D.; Andersen, H.C. *J. Chem. Phys.* **1971**, *54*, 5237.
14. Israelachvili, J.N. *Intermolecular and Surface Forces*; Academic Press: London, 1992.
15. Evans, R. In *Inhomogeneous Fluids*; Henderson, D., Ed.; Marcel Dekker: New York, 1992; Chapter 5.

16. Tarazona, P. *Phys. Rev. A* **1985**, *31*, 2672; ibid, **1985**, *32*, 3148. Tarazona, P.; Marini Bettolo Marconi, U.; Evans, R. *Mol. Phys.* **1987**, *60*, 5743.

17. Carnahan, N.F.; Starling, K.E. *J. Chem. Phys.* **1969**, *51*, 635.

18. Barker, J.A.; Henderson, D. *J. Chem. Phys.* **1967**, *47*, 4714.

19. Neimark, A.V.; Ravikovitch, P.I. *Langmuir* **1997**, *13*, 5148.

20. *CRC Handbook of Chemistry and Physics*, 61st ed.; Weast, R., Ed.; CRC Press: West Palm Beach, FL, 1981.

21. Neimark, A.V.; Ravikovitch, P.I.; Grun, M.; Schuth, F.; Unger, K.K. *J. Coll. Int. Sci.* **1998**, *207*, 159.

22. de Boer, J.H.; Linsen, B.G.; Osinga, T.J. *J. Catal.* **1965**, *4*, 643.

23. Olivier, J.P. In *Proceedings of the Fifth International Conference on Fundamentals of Adsorption*; LeVan, M.D., Ed.; Kluwer Academic Publishers: Boston, 1996; p. 699.

24. Olivier, J.P. In *Proceedings of the Sixth International Conference on Fundamentals of Adsorption*; Elsevier: Amsterdam, 1998; p. 207.

25. Quirke, N.; Tennison, S.R.R. *Carbon* **1996**, *34*, 1281.

26. Lopez-Ramon, M.V.; Jagiello, J.; Bandosz, T.J.; Seaton, N.A. *Langmuir* **1997**, *13*, 4435.

27. V. Szombathely, M.; Brauer, P.; Jaroniec, M. *J. Comp. Chem.* **1992**, *13*, 17.

28. Davies, G.M.; Seaton, N.A. *Carbon* **1998**, *36*, 1473.

Chapter 3.

Carbon Nanotubes as an Alternate Reference Adsorbent

3.1. Introduction

Carbon nanotubes were first discovered by Iijima[1] in 1991, and have been found to have excellent physical and electrical properties. Nanotubes are fullerene molecules that have repeat hexagonal units that extend their length, essentially becoming sheets of graphite that are rolled upon themselves [2]. Nanotubes may be either single or multi-layered dependent upon the means used to produce them. The size of a typical nanotube diameter varies between 1 and 20 nm for multi-layered tubes [3], with lengths that are typically greater than 100 times the diameter or nearly infinite on a molecular scale[4]. The nanotube length can be dramatically shortened by sonication in acid to a length that is more desirable [5]. The mean tube diameter may also be tuned during the production process by altering the production conditions [4]. Consequently nanotubes can be modified to suit a particular application via altering their thickness resulting in stronger surface potentials, their diameters resulting in higher selectivity, and their lengths to maximize transport properties.

Carbon nanotubes have attracted much attention due to their electrical properties and their mechanical strength; these same attributes make them appealing lattice material [3] or size selective catalysts. Carbon nanotubes have potential applications as a means to separate mixtures of molecules based upon their relative size [6]. Another practical application is safer cheaper gas storage through adsorption [7,8]. In either application the diameter of the tube is the controlling factor in determining the relative affinity for the

adsorbates of different sizes [6]. Varying the diameter of the buckytube by even a nanometer can change the selectivity for one molecule by several orders of magnitude [6].

The determination of the size of a nanotube can be performed via several methods, each with benefits and associated problems. Transmission electron microscopy (TEM) can be used to generate cross sectional images of tubes, which can then be directly measured to find the tube diameter [4]. Although, the measurement of the tube image can give precise measurements for particular nanotube, this is a time consuming process when applied to many nanotubes and does not measure tube length. While the information gained from TEM may be exact for determining the PSD for tubes interior diameters it gives no indication of the exterior properties of the tubes. The exterior surface properties, such as the effect of the interstitial spaces between the tubes, are extractable using isotherms [9]. Although evidence has recently come to light that the interstitial channels within tube bundles do not adsorb gases [10] there is however a great deal of evidence of sorption to the exteriors of nanotubes [7,8,9]. The importance of the exterior properties are shown in their application, for storage purposes optimizing the interstitial spaces between tubes is just as imperative as optimizing the actual tube size [7,8] for gases.

The isotherm may yield data on the size heterogeneity through inversion of the adsorption integral for cylindrical pores which is equivalent to the slit pore Equation (1.1)

$$\Gamma(P) = \int_{R_{min}}^{R_{max}} \Gamma(P,R) F(R) dR \qquad (3.1)$$

Where R is the physical pore radius and the subscripts refer to the maximum and minimum values, P is the pressure, $\Gamma(P)$ is the excess adsorption, $\Gamma(P,R)$ is thermodynamic model isotherm, and $F(R)$ is the pore size distribution. The thermodynamic model must be based upon a model that matches the physical properties of the system, such as pore shape, potential function, and solid fluid interaction energies. In the case of a single walled nanotubes (SWNT) a model that represents the system is a cylinder of infinite length, with a single shell of carbon atoms. For a given thermodynamic model, $\rho(P,R)$, a PSD, $F(R)$, may be chosen that reproduces the excess adsorption isotherm $\Gamma(P)$ when combined in Equation (3.1). Although, the uniqueness of any particular solution may be questioned, applying the following rules minimizes the likelihood of obtaining multiple solutions:

i. There can be no negative pore volumes.

ii. The pore width must be large enough to avoid steric repulsion, usually two adsorbate molecular diameters.

iii. The filling pressures of the thermodynamic models must be within the pressure range measured experimentally.

Potential parameters are fitted based upon the adsorption integral found in equation (3.1). One typically measures an isotherm of a reference material under the same conditions as the unknown sample isotherm. Of the three variables in the adsorption equation two must be known to obtain an estimate of the third. The easiest of the variables to know is the experimental excess isotherm $\Gamma(P)$, followed by the PSD, $F(R)$. In this chapter the thermodynamic model $\Gamma(P,R)$ is chosen to be the density functional theory model, which is based upon the Lennard-Jones interaction potential.

Carbon nanotubes have regular structure, high surface area [9] and are chemically homogeneous, which makes them an excellent standard for determining reference isotherms. Additionally the length of a nanotube is typically over 100 nanometers, while the end effects of the tube determined by molecular simulation extend 2 nanometers into the tube [11]. The micropore size distribution of a SWNTs can be determined using TEM for a relatively small but representative sample. Once the PSD is known a solid-fluid energy well depth can be chosen to determine the thermodynamic models used in equation (3.1) that result in reproducing the initial filling pressure of the reference isotherm.

3.2. Thermodynamic Model

The density functional theory (DFT) is explained for the cylindrical geometry in several other sources, therefore a brief summary is offered [12,13,14,15]. The grand potential function Ω for a cylindrical pore is given by equation (3.2).

$$\Omega[\rho(\mathbf{r})] = F[\rho(\mathbf{r})] - \int d\mathbf{r}\rho(\mathbf{r})[\mu - V_{ext}(\mathbf{r})] \qquad (3.2)$$

Where F is the Helmholtz energy, μ is the chemical potential, and V_{ext} is the potential energy field between the fluid and the solid. The local density $\rho(r)$ is chosen to minimize the overall grand potential. The potential energy V_{ext} is a function of the pore radius and spatially varies with the distance from the centerline of the pore and represents an integrated form of the 12-6 Lennard-Jones potential [16,17].

$$\frac{V_{ext}(r,R)}{\kappa T} = \frac{1}{T}\varepsilon_{sf}\pi^2\sigma_{sf}^2\left[\begin{array}{l}\frac{63}{32}\left[\frac{r}{\sigma_{sf}}\left(2-\frac{r}{R}\right)\right]^{-10} F\left[-\frac{9}{2},-\frac{9}{2};1;\left(1-\frac{r}{R}\right)^2\right] \\ -3\left[\frac{r}{\sigma_{sf}}\left(2-\frac{r}{R}\right)\right]^{-4} F\left[-\frac{3}{2},-\frac{3}{2};1;\left(1-\frac{r}{R}\right)^2\right]\end{array}\right] \qquad (3.3)$$

Where $F[\alpha,\beta;\gamma;\chi]$ is the hypergeometric series, ε_{sf} is an energetic parameter, σ_{sf} is the solid fluid intermolecular diameter, r is the distance from the pore centerline, R is the tube radius, κ is the Boltzman constant, and T is the temperature. The values of ε_{sf} and σ_{sf} are determined by the methods found in section 3.3. It is important to note that the potential function is solely for the interior of the pore, and approaches the limit of a 10-4 potential of a flat slab as the radius R approaches infinity. The potential of an isolated nanotube exterior is less than that of an infinite plane [18], however the difference in the potential minimum is small. The occurrence of an isolated nanotube is doubtful, as the tubes are known to grow in bundles. The exterior environment of a nanotube, or the interstitial space between tubes can be modeled as a nanotube with a larger radius to match the appropriate potential. For the limits of this calculation a flat plane is used to model the potential of a very large tube.

The DFT method for a cylindrical pore is very similar to the method described in Section 2.2, with the exception that the externally varying potential function is that outlined by Equation 3.3. The Helmholtz free energy F is a function of the smoothed local density $\overline{\rho}(\mathbf{r})$. The smoothed local density is weighted based upon the Tarazona method, although it is modified to match the cylindrical geometry[19]. The method that Tarazona [19] describes uses a power series expansion, of which the first three terms are used to give very good agreement for the density profiles of Lennard-Jones fluids near

attractive walls, which is given in Equation 2.8. The grand potential is minimized with respect to the local density profile, which may result in multiple minimums, representing a condensed and expanded phase. The phase change occurs when the grand potential is equal for both the liquid and vapor minimum. The stable or equilibrium minimum is the one that has the lowest grand potential.

3.3. Method for Fitting the Potential Parameters

3.3.1 Potential Function

The potential parameters used in this paper refer to the Lennard-Jones 12-6 parameters, which are related to the size and potential well depth associated with any two molecules or atoms. The Lennard-Jones potential function consists of an attractive term raised to the sixth power and a repulsive term raised to the twelfth power.

$$\phi_{ij} = 4\varepsilon_{ij}\left[\left(\frac{\sigma_{ij}}{d}\right)^{12} - \left(\frac{\sigma_{ij}}{d}\right)^{6}\right] \tag{3.4}$$

Where ε_{ij} is the potential well depth between i and j type atoms, σ_{ij} is the collision diameter of i and j type atoms, and d is the distance that separates atoms i and j. Although isolating two atoms and measuring their interactions is a very difficult task, the individual terms can be resolved from bulk data. The fluid-fluid Lennard-Jones parameters may be calculated from the saturation data of the adsorbate at the experimental temperature. Relating the liquid molar density ρ, the pressure P, and the temperature T to their corresponding non-dimensional units one can determine the values of σ and ε.

$$\frac{P}{\rho RT} = \left(\frac{P\sigma^3}{\varepsilon}\right)\left(\frac{\varepsilon}{kT}\right)\left(\frac{1}{\rho\sigma^3 N_{av}}\right) = \frac{P^*}{\rho^* T^*} \tag{3.5}$$

At the saturation there is a single degree of freedom, therefore specifying a particular temperature would constrain the remaining parameters for both the condensed and gas phases. The correct values of T*, P* and ρ^* and therefore ε and σ are found by equating the values for both phases at saturation. The carbon molecular diameter is well known to be 3.35 Å for a graphitic carbon [20]. The arithmetic mean is used to determine the interaction distance between the carbon molecule and the adsorbate. Matching the solid to fluid potential well depth is slightly more difficult. The adsorption integral in equation (3.1) is the key to this dilemma, one must use the reference isotherm $\Gamma(P)$ and the PSD $F(R)$ to ascertain the parameters which influence the thermodynamic model. The thermodynamic model may be chosen at the discretion of the user. However, for a given pore size and chemical composition Molecular Simulations MS and DFT are generally considered to be exact. There are however semi-empirical methods such as the Horvath-Kawazoe HK model, which produce results that are similar to the DFT with a reasonable tradeoff in accuracy [21,29]. The fore mentioned techniques all depend upon the potential interaction between the adsorbate and adsorbent. Other classical models such as the Kelvin equation, may also be used, however they do not accurately predict the results in pores that are smaller than 75 Å and are not dependent upon the adsorbate-adsorbent interaction, therefore will not be considered in this paper. Although the MS method is the most exact means to determine a thermodynamic model its results are rivaled by DFT, which requires 1% of the computational time. The HK model although recently shown to have surprising accuracy [21,29] has not been improved sufficiently for the

pores with a single filling step and cylindrical geometry. The DFT thermodynamic model will therefore be utilized to determine the Lennard-Jones interaction parameters between the solid and fluid. The DFT model as previously mentioned is based upon the Lennard-Jones parameters all of which are determined from the saturation data except the solid fluid potential well depth ε_{sf}.

3.3.2 Electric properties

Although, the most accurate data is obtained through fitting the Lennard-Jones parameters at the experimental conditions, they may also be determined via several schemes based upon the electric properties of the atoms. Due to the range of the forces it is easily shown that ion to ion and ion to dipole interactions account for the bulk of the electrostatic forces, followed by dipole interactions then greater multi-pole interactions. In the absence of ions the dipole-to-dipole interaction accounts for over 85% of the attractive force [22]. It is well known that dipoles maybe induced in an electric field, even a field generated by an adjacent dipole. It is easily shown that dipoles with their orientations weighted upon the energy, dipole to induced dipole, and induced dipole to induced dipole interactions all are dependant on the inverse r^6 dependence [22,23]. The value of the potential due to dipole attraction is determined in the following ways [22]:

$$U = \frac{-C_1}{r^6} + \frac{-C_2}{r^6} + \frac{-C_3}{r^6} \qquad 3.6$$

$$C_1 = \frac{2}{3kT}\left(\frac{\mu_i \mu_j}{4\pi\varepsilon_0}\right)^2$$

$$C_2 \approx \frac{\mu_i^2 \alpha_j'}{4\pi\varepsilon_0}$$

$$C_3 = \frac{3}{2}\alpha_i' \alpha_j' \left(\frac{I_i I_j}{I_i + I_j}\right)$$

where U represents the attractive potential, C_1 is the dipole to dipole interaction,C_2 is the dipole to induced dipole, and C_3 is the induced dipole to induced dipole interaction μ is the dipole moment, k is Boltzman's constant, ε_0 is the permittivity of free space, α is the polarizability volume, I is the ionization energy, and the subscripts i and j refer to atoms i and j. The natural radial dependence of a dipole can be shown to vary as the inverse of r^6. The radial dependence of quadrupoles varies with the inverse of r^8, and r^{10} for dipole and quadrupole interactions of freely rotating molecules based upon and energy weighted orientation. Therefore the methods that fit the Lennard-Jones parameters to the properties of the dipole neglect all other multipole interactions, and may yield potential well depths that are to shallow.

The Lennard-Jones potential may be integrated over the dimensions of a flat surface to yield the 10-4 potential, or over an infinite cylinder to yield Equation 3.3. Alternate theories exist to determine the potential well depth. The concept, first put forth in the Frenkel Hasley Hills FHH adsorption theory, is that the excess free energy change of adsorption is equal to the difference in the interaction energy of the adsorbate molecule with the slab of adsorbent, *less* the adsorbate interaction energy with a similar slab of pure adsorbate [24]. Horvath and Kawazoe used FHH theory to determine the potential ϕ between two infinite sheets of graphite separated by a distance H, as demonstrated in the following equation (corrected from its form shown in the reference [25]):

$$\phi(z)=\phi_{sf}(z)-\phi_{ff}(z)=\frac{N_s A_{sf}-N_f A_{ff}}{2\sigma^4}\left[\left(\frac{\sigma}{z}\right)^{10}-\left(\frac{\sigma}{z}\right)^{4}+\left(\frac{\sigma}{H-z}\right)^{10}-\left(\frac{\sigma}{H-z}\right)^{4}\right] \qquad 3.7$$

where z is the distance from the surface; σ is the solid fluid molecular diameter; N is the molecular density (the number of molecules per unit surface area); A is the dispersion

coefficient; the subscripts s and f refer to the adsorbent and adsorbate, respectively, and the dispersion coefficients are calculated using the Kirkwood-Muller equations [26]:

$$A_{sf} = \frac{6mc^2\alpha_s\alpha_f}{\frac{\alpha_s}{\chi_s}+\frac{\alpha_f}{\chi_f}} \qquad 3.8$$

$$A_{ff} = 3mc^2\alpha_f\chi_f \qquad 3.9$$

In the above equations, m is the mass of an electron; c is the velocity of light; and α and χ are the polarizability and magnetic susceptibility, respectively, of the adsorbent atom or adsorbate molecule. In both of the methods presented the potential well depth is determined by the polarizability of the molecule. This method however predicts a potential well depth that is only 40% of the values obtained via fitting methods [21,29].

3.3.3 Nonporous carbon method

One method to fit the Lennard-Jones parameters is to find an experimental isotherm of a sample with a known PSD, then to determine the LJ that allows the thermodynamic model to minimize the error in the adsorption integral Equation 3.1. Utilizing the slit shaped pore DFT thermodynamic model with the adsorbate-adsorbate data fit to the saturation properties of the system the remaining variable is solid fluid potential well depth. Large pores have been shown to fill in layers [27,28,29] with the monolayer relative filling pressure approaching a maximum value as the pore exceeds 20 molecular diameters in width. The filling pressure is controlled predominately by relative temperature, molecular size and solid-fluid potential well depth. The temperature may be controlled using a temperature bath or a cryostat. However, the potential well depth and size are fixed for a given adsorbate-adsorbent system. The energetic

heterogeneity is assumed to be due to physical separation of opposing pore walls, hence for sufficiently large pores the superposition of potential is negligible and the monolayer filling pressure is determined by the potential exerted by only one wall. The limiting value of the monolayer filling pressure is fortuitous because it allows one to treat the pore size distribution of a nonporous solid as a mono-disperse PSD despite the ambiguity of its actual size distribution as shown in figure 3.1. The thermodynamic model can be related to the experimental isotherm though the following relationship for a Dirac distribution for slit pores.

$$V_{ads}(P) = \frac{1}{2}\frac{R^* S\Gamma(P,R^*)}{\sigma_{ff}^2 N_{av}} \qquad 3.10$$

Where $V_{ads}(P)$ is the volume adsorbed, R^* is the mono-disperse pore size, S is the surface area of the sample, and $\Gamma(P,R^*)$ is the thermodynamic model. The thermodynamic model is often sharper than the reference isotherm, in which case the inflection points of the monolayer filling should be matched.

The shortcomings of fitting the parameters to a nonporous surface are the ambiguity of the shape and size of a pore in a "nonporous" carbon, measuring the high relative pressure of the monolayer for some gases, matching the distribution of the pore sizes and the reduced sensitivity to potential well changes. The ambiguous size of an appropriate isotherm makes an exact fit less likely, although the monolayer filling approaches a maximum it still is a function of the pore size and increases with pore size. Additionally nonporous references generally contain a distribution of meso and macropores which results in a reference isotherm which displays heterogeneity resulting

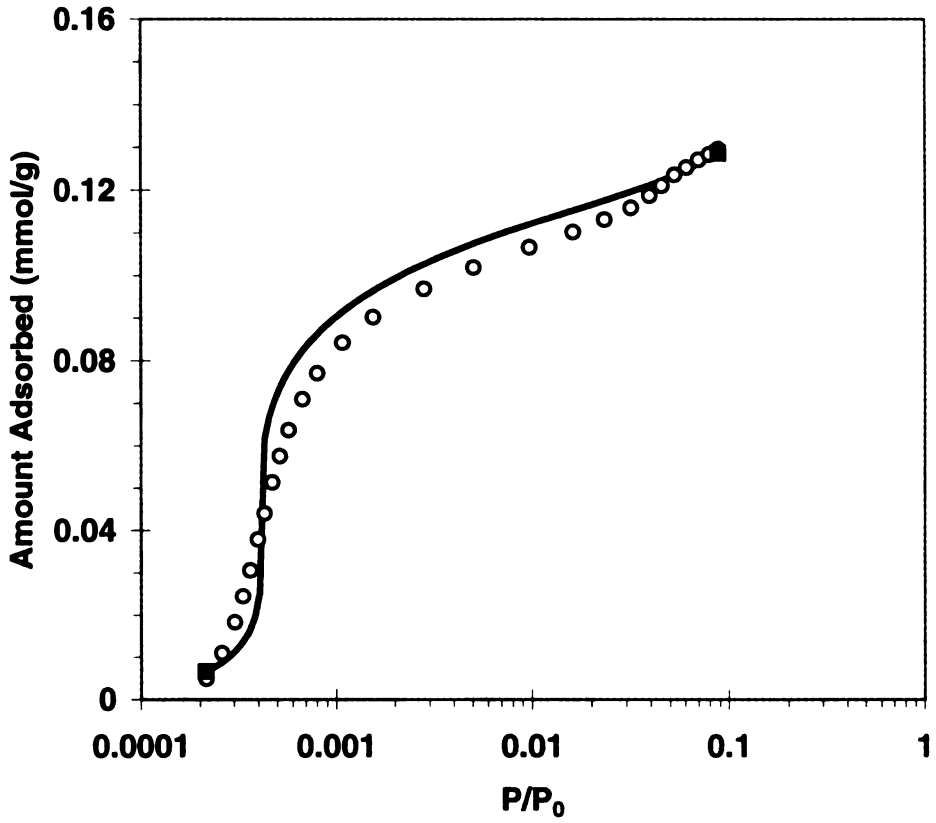

Figure 3.1 Argon adsorption on a nonporous graphitic carbon surface at 77K. The circles are the experimental isotherm and the solid line represents the fitted slit pore isotherm with a pore width of 67.5 Å.

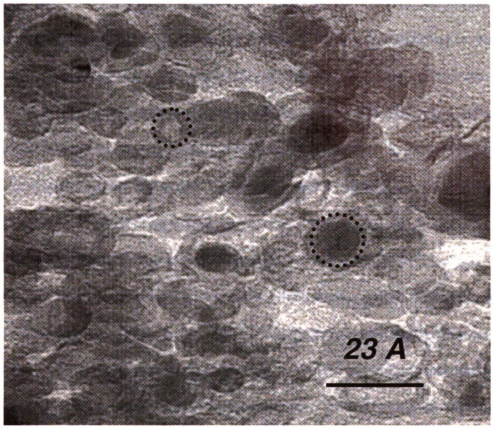

Figure 3.2 TEM photograph of single-walled carbon nanotubes. The dotted circles represent the least squares fit circle to the SWNT wall.

in filling over a broader range of relative pressures. The exact point of inflection may not lie on a measured data point reducing the ability to correctly fit the isotherms. The nonporous standard has the shortcoming of a relative filling pressure that is much higher than that of a micropore. Some gases such as carbon dioxide require pressure vessels to reach the monolayer filling pressures at room temperature, which may increase cost. The approximation of a nonporous solid indicates that the adsorbate is influenced by only one wall. The superposition of potentials results in greater sensitivity to potential well depth in micropores compared to meso and macropores.

3.3.4 Nanotubes as a Reference Adsorbent

The use of a microporous reference can obviate many of the difficulties associated with the nonporous reference. Nanotubes have properties that make them an excellent alternative reference material, such as their simple geometric structure, chemical homogeneity, and multiple means of measuring their size. Using a micropore will have the result of increased sensitivity to the potential well depth due to the super position of potential wells. Additionally the model of a cylindrical pore represents nanotubes well, whereas a nonporous carbon may have structural heterogeneity due to the varying shape and size of the surface. As stated earlier it is necessary to determine the PSD of the reference adsorbent. The PSD of a nanotube sample may be determined via measuring the cross section of a nanotube photographed using transmission electron microscopy (TEM). Nanotubes diameters may be found using a least squares approximation to fit a circle to points that lay midway in the pore wall as shown in Figure 3.2. Utilizing a method similar to that of the nonporous surface a solid fluid potential chosen and used to generate a series of thermodynamic model isotherms, which are used in the inversion of

the adsorption integral Equation (3.1). The PSD which is generated for a particular solid-fluid potential well depth may be compared to a simple histogram of the pore sizes measured by the TEM to reveal the validity of the chosen potential

Both the nonporous and nanotube reference isotherms contain extraneous information at relative pressures greater than the monolayer filling pressure. In the case of the nonporous reference the isotherm the data obtained at pressures greater than the monolayer "knee" may be misleading. Whereas for a nanotube the relative pressure range is bounded by the monolayer filling pressure of the smallest and largest pore in the distribution determined by TEM. As shown in Figure 3.3 the monolayer region as defined by the thermodynamic model, is the most relevant region for fitting the potential parameters. At relative pressures larger than the monolayer filling pressure the fluid-fluid interactions play a larger relative role in pore condensation, therefore are less reliable for determining the solid-fluid potentials. For nonporous surfaces the heterogeneity of the meso and macropore sizes is also evident in the second layer transition, reducing the reliability of data fitted to that region of the reference isotherm. Data obtained from microporous references at relative pressures higher than the monolayer filling pressures are suspect for the same reason as the nonporous reference with the addition of ambiguity associated with the sorption to the tube exteriors and interstitial spaces.

3.4. Results

3.4.1 General information

A sample of purified single walled carbon nanotubes, which was sonicated in strong acid for 48 hours to shorten the nanotubes, remove the end caps and impurities, was dried and

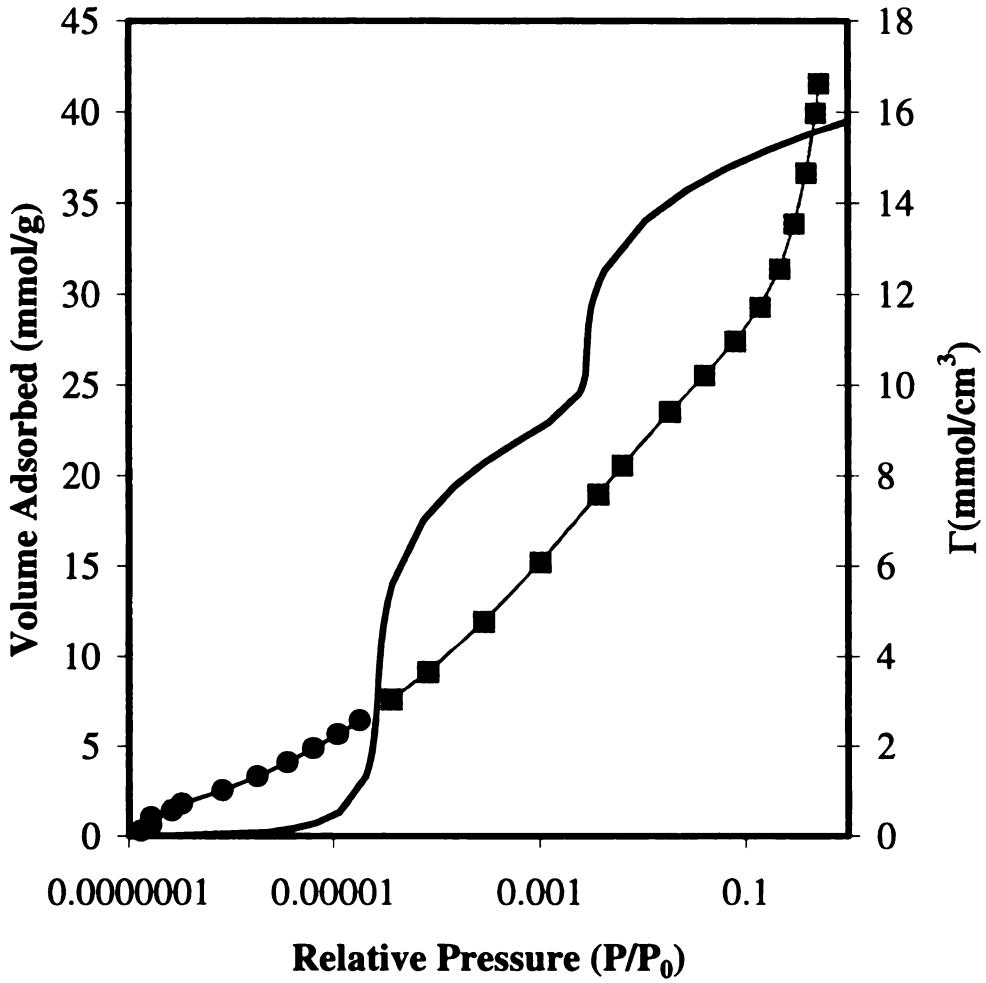

Figure 3.3 The relevant region of the isotherm to fitting is determined by the isotherm generated predicted by the largest pore in the TEM photo(solid line). The circles show the relevant region of the isotherm while the squares represent data from the nanotube exterior.

photographed using TEM. The TEM photographs were then analyzed to determine the histogram of pore sizes, based upon the least squares fit of a circle to the cross-section of a nanotube, as shown in Figure 3.2. The mode pore size was determined to be 12.5 Å as specified by the manufacturer using TEM (see Figure 3.4). The preparation of the SWNT for the TEM photograph may alter their relative positions to one another, therefore no information about the interstitial spaces between tubes or tube bundles may be ascertained from the analysis of the TEM data. The PSD obtained via TEM therefore contains data based upon the tube diameter alone and is independent of the external tube conditions.

3.4.2Verifying validity

The validity of the nanotube as a standard reference may be verified by comparing the TEM PSD with the PSD obtained by porosimetry measurements based upon nonporous references. Nitrogen and Argon Lennard-Jones parameters obtained for graphitic nonporous carbons in the method described in section 3.3 [20,28], were used to generate a series of cylindrical pore isotherms shown in Figures 3.5 and 3.6 respectively. For convenience the pores were assumed to be in a trimodial gamma distribution (M=3), although the PSD could have been determined over discrete intervals or with another distribution function [20].

$$f(H) = \sum_{i=1}^{m} \frac{\alpha_i (\gamma_i H)^{\beta_i}}{\Gamma(\beta_i) H} \exp(-\gamma_i H) \qquad 3.11$$

It has been demonstrated that during the manufacture of SWNT, bundles of tubes are formed rather than individual tubes. The external surface of a tube is available for sorption, however it has been shown that the interstitial spaces between tubes in bundles

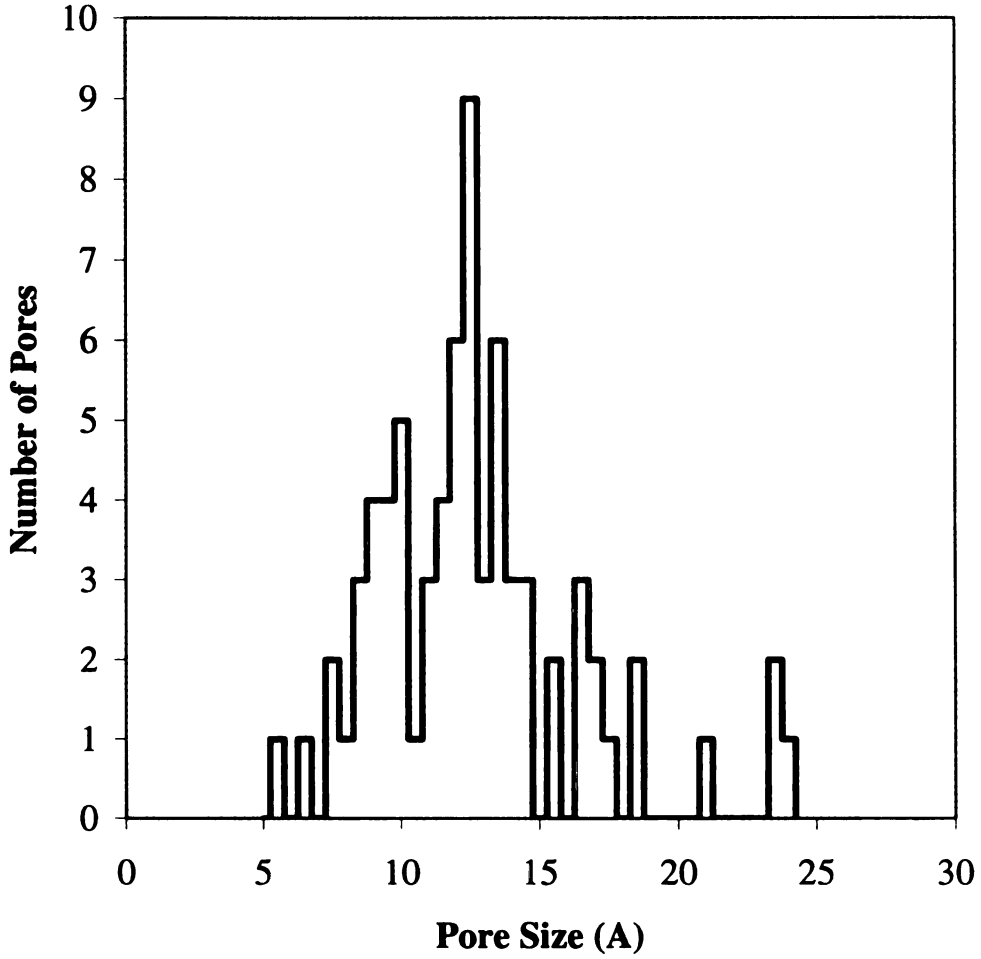

Figure 3.4 TEM Pore size distribution. The number of pores with a diameter that lies between half-angstrom intervals is displayed; the total number of pores measured is 72. The mode in the distribution is the same as that predicted by the manufacturer. [4]

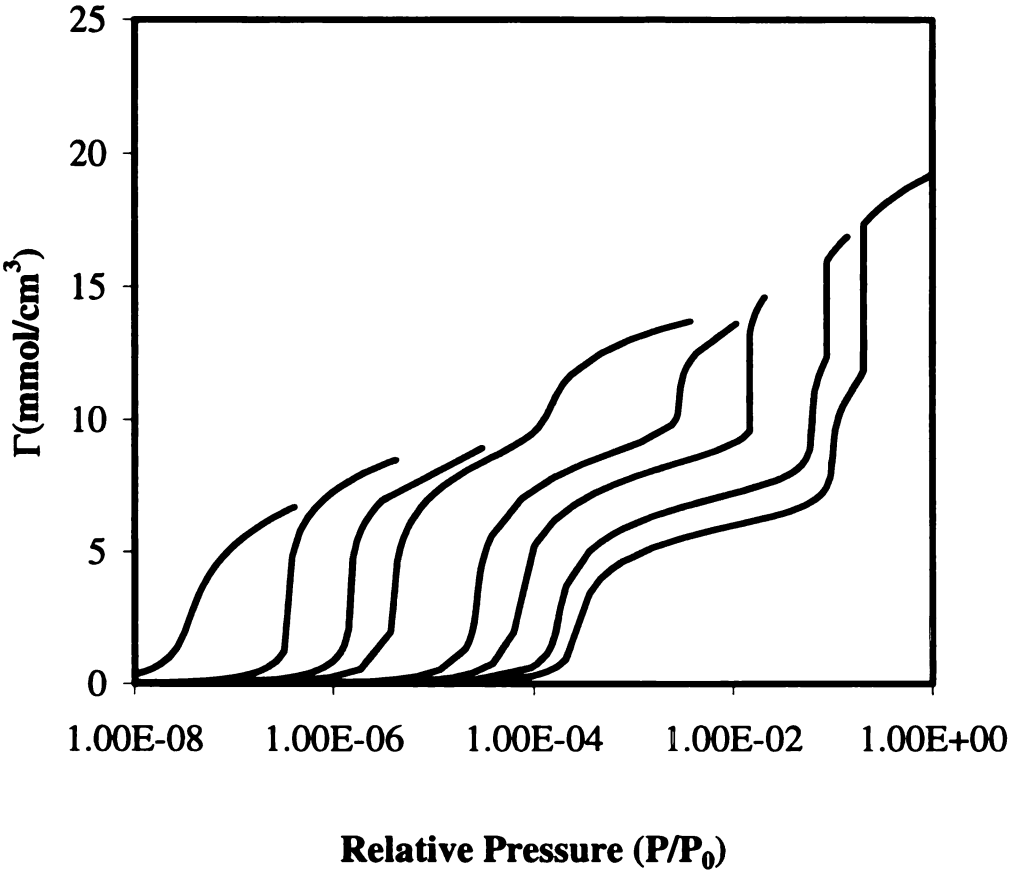

Figure 3.5 Nitrogen specific excess adsorption in model single walled carbon nanotubes at 77K. The isotherms shown from left to right have physical pore diameters of 10.7, 12.1, 13.2, 14.3, 17.9, 21.4, 28.6, and 35.7 Å.

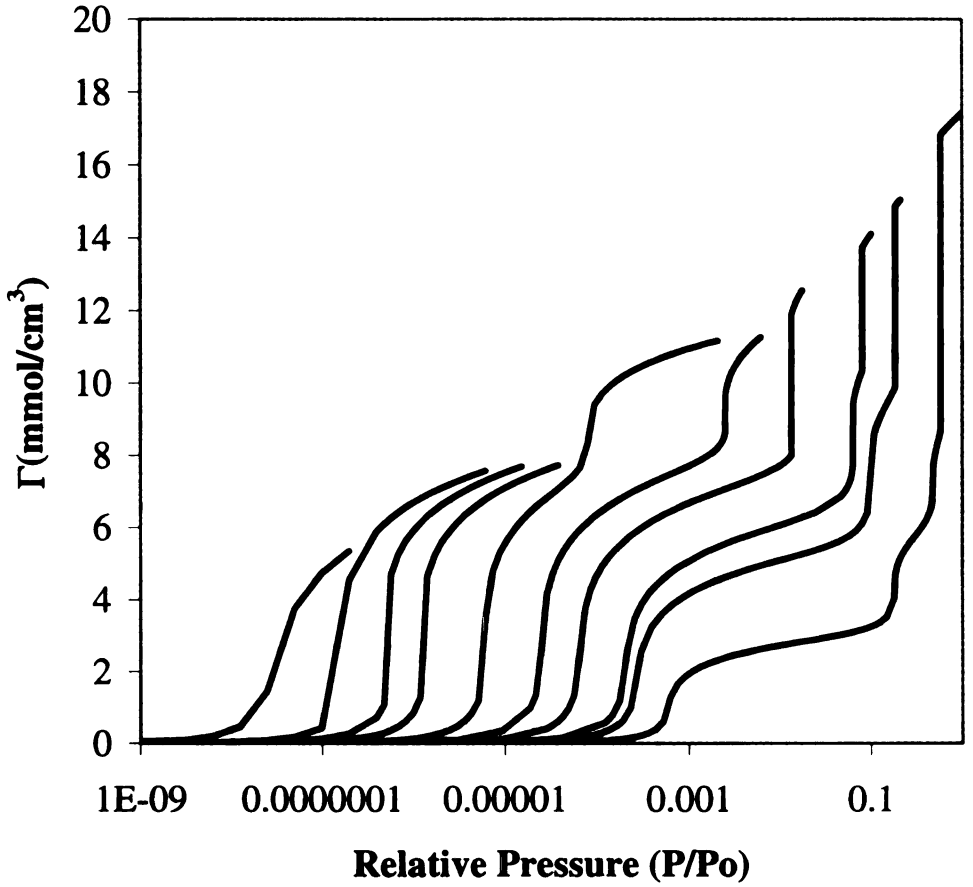

Figure 3.6 Argon specific excess adsorption in model single walled carbon nanotubes at 87K. The isotherms shown from left to right have physical pore diameters of 11.3, 12.4, 13.1, 13.9, 15.8, 18.8, 22.5, 30, 37.5, and 75 Å.

are too small for sorption to occur, [30,31] however modified tubes will adsorb on the exterior [8,32,33]. The external surface of a SWNT has a weaker potential than a flat surface [18], therefore tends to adsorb gases at a higher pressure. However, bundles of tubes will have interstitial spaces that may be approximated as the interior of a tube with a radius that is larger than the separation of tube bundles. These interstitial spaces of tube bundles are expected to be larger than the size of an actual nanotube. Therefore the first mode of the gamma distribution is anticipated to measure the PSD of the SWNT interiors, while the remaining modes are due to the external surface area of the tube bundles. As shown in Figure (3.7) the first mode of both the Ar and N2 overlap the PSD determined via TEM and each falls within the binning of the histogram and within 2% of the center of the peak. The two probe gases also predict a second mode that is within 4% of one another, which was not be detected via TEM, presumably due to interstitial spaces.

3.4.3 Carbon dioxide adsorption

Carbon dioxide is a linear three-centered molecule with a permanent quadrupole moment, with properties that make it a desirable alternate probe gas. Carbon dioxide is subcritical at room temperature, making it a desirable probe gas where equilibrium cannot be achieved in reasonable time scales at cryogenic temperatures. Unfortunately, the high saturation pressures require special apparatus to measure isotherms above the monolayer filling pressure at room temperature. The filling pressures of micropores however are at low enough pressures to be measured with common machinery. The saturation properties of carbon dioxide were used to determine the Lennard-Jones potential for fluid-fluid interactions and may be found in Table 3.1. An isotherm was measured for carbon

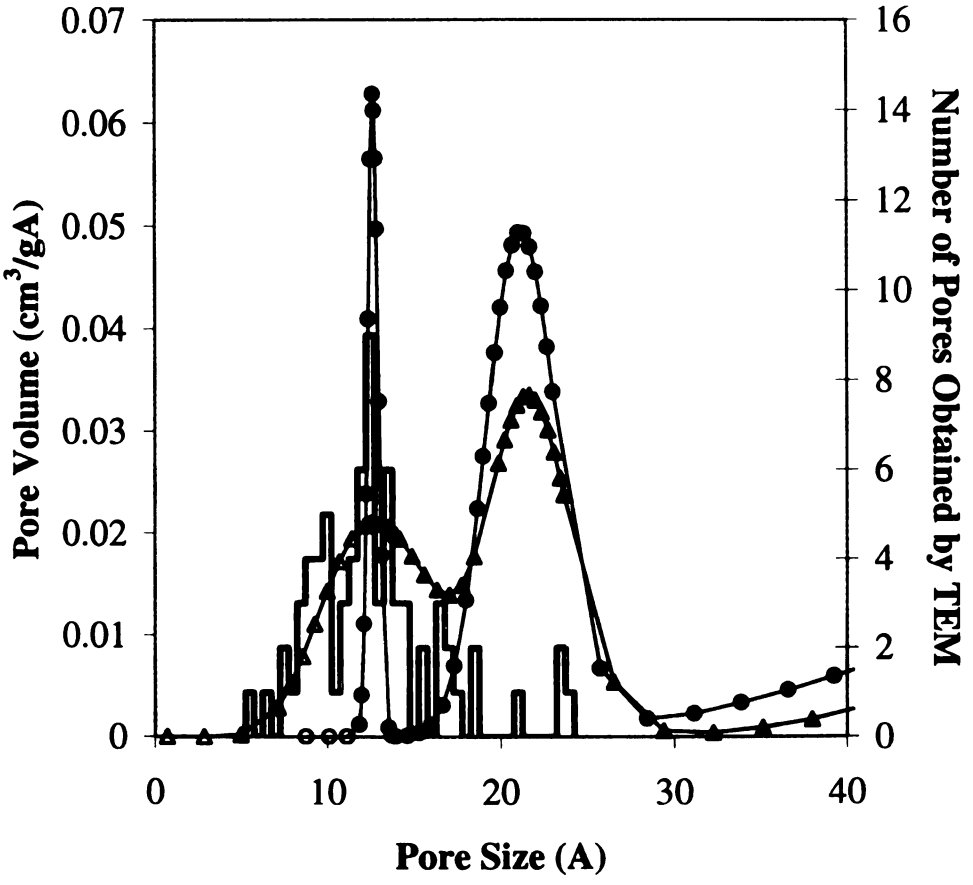

Figure 3.7 Comparison of the TEM, argon and nitrogen PSD, note that the first peak of each of the distributions are within 3% of one another. Also note that the TEM is incapable of generating the secondary mode predicted by both probe gases.

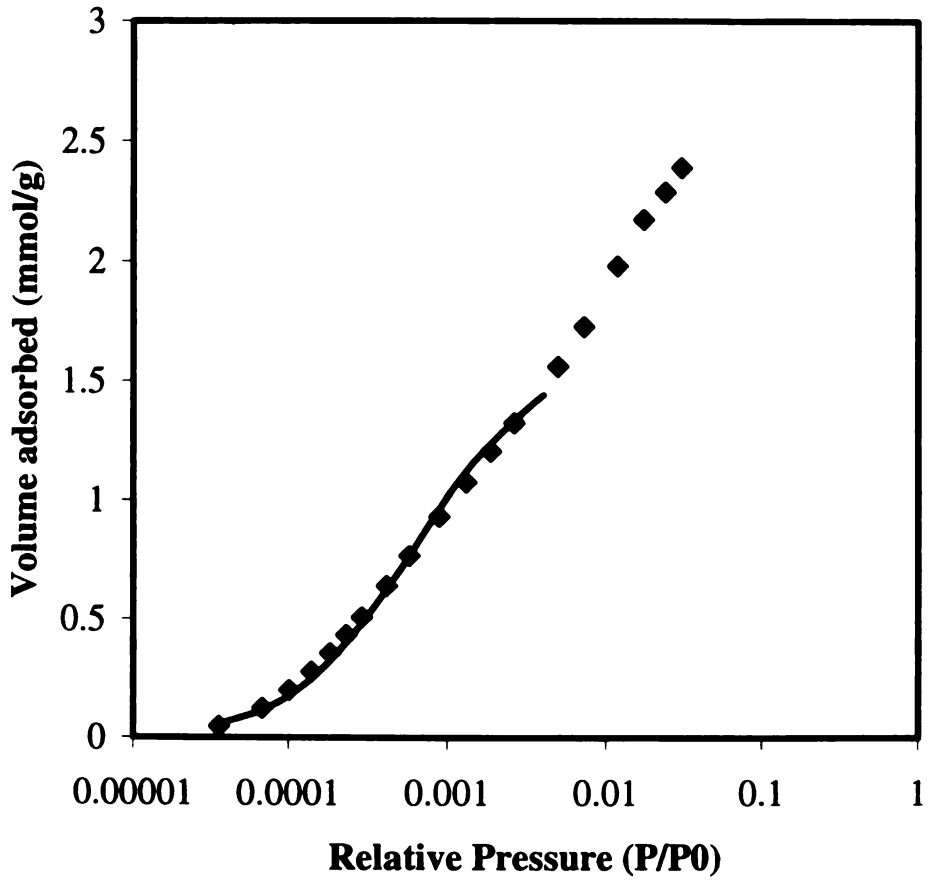

Figure 3.8 A carbon dioxide adsorption isotherm measured on single walled carbon nanotubes at 273K the squares represent the isotherm data and the line represents the best fit DFT model isotherm for carbon dioxide.

dioxide on SWNT at 273Kas shown in figure (3.8) A series of cylindrical pore isotherms were generated using a guess for the solid-fluid potential well depth as shown in figure 3.9. The isotherms were used in conjunction with the isotherm measured for SWNT to determine a PSD, which would likely reproduce the reference isotherm. The value of the solid-fluid potential well depth was adjusted to cause the first mode of the PSD to align with the PSD obtained by TEM. The solid-fluid potential well depth which best reproduced the mode in the PSD was 110K*k_B and was then used to generate slit pore isotherms for carbon dioxide between graphitic slabs. It was found that increasing the magnitude of the potential well depth increased the size of the mode of the distribution. The carbon dioxide slit pore isotherms are shown in figure 3.10 using the potential parameters found in Table 3.1. The carbon dioxide slit pore isotherms are at a

Table 3.1 Potential Parameters

Parameter	Argon	Nitrogen	Carbon dioxide
σ_{ff} (Å)	3.375	3.572	3.562
ε_{ff}/k (K)	110.2	93.98	225.3
σ_{sf} (Å)	3.362	3.494	3.456
ε_{sf}/k (K)	58.02	53.22	110.1

considerably higher relative temperature and therefore contain considerably less structure than either the argon or nitrogen isotherms, which were generated for 87K and 77K respectively. Like the argon and nitrogen slit pore isotherms [28] (Figures 2.4 and 2.5), a transition is noted near 3.7σ marking the transition to multilayering isotherms [29]. Carbon dioxide however has the monolayer filling pressure of large pores over a broader range for a particular pore size, which would result in difficulty fitting the Lennard-Jones potential parameters with a nonporous carbon. As shown in figure 3.11 the carbon

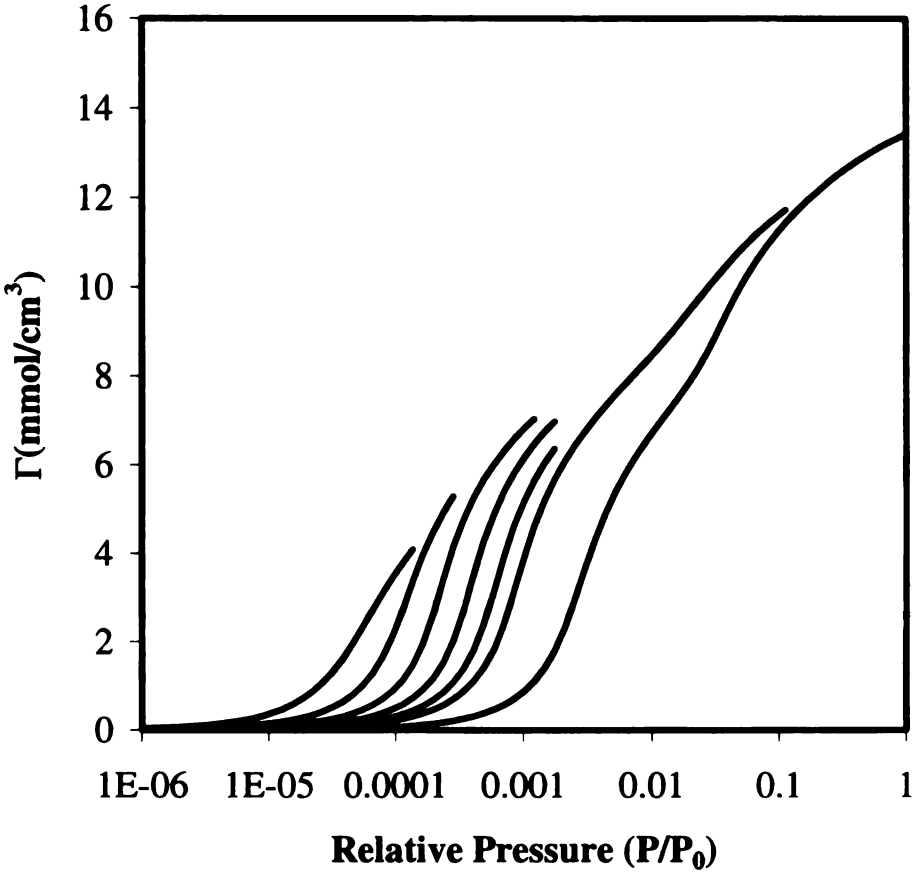

Figure 3.9 Excess carbon dioxide adsorption isotherms in model single walled carbon nanotubes at 273K for a solid fluid potential well depth of 110K*k_B. From left to right the pores are 10.7, 11.4, 12.1, 12.8, 13.5, 14.3, and 17.8 Å.

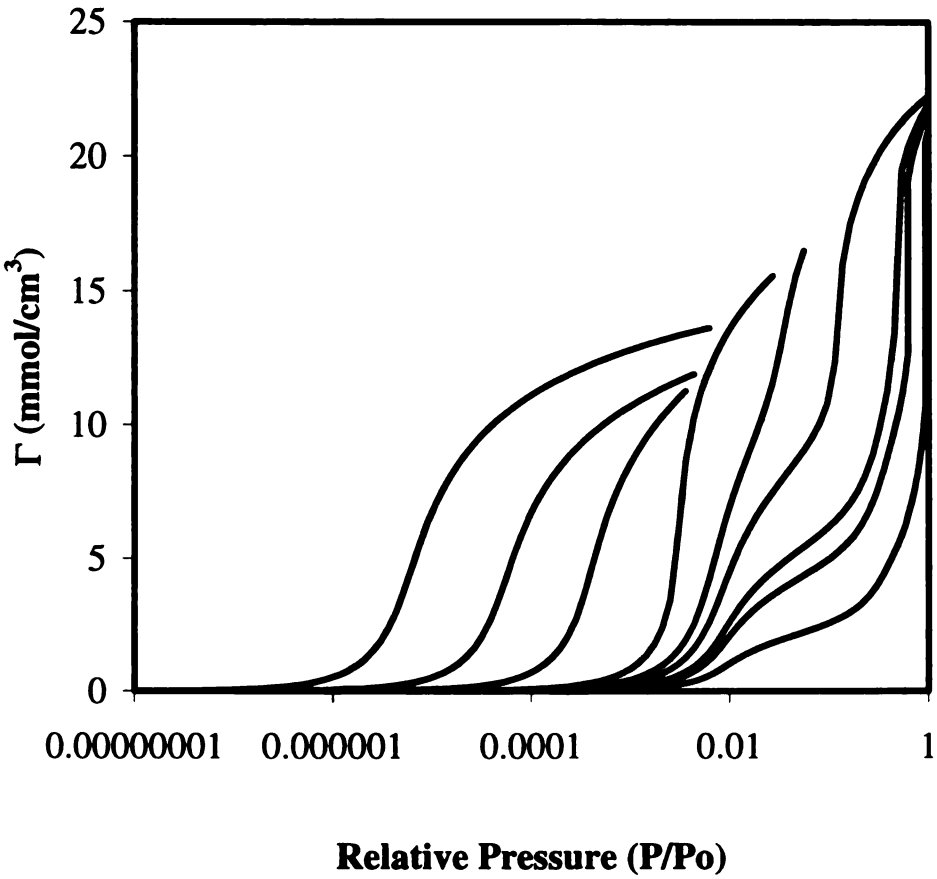

Figure 3.10 Carbon dioxide excess adsorption isotherms in model graphitic slit pores at 273 K Calculated using DFT. The isotherms shown left to right for pores having physical widths of 7.1, 8.0, 8.9, 11.6, 14.2, 17.8, 21.4, 35.6 and 71.2 Å.

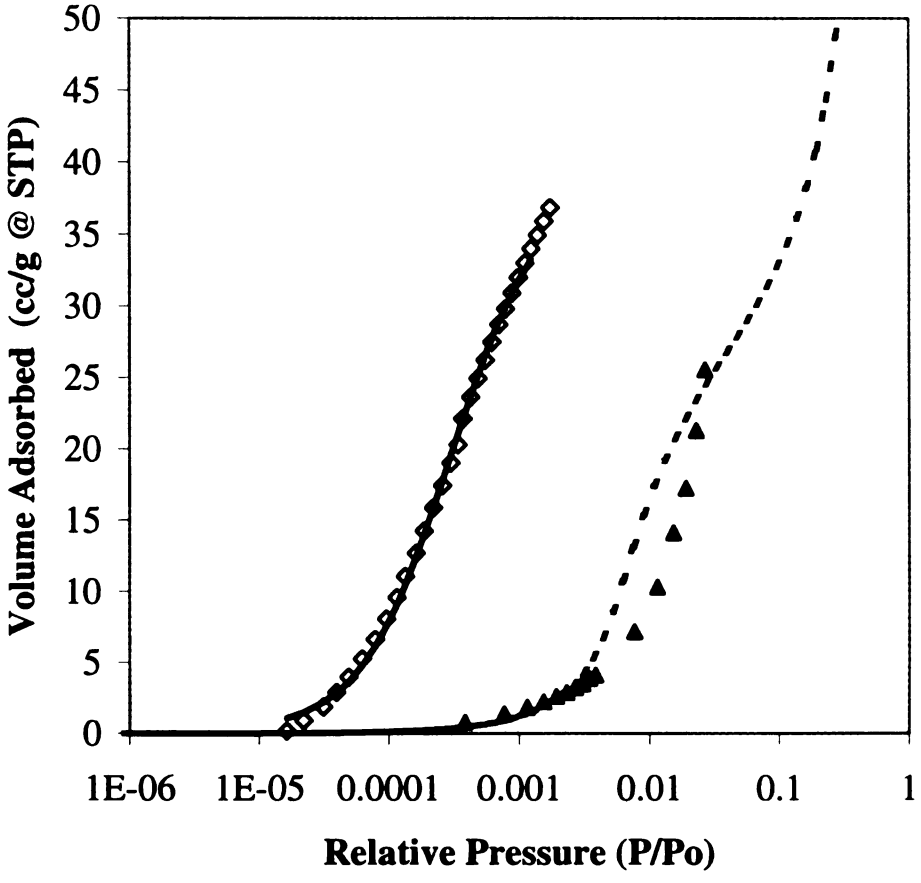

Figure 3.11 Comparison of surfaces for fitting. The nonporous carbon dioxide isotherm measured by Bottani [34]is represented by triangles, the open diamonds are experimental data for carbon dioxide adsorption on single walled carbon nanotubes, the solid line is the fit of the DFT potential parameters and the dotted line is the DFT slit pore isotherm with the potential determined via fitting to nanotube data.

dioxide isotherm obtained on a nonporous carbon does not display the characteristic "knee" required to utilize the standard nonporous fitting technique. However, as seen in the SWNT isotherm(figure 3.8) and the cylindrical pore model isotherms (figure 3.9) one is capable of measuring the PSD.

3.4.4 Test of the Carbon dioxide Parameters

To test the reliability of the potential parameters obtained via the nanotube reference, a comparison was made between carbon dioxide parameters fit to SWNT and argon and nitrogen parameters, which were fit, based upon a nonporous surface. A granular activated carbon (BPL 4x6) was examined with argon, nitrogen and carbon dioxide probe gases to determine their respective isotherms as shown in figure 3.12. The argon and nitrogen isotherms were determined at 77K and the carbon dioxide measurements were preformed at 273K. It is not unexpected that the carbon dioxide isotherm should fill at higher relative pressures at this higher relative temperature. The PSD for each gas was determined based upon the inversion of the adsorption integral and is displayed in figure 3.13. The mode of each distribution was found to reside in a narrow range between 11.86 and 14.42 A. The argon and carbon dioxide modes were within –10% and +11% of the nitrogen mode. As determined by the following equation:

$$Percentdiffernce = \frac{|ModeofGasX - NitrogenMode|}{NitrogenMode} \times 100\% \qquad 3.12$$

The PSD predicted by the carbon dioxide isotherm is within a reasonable degree of error when compared to the either nitrogen or argon probe gases. The relative proximity of the carbon dioxide and nitrogen modes indicated a reasonable fit of the potential parameters. There are several reasons why one would not anticipate the same result for all three probe gases: (1) the precision of the experimental isotherm measurement; (2) the accuracy of

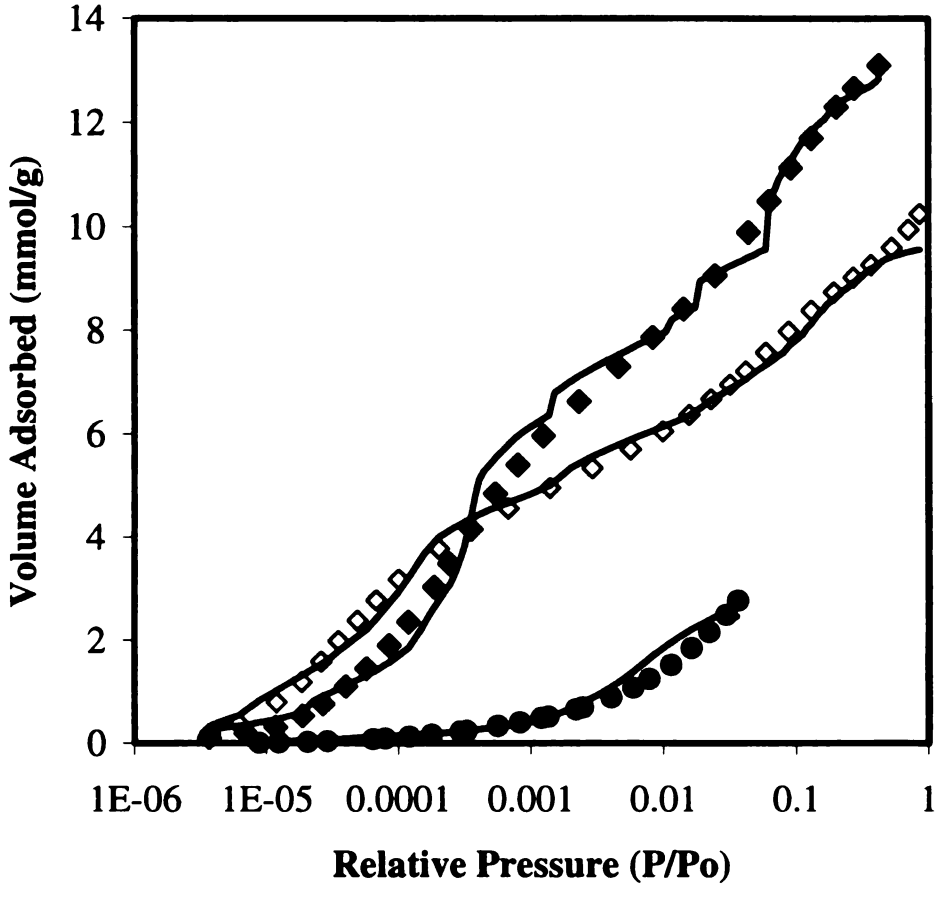

Figure 3.12 Adsorption isotherms on Granular activated carbon at 77K for argon and nitrogen represented by filled and open squares and carbon dioxide at 273K represented by filled circles. The solid lines represent the respective best fit DFT model to the experimental isotherm, each of which was fitted separately under the same conditions as the experiment.

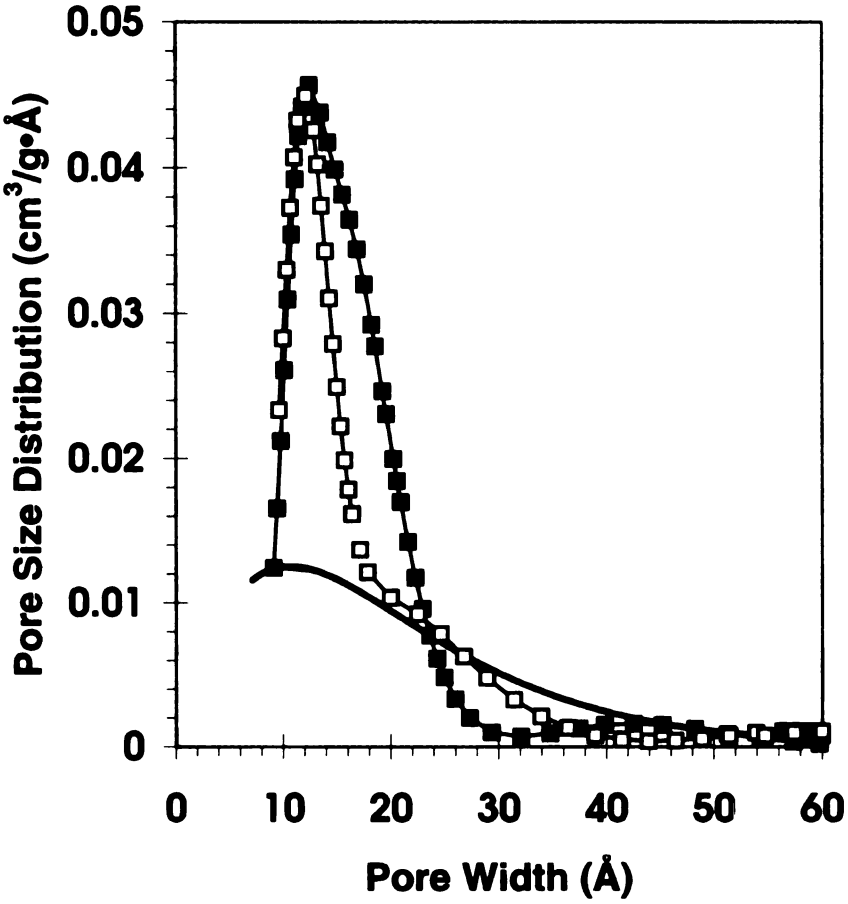

Figure 3.13 PSD obtained from the best fit DFT model isotherms on granular activated carbon. The argon is represented by the filled squares the nitrogen by the open squares and the carbon dioxide by the solid line.

the DFT pore filling model; and (3) the soundness of the numerical method used to invert the Fredholm integral of Equation 3.1 to obtain the PSD. The assumptions made in determining the DFT Model isotherms are a simplification of the actual systems and therefore will necessarily involve some degree of error. Neither nitrogen nor carbon dioxide are actually single centered molecules as used in the model, therefore their anisotropy is neglected. The model also simplifies the structure of the sorbent, the assumptions of slit shape, no connectivity, and perfectly homogeneous surfaces are simplifications to make the problem more tractable [28]. Results indicate that either a nonporous surface or a SWNT will yield comparable potential parameters, however the equilibrium isotherm may be questioned for the validity. Further investigations are required to verify the isotherms. Due to the protracted times required for diffusion in the nanotubes it is questionable whether the nanotubes are in true equilibrium with the surroundings. One test to determine if an isotherm is in equilibrium is to increase the temperature at which the isotherm is measured, DFT and MS predict that increasing the temperature will increase the filling pressure and decrease the total volume adsorbed. Changing the cryostatic temperature bath from liquid nitrogen to liquid argon shifts the temperature from 77K to 87K, however the saturation pressure of the adsorbate is not concurrently measured. As seen in Figure 3.14 sets of nitrogen and carbon dioxide isotherms taken at different temperatures yield results that overlap one another. The nitrogen isotherms are nearly overlapping and do not display significant differences despite the prediction that at 87K the pores should fill at higher relative pressures. The carbon dioxide isotherms display significant deviations from the anticipated results. The reason for these deviations remain unclear, both temperature measurements are taken at

high relative temperatures and should display the opposite results. Possible reasons for the unanticipated results include stretching of the bonds in the nanotubes at higher temperatures, resulting in larger tubes with greater storage capacity. An alternate view is that the rate of diffusion through the nanotubes is very slow, giving rise to non-equilibrium isotherms.

3.5. Conclusions

The nanotubes are capable of serving as alternate reference adsorbents to nonporous carbons, as illustrated by the overlap in the predicted PSD of the argon and nitrogen on the SWNT and carbon dioxide on activated carbon, despite the apparent non-equilibrium state. The data taken with a reference fluid at saturation indicates that the nanotubes fill at the anticipated pressures, however deviations are noted for fluids that do not have a saturated reference fluid. The apparent success in fitting the carbon dioxide potential parameters cannot be trusted entirely despite its ability to match the PSD predicted by both argon and nitrogen with a high degree of accuracy. When the temperature is altered the values for these constants tend to change significantly therefore their validity is questioned. Further analysis over a wider array of temperatures is required to determine the appropriate equilibrium isotherms. While the mechanism responsible for the non-equilibrium status is poorly understood it is known that increasing the temperature has the result of faster diffusion times, it is therefore more likely that the higher temperature isotherms are closer to the equilibrium isotherms.

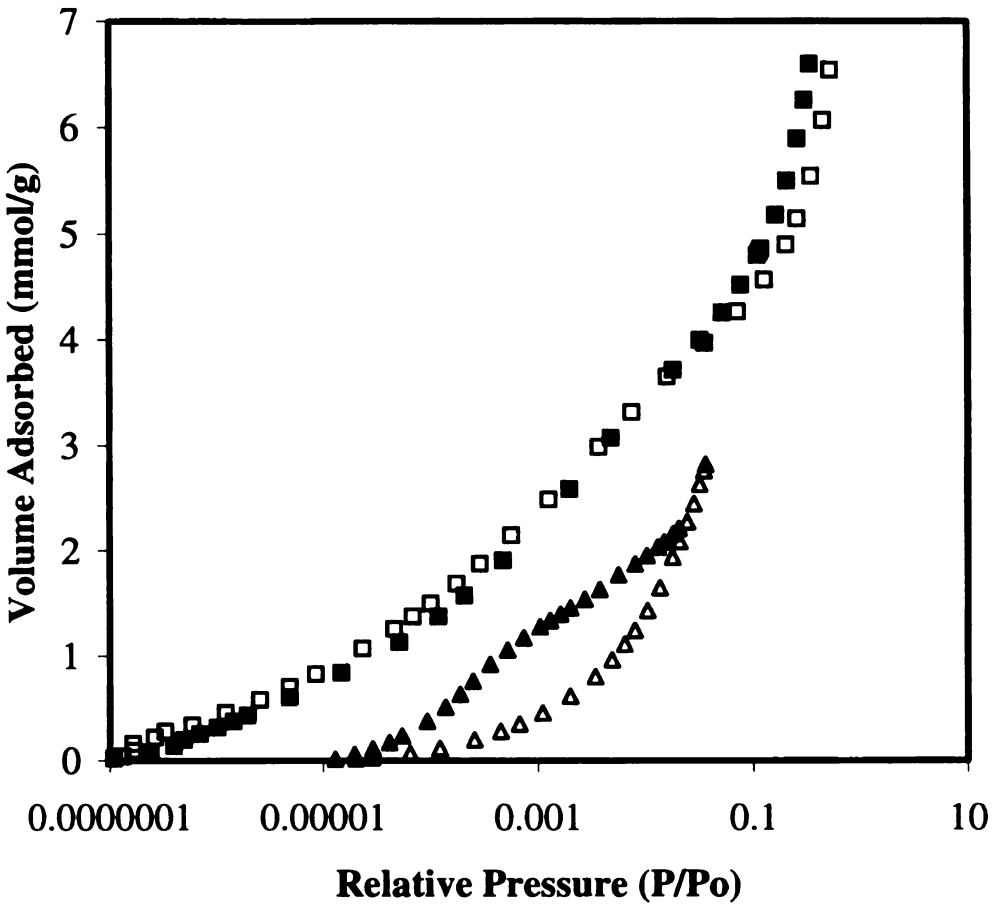

Figure 3.14 Adsorption isotherms of on single walled carbon nanotubes of nitrogen at 77K (open squares) and 87K (filled squares), and carbon dioxide at 273k (open triangles) and 293K (filled triangles).

3.6. References:

1. Iijima, S. Nature1991; 354: 56.
2. Ebbesen, T. W. *"Cones and Tubes: Geometry in the chemistry of Carbon."* Accounts of Chemical Research. 1998;31 558.
3. Dujaurdin, E,; Ebbesen, T.; Krishnan, A. and Treacy M. *Wetting of Single Shell Carbon Nanotubes.* Advances Materials 1998;10, 1472.
4. Rinzler, A.G.; Liu, J.; Dai, H.; Nikolaev, P.; Huffman, C. B.; Rodriguez-Macias, F.J.; Boul ,P.J.; Lu, A.H.; Heymann, D.; Colbert, D. T.; Lee, R. S., Fischer, J. E., Rao, A.M. Eklund, P.C. Smalley R. E. Large Scale purification of single-wall carbon nanotubes: process, product, and characterization. Appl. Phys. A.. 1998, 67, 29.
5. Lui, J.; Rinzler, A.G.; Dai, H.; Hafner, J.H.; Bradley R. K.; Boul ,P.J.; Lu, A. H.; .Iverson, T.; Shelimov, K.; Huffman, C. B; Rodriguez-Macias, F.J.; Shon, Y.; Lee, R. S.; Colbert, D. T.; Smalley R. E. Fullerene Pipes. Science 1998; 280,1253.
6. Maddox, M.W.; Sowers S.L.; Gubbins, K.E. Molecular Simulation of Binary Mixture Adsorption in Buckytubes and MCM-41. Adsorption 1996; 2, 23.
7. Darkim, F. and Levensque, D. Monte Carlo Simulations of Hydrogen Adsorption in Single-Walled Carbon Nanotubes. Journal of Chemical Physics 1998; 109 4981.
8. Wang, Q.; Johnson, K. Journal of Chemical Physics 1999, 110, 577.

9. Eswaramoorthy, M.; Sen, R.; Rao, C.N.R. Chemical Physics Letters 1999; 304, 207.

10. Talapatra, s.; Zambano, A.E.; Weber, S.E. and Migone, A. D. Gases Do Not Adsorb on the Interstitial Channels of Closed-Ended Single-Walled Carbon Nanotube Bundles Physical review letters 2000, 85 138.

11. Maddox M.W, and Gubbins KE. Molecular Simulation of Fluid Adsorption in Buckytubes. Langmuir 1995; 11 3988.

12. Lastoskie, C.M.; Quirke, N.; Gubbins, K.E. Stud Surf Sci and Cat 1997, 104, 745.

13. Schumacher, K., Ravikovitch, A. Du Chesne, A. , Neimark, A., Unger , K. Characterization of MCM-48 Materials Langmuir, 2000; 16, 4648.

14. Ravikovitch, P.,Haller, G., Neimark, A. Density Functional Theory Model for Calculating Size Distributions: Pore Structure of Nanoporous Catalysis. Advances in Colloid and Interface Science 1998; 76 203.

15. Ravikovitch, P., Domhanaill, S. C., Neimark, A. Schuth, F. and Unger K.K. Caplary Hysteresis in Nanopores: Theoretical and Experimental Studies of Nitrogen Adsorption on MCM-41. Langmuir 1995; 11, 4765.

16. Balbuena PB, Gubbins KE.The Effect of Pore Geometry on Adsorption Behavior COPS III International Symposium on the Characterization of Porous Solids Marseille May 1993.

17. Tjatjopoulos GJ, Feke DL, Mann JA. Molecule-Micropore Interaction Potentials J.Phys. Chem 1988; 92:4006-4007.

18. Stan, G.; Cole, M.W. Low Coverage Adsorption in Cylindrical Pores. Surface Science 1998; 395, 280.

19 Tarzona, P. Phys. Rev. A 1987, 60, 573

20. Lastoskie, C.; Gubbins, K.E.; Quirke, N. *J. Phys. Chem.* **1993**, *97*, 4786.

21. Dombrowski RJ, Hyduke DR, Lasktoskie CM. The Horvath-Kawazoe Method Revisited Colloid and Surfaces, A: Physiochem. and Eng. ASAP

22. Atkins PW. Physical Chemistry Fourth Edition. New York NY: W. H. Freeman and Company. 1990:645-662.

23. Gregg, S.J.; Sing, K.S.W. Adsorption, Surface Area and Porosity; Academic Press: New York, 1982.

24. J. Frenkel, "Kinetic Theory of Liquids," Clarendon Press, Oxford (1946).

25. Horvath, G.; Kawazoe, K. J. Chem. Eng. Japan **1983**, 16, 474.

26. A. Muller, Proc. Roy. Soc. London **A154** 624 (1936).

27. Lastoskie, C.; Gubbins, K.E.; Quirke, N. *Langmuir* **1993**, *9*, 2693.

28. Dombrowski RJ, Hyduke DR, and Lastoskie CM. Langmuir 2000, 5040?

29. Dombrowski R, and Lastoskie C Submitted to AICHE Journal.

30. Talapatra S, Zambano AZ, Weber SE, Migone AD. Gases Do Not Adsorb on the Interstitial Channels of Closed-Ended Single-Walled CarbonNanotube Bundles. Physical Review Letters 2000; 85(1):138-141.

31. Darkrim F, Levesque D. High Adsorptive property of Opened Carbon Nanotubes at 77K. J. Phys Chem B. 2000; 104 6773-76.

32. Mao Z, Sinnott SB. A Computational Study of Molecular Diffusion and Dynamic Flow through Carbon Nanotubes. J. Phys Chem B. 2000; 104 4618-24.

33. Yin YF, Mays T, McEnaney B. Adsorption of nitrogen in Carbon Nanotube Arrays. Langmuir 1999; 15 8715-8718.

34. deTorre LEC, Bottani EJ, Steele WA Amorphous carbons: Surface structure and adsorptive properties.LANGMUIR1996 12 (22): 5399-5406.

Chapter 4.

Dombrowski RJ, Hyduke DR, Lastoskie CM . The Horvath-Kawazoe method revisited. Colloid and Surfaces, A: Physiochem. and Eng. Vol 187-188, pp 23-39 ASAP.

Chapter 4.

The Horvath-Kawazoe Method Revisited

4.1 Introduction

The determination of the pore size distribution (PSD) of microporous adsorbents and catalysts continues to be an important research problem. Gas adsorption porosimetry remains a convenient and popular technique for probing the PSD of a microporous solid. Recently, novel methods have been proposed for characterizing the structure and adsorbent properties of disordered porous solids. However, these promising new approaches are not yet developed to a point where their widespread implementation is possible. The PSD characterization problem, therefore, becomes one of selecting the best available thermodynamic adsorption model $\Gamma(P,H)$ to describe gas uptake in pores of different width over the experimentally-sampled range of bulk gas pressures and temperatures. An assortment of pore filling models have been put forth for this purpose; among the first models suggested were the BET equation [1], the Dubinin-Radushkevich equation [2], and the Kelvin equation [3]. It has been recognized for some time that these "classic" models of adsorption do not accurately represent the filling process in micropores; therefore, more recent models have been proposed that, in some manner, incorporate gas-solid energies of interaction into the calculation of the model isotherm. These include methods based upon statistical thermodynamics, such as density functional

theory [4] and molecular simulation [5]; and semi-empirical models such as the Horvath-Kawazoe (HK) method [6].

The HK method is the first pore filling model specifically developed to describe adsorption in microporous solids. In the original HK method, an analytic pore filling correlation is obtained by calculating the mean free energy change of adsorption $\bar{\phi}$ that occurs when an adsorbate molecule is transferred from the bulk gaseous phase to the condensed phase in a slit pore of width H:

$$\ln(P_c/P_0) = \bar{\phi}(H)/kT \qquad 4.1$$

In equation (4.1), P_0 is the bulk gas saturation pressure; P_c is the pore filling pressure; k is the Boltzmann constant; and T is the temperature. The assumed exponential dependence of filling pressure on the free energy change of adsorption is also invoked in Polanyi potential theory [7] and in the Frenkel-Halsey-Hill or FHH theory [8-10]. In the original HK method, the mean free energy change upon adsorption is calculated from an unweighted average of the adsorbate interaction potential ϕ, measured over the volume of the slit pore located between $z = \sigma_{sf}$ and $z = H - \sigma_{sf}$:

$$\bar{\phi} = \frac{\int_{\sigma_{sf}}^{H-\sigma_{sf}} \phi(z)dz}{\int_{\sigma_{sf}}^{H-\sigma_{sf}} dz} = \frac{\int_{\sigma_{sf}}^{H-\sigma_{sf}} \phi(z)dz}{H-2\sigma_{sf}} \qquad 4.2$$

where z is the perpendicular distance of the adsorbate molecule center-of-mass from the plane of atomic nuclei in the solid surface layer, and σ_{sf} is the arithmetic mean of the adsorbate molecule and adsorbent atom diameters. The interaction energy between the adsorbate molecule and a slit pore wall is represented by the 10-4 potential

$$\phi_{10-4}(z) = \frac{NA}{2d^4}\left[\left(\frac{d}{z}\right)^{10} - \left(\frac{d}{z}\right)^{4}\right] \qquad 4.3$$

which is obtained by integrating the Lennard-Jones 12-6 pair potential over an unbounded planar surface [11]. In equation (4.3), N is the molecular density (the number of molecules per unit surface area); A is the dispersion coefficient; and $d = (2/5)^{1/6}\sigma_{sf} = 0.858\sigma_{sf}$ is the distance from the solid surface at which the 10-4 potential has a zero interaction energy.

The adsorbate potential within the slit pore, ϕ in equation (4.2), is modeled in the original HK method as the sum of the gas-solid potential ϕ_{sf} and a second term representing the adsorbate-adsorbate interaction, ϕ_{ff}:

$$\phi(z) = \phi_{sf}(z) + \phi_{ff}(z) = \frac{N_s A_{sf} + N_f A_{ff}}{2\sigma^4}\left[\left(\frac{\sigma}{z}\right)^{10} - \left(\frac{\sigma}{z}\right)^{4} + \left(\frac{\sigma}{H-z}\right)^{10} - \left(\frac{\sigma}{H-z}\right)^{4}\right] \qquad 4.4$$

where the subscripts s and f refer to the adsorbent and adsorbate, respectively, and the dispersion coefficients are calculated using the Kirkwood-Muller equations (as reported in reference [6]):

$$A_{sf} = \frac{6mc^2\alpha_s\alpha_f}{\frac{\alpha_s}{\chi_s} + \frac{\alpha_f}{\chi_f}} \qquad 4.5$$

$$A_{ff} = \frac{3}{2}mc^2\alpha_f\chi_f \qquad 4.6$$

In the above equations, m is the mass of an electron; c is the velocity of light; and α and χ are the polarizability and magnetic susceptibility, respectively, of the adsorbent atom or adsorbate molecule. Substitution of equation (4.4) into equation (4.2) and integration

yields, when combined with equation (4.1), the original analytic HK correlation between the pore filling pressure and the slit pore width:

$$\ln(P_c/P_0)=\frac{N_s A_{sf}+N_f A_{ff}}{kT\sigma^3(H-2d)}\left[\frac{1}{9}\left(\frac{\sigma}{d}\right)^9-\frac{1}{3}\left(\frac{\sigma}{d}\right)^3-\frac{1}{9}\left(\frac{\sigma}{H-d}\right)^9+\frac{1}{3}\left(\frac{\sigma}{H-d}\right)^3\right] \qquad 4.7$$

Correlations similar to equation (4.7) have also been derived for cylindrical [12] and spherical [13] pore geometries. The pore filling correlation predicted by the original HK equation for nitrogen adsorption in carbon slit pores at 77 K is shown in Figure 4.1. It can be seen that the original HK method correctly predicts lower micropore filling pressures than are obtained from Kelvin-equation based pore-filling models such as the Barrett-Joyner-Halenda (BJH) method [3]. The introduction of the HK method thus brought about a major improvement to the PSD analysis of microporous solids, since unlike the Kelvin equation, the HK model yields physically realistic PSDs for adsorbents that uptake gases at very low relative pressures (i.e. at $P/P_0 < 0.01$).

In the last decade, a dramatic improvement in computer capabilities has led to the application of numerically intensive statistical thermodynamics methods to model adsorption in microporous solids. The advantage of using molecular simulation to calculate the theoretical adsorption isotherms $\Gamma(P,H)$ is that the isotherms so obtained may be considered "exact" for the assumed pore geometry, surface composition and intermolecular potential functions. For adsorbents with pore structures that are well approximated by simple geometries such as slits or cylinders, theoretical adsorption isotherms can be efficiently calculated using density functional theory (DFT) [4, 14-15]. Adsorption isotherms and pore filling correlations obtained from DFT rival molecular

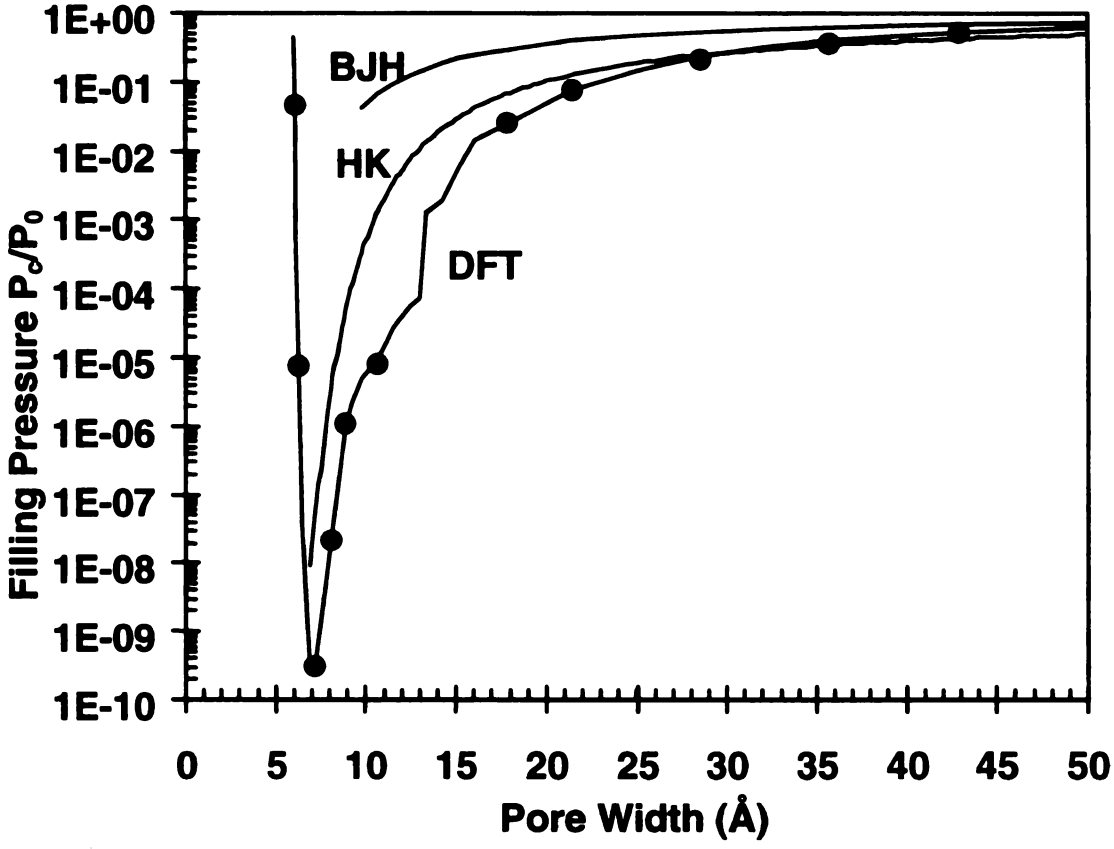

Figure 4.1: Pore filling correlations predicted by the Barrett-Joyner-Halenda (BJH) method, the original Horvath-Kawazoe method (HK), density functional theory (DFT), and Gibbs ensemble Monte Carlo molecular simulation (points) for nitrogen adsorption in carbon slit pores at 77 K [19].

simulation results in accuracy (Figure 4.1) and can be computed in a small fraction of the time required for molecular simulations. Molecular simulation, however, remains the principal method of modeling adsorption in materials that have irregular pore geometries (e.g. controlled pore glasses) or interconnected pore structures (e.g. zeolites) [16-18].

4.2 Critique of Original HK Method

The original HK model yields an analytic equation that is easily applied to adsorbent PSD analysis by using a simple spreadsheet, whereas a Fortran or C++ computer algorithm must typically be written and executed to obtain theoretical isotherms from DFT or Monte Carlo simulation. A comparison of the pore filling correlations obtained for the original HK, DFT, and Gibbs ensemble Monte Carlo (GEMC) adsorption models is shown in Figure 4.1 for nitrogen adsorption in graphitic slit pores at 77 K [19]. It can be seen that, relative to the DFT and GEMC results, the HK model, as originally posed, overestimates the nitrogen condensation pressure in carbon micropores. There are several reasons for the difference in the predicted HK and DFT/GEMC pore filling correlations:

(1) *The gas-solid interaction potentials that were used in the HK model and in the DFT/molecular simulation approach are not the same.* The original HK method uses the 10-4 potential for adsorbate interaction in a slit pore bounded by a single graphitic carbon layer. In the reported comparisons with DFT and Monte Carlo simulation, meanwhile, the 10-4-3 potential [20] for adsorbate interaction in a slit pore bounded by layered, semi-infinite graphitic *slabs* has been used. The 10-4-3 potential for an adsorbate molecule at distance z from a single graphite slab is

$$\phi_{10-4-3} = 2\pi\varepsilon_{sf}\rho_s\sigma_{sf}^2\Delta\left[\frac{2}{5}\left(\frac{\sigma_{sf}}{z}\right)^{10} - \left(\frac{\sigma_{sf}}{z}\right)^4 - \frac{\sigma_{sf}^4}{3\Delta(z+0.61\Delta)^3}\right] \qquad 4.8$$

where ρ_s = 0.114 Å^{-3} and Δ = 3.35 Å are the graphite density and graphite layer spacing, respectively; and ε_{sf} and σ_{sf} are the Lennard-Jones well depth and effective molecular diameter, respectively, for the gas-solid interaction potential. The "3" term of the 10-4-3 potential represents the dispersion energy between the adsorbate molecule and the subsurface layers of the graphite slab. If equation (4.3) is written in terms of the Lennard-Jones gas-solid potential parameters, one obtains the result

$$\phi_{10-4-3} = 2\pi\varepsilon_{sf}\rho_s\sigma_{sf}^2\Delta\left[\frac{2}{5}\left(\frac{\sigma_{sf}}{z}\right)^{10} - \left(\frac{\sigma_{sf}}{z}\right)^4\right] \qquad 4.9$$

with $NA = 10\pi\varepsilon_{sf}\rho_s\Delta d^6$ from equation (4.3). Comparing equations (4.8) and (4.9), it can be seen that, for the same potential parameters, the 10-4-3 potential has a greater net attraction for the adsorbate molecule at all distances z than does the 10-4 potential. Therefore, the DFT adsorption model with the 10-4-3 potential might be expected to predict lower pore filling pressures than the HK model with the 10-4 potential.

(2) *The gas-solid potential parameters selected for the HK model are not the same as the parameters fitted in the DFT model.* In the original HK method, the dispersion coefficients are fitted using the polarizability and magnetic susceptibility of the bulk adsorbate (nitrogen) and adsorbent (carbon), as noted in equations (4.5) and (4.6). Values of these and other needed physical properties, such as the molecular diameter and the monolayer density, are culled from various references [6]. In the DFT method, the Lennard-Jones parameters for the adsorbate-adsorbate pair potential are fitted to the

physical properties of bulk saturated liquid nitrogen, and the parameters for the adsorbate-adsorbent potential are fitted to the monolayer uptake region of the nitrogen adsorption isotherm on a nonporous graphitized carbon black. The gas-solid potential parameters obtained in the DFT model for nitrogen adsorption at 77 K were σ_{sf} = 3.49 Å and ε_{sf}/k = 53.2 K. By converting the parameter values *NA* and *d* in equation (4.3) to their Lennard-Jones potential equivalents as written in equation (4.9), one recovers σ_{sf} = 3.20 Å and ε_{sf}/k = 21.3 K as the values used in the original HK model. Thus, there is substantial disagreement in both the form of the potential and the values of the potential parameters used in previous comparisons of the HK and DFT pore filling correlations. The HK solid-fluid diameter is smaller than the DFT σ_{sf} value because a nitrogen molecular diameter of 3.0 Å was selected for the HK calculation [6]. This is an unusually small value for the nitrogen molecular diameter; it is generally accepted that diatomic nitrogen has an effective diameter that is larger than a carbon atom, with a value typically in the range 3.5 to 3.8 Å. The gas-solid well depth in the HK model is also smaller than that used in the DFT model; in this case, the ε_{sf} value for the HK method is only 40% of the fitted DFT well depth. This amplifies into a large difference between the HK and DFT micropore filling pressures because the filling pressure varies exponentially with the free energy change on adsorption in equation (4.1).

(3) *The adsorbate-adsorbate interaction energy is not calculated correctly in the original HK model.* Four conceptual flaws have been identified in the derivation of the original HK pore filling correlation shown in equation (8). First, there is a factor of two error in the Kirkwood-Muller formula reported in the original HK paper for the adsorbate

dispersion coefficient (equation (4.6)). The correct formula for A_{ff} is noted by Muller [see the appendix of reference 21] and should read as

$$A_{ff} = 3mc^2 \alpha_f \chi_f \qquad 4.10$$

A second error related to the adsorbate-adsorbate energy contribution is that the adsorbate pair interaction should be *subtracted* from the adsorbate-adsorbent interaction, rather than added to it as is done in the original HK method. The concept, first put forth in the FHH adsorption theory, is that the excess free energy change of adsorption is equal to the difference in the interaction energy of the adsorbate molecule with the slab of adsorbent, *less* the adsorbate interaction energy with a similar slab of pure adsorbate [7]. In effect, one must remove a slab of adsorbate and replace it with a similarly-shaped slab of the solid adsorbent to obtain the correct free energy change due to adsorption. In the original HK treatment, however, the two free energies are not subtracted from one another but instead are added together. No justification is given for summing the interaction energies rather than taking the difference. Using the values reported in the original HK paper for the monolayer densities and dispersion coefficients, the HK potential parameters are given by equations (4.5) and (4.6) as $N_s A_{sf} = 3.50 \times 10^{-18}$ J Å^4 for the adsorbate-adsorbent potential and $N_f A_{ff} = 2.40 \times 10^{-19}$ J Å^4 for the adsorbate-adsorbate potential [6]. Since the adsorbate-adsorbate parameter is about 7% of the magnitude of the adsorbate-adsorbent parameter, the error in the size and sign of the adsorbate pair potential term in equation (4.7) slightly changes the HK pore filling correlation. Using the FHH form of the free energy difference $NA = N_s A_{sf} - N_f A_{ff}$, with A_{ff} given by equation (4.10), the corrected value of NA is 3.02×10^{-18} J Å^4, 19% less than the originally reported

HK value of 3.74×10^{-18} J $Å^4$ for nitrogen adsorption on a carbon surface. This correction actually shifts the HK pore filling correlation to higher condensation pressures, in greater disparity with the DFT correlation of Figure 4.1.

A third defect of the original HK method is the *ad hoc* manner in which the adsorbate-adsorbate potential is modeled. Equation (4.7) implies that the adsorbate pair interaction energy can be calculated by placing the adsorbate molecules in the same region of space occupied by the solid adsorbent atoms. This is physically unrealistic, since pairwise adsorbate energetic contributions must clearly arise from adsorbate molecules situated within the accessible volume of the slit pore, and not within the slab wall. The original HK paper gives no explanation for superimposing the adsorbate-adsorbent and adsorbate-adsorbate interactions onto exactly the same 10-4 potential, aside from a nonspecific reference to the latter as being "an implicit function of the adsorbate-adsorbate-adsorbent interactions" [6].

A possible fourth shortcoming of the adsorbate-adsorbate energy calculation in the original HK method is that the mean free energy change due to adsorption is calculated from an unweighted average over the accessible volume of the micropore. It is known from molecular simulation studies that the local adsorbate density in the pore varies strongly with position due to fluid layering near the pore walls. In particular, the contact layer or monolayer is highly structured because it adsorbs within the large energy well that is present in both the 10-4 and the 10-4-3 potential at a distance of one molecular diameter from the pore wall. Other fluid layers similarly are not uniform, but occupy discrete positions within the pore, giving rise to a structured local density profile that is oscillatory. By neglecting the high degree of ordering in the adsorbed fluid, and in

particular by undercounting the adsorbate density in the monolayer region, the HK method, as originally posed, underestimates the mean heat of adsorption computed by equation (4.2), and thus overestimates the micropore filling pressures calculated from equation (4.1). Consequently, the PSD results obtained for the original HK model in equation (1.1) are less accurate than those given by DFT or molecular simulation.

Although several limitations of the HK method have been recounted here, the original HK concept should not be dismissed. The basic concept of the model is meritorious in that it attempts to relate the micropore filling pressure to the solid-fluid interaction potential. One method of improving the HK correlation that is suggested by the previous discussion is to represent the local density in the slit pore as a weighted profile rather than as an unweighted profile. If the mean free energy change upon adsorption is then calculated from an integration of the potential that is property weighted with respect to the local adsorbate density $\rho(z)$

$$\bar{\phi} = \frac{\int_{\sigma_{sf}}^{H-\sigma_{sf}} \rho(z)\phi(z)dz}{\int_{\sigma_{sf}}^{H-\sigma_{sf}} \rho(z)dz} \qquad 4.11$$

the HK pore filling correlation given by equation (4.1) should be in better agreement with the DFT and simulation results. In a recent paper, an improved HK pore filling correlation for argon adsorption in carbon slit pores at 77 K was reported in which the local density profile was represented by a sum of Gaussian distributions [22]. The Gaussian distribution modes were fitted with a uniform amplitude and variance; the shape parameter values were chosen so as to give the best agreement with local density profiles calculated from DFT over a range of micropore widths. It was found, using equation

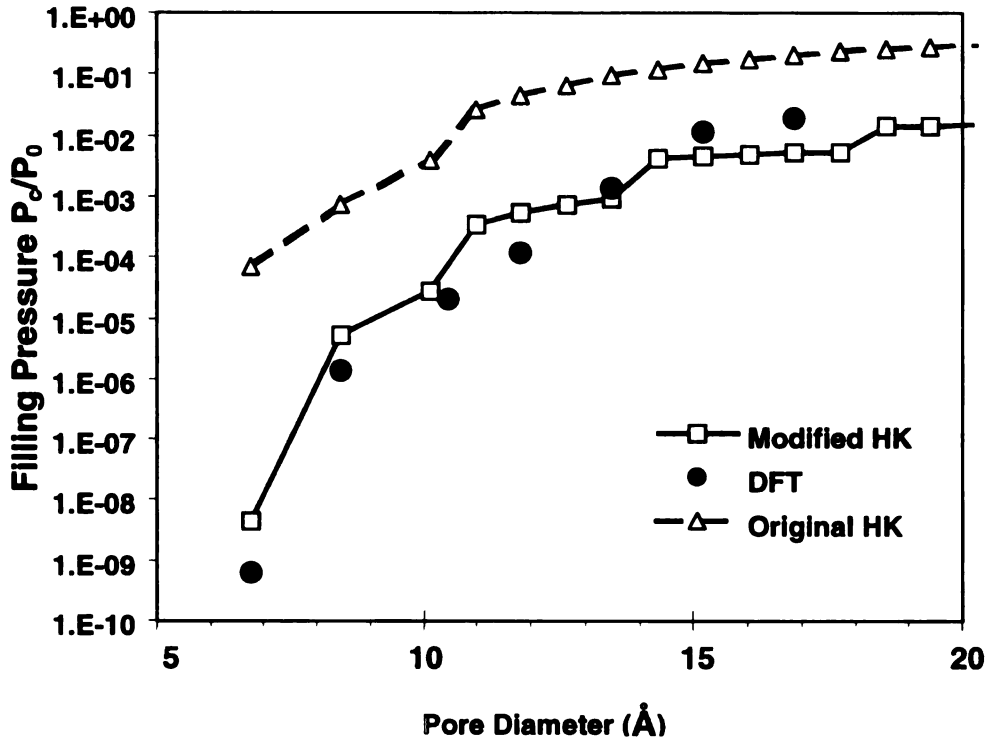

Figure 4.2: Comparison of pore filling correlations for argon adsorption in carbon slit pores at 77 K using DFT, the original HK method, and a modified HK method in which the local adsorbate density profile is represented as a sum of Gaussian distributions [22].

(4.4) for the interaction potential as in the original HK paper, that substituting the weighted local density profile in place of the unweighted density profile improved the agreement between the HK and DFT pore filling correlations (Figure 4.2). However, a general method of calculating the Gaussian shape parameters of the local density profile from the adsorbate-adsorbent physical properties was not reported in this work.

In this paper, a generalized HK method is described for the PSD analysis of adsorbents that have slit-shaped pores. Methods of calculating the micropore filling pressure correlation for the unweighted and weighted local density assumption are presented. A comparison of the HK and DFT predictions is also reported for the first time using the same adsorbate-adsorbent potential (the 10-4-3 potential) and the same potential parameter values in the comparison. By representing the gas-solid interactions equivalently in both adsorption models, a truer comparison of the models is achieved.

4.3 Description of Generalized HK Method

In the generalized HK model, the filling pressure of a micropore is determined exclusively from the characteristic temperature $T^* = kT/\varepsilon_{ff}$ and solid-fluid potential strength $E^* = \varepsilon_{sf}/\varepsilon_{ff}$ of the adsorbate-adsorbent system. A description of the generalized adsorption model follows.

Solid-fluid interaction potential: The adsorbate-adsorbent interactions are modeled using a 10-4-3 potential in which there is a single characteristic molecular diameter σ, that of the adsorbate molecule. With this approximation, $\sigma_{sf} = \Delta = \sigma$ and the 10-4-3 potential of equation (4.8) reduces to

$$\phi^*(z^*) = \frac{\phi}{\varepsilon_{ff}} = 2\pi E^* \rho_s^* \left[\frac{2}{5}(z^*)^{-10} - (z^*)^{-4} - \frac{1}{3}(z^* + 0.61)^{-3} \right] \qquad 4.12$$

where $z^* = z/\sigma$ and $\rho_s^* = \rho_s \sigma^3 = 5.2$ for graphitic carbon [20]. The simplification in the 10-4-3 potential per equation (4.12) is justified on the grounds that, for most probe gases used to characterize the PSDs of activated carbons, the adsorbate molecular diameter is nearly equal in size to the carbon atom spacing in the porous solid. For example, for nitrogen as the probe gas and graphitic carbon as the adsorbent, $\sigma = 3.57$ Å and $\sigma_{sf} = 3.49$ Å $= 0.98\sigma \cong \sigma$ [23]. Helium is a notable exception to this rule; however, this is not a concern in the development of our adsorption model because helium is usually employed to characterize the pore volume of the adsorbent, rather than the pore size distribution.

The adsorbate-adsorbate potential is not included in the calculation of the HK pore filling correlation presented in this dissertation. As noted in the introductory section, the adsorbate-adsorbate interaction is erroneously interpreted in the original HK model. In the absence of a suitable method of correcting this defect, the adsorbate pair interaction energy is simply excluded from the free energy calculation. This decision is justified on the grounds that the adsorbate-adsorbate potential is relatively small compared with the adsorbate-adsorbent potential, and thus it is the gas-solid interaction energy that primarily determines the filling pressure of a micropore.

With the imposed uniformity of the adsorbent layer spacing to match the adsorbate molecular diameter, the conditions of the adsorbate-adsorbent system are described by two only independently variable parameters, the dimensionless solid-fluid potential strength E^* and the dimensionless temperature T^*.

Unweighted density representation: In the unweighted HK method, the local adsorbate density in the slit pore is assumed to be uniform everywhere in the accessible volume of the pore. The accessible pore volume is defined as the region of the pore where the solid-fluid potential has a negative value; i.e. where there is a net attractive interaction between the adsorbate molecule and the adsorbent surface. The local density profile in the unweighted density approach is therefore represented as $\rho(z) = \rho_{av}$ for $d < z < H - d$; and $\rho(z) = 0$ for $z < d$ and $z > H - d$, where $d \cong 0.851\sigma$ is the distance from the surface at which the 10-4-3 potential has a zero energy. The unweighted HK model thus yields an analytic equation for the mean free energy change of adsorption:

$$\begin{aligned}\bar{\phi}^* &= \frac{\int_{d^*}^{H^*-d^*} \rho_{av}\phi^*(z^*)dz^*}{\int_{d^*}^{H^*-d^*} \rho_{av}dz^*} \\ &= \frac{2\pi E^* \rho_s^*}{H^*-2d^*}\left\{\frac{4}{45}\left[(d^*)^{-9} - (H^*-d^*)^{-9}\right]\right. \\ &\left. + \frac{2}{3}\left[-(d^*)^{-3} + (H^*-d^*)^{-3}\right] + \frac{1}{3}\left[-(d^*+0.61)^{-2} + (H^*-d^*+0.61)^{-2}\right]\right\}\end{aligned} \qquad 4.13$$

The adsorption isotherm $\Gamma(P,H)$ is then calculated as

$$\Gamma(P,H) = 0 \qquad \text{for } P < P_c$$

$$\Gamma(P,H) = \rho_{av}(H - 2d)/H \qquad \text{for } P > P_c \qquad 4.14$$

where $P_c = P_0 \exp\left(\bar{\phi}^*/T^*\right)$ is the filling pressure for a pore of width H calculated from equations (4.1) and (4.13). The unweighted density $\rho_{av}(T^*, E^*)$ is obtained from a correlation to DFT results as described later in this section. Note that in both the unweighted and the weighted HK model, the specific excess adsorption is assumed to be

equal to the absolute amount adsorbed, because for temperatures that are well below the bulk adsorbate critical temperature, the gas-phase adsorbate density is very small.

Weighted density representation: In the density-weighted HK method, the local adsorbate density profile in the slit pore is modeled as an n-modal Gaussian distribution

$$\rho(z)=\sum_{i=1}^{n} A_i \exp\left[\frac{-(z-\mu_i)^2}{2V_i^2}\right] \qquad 4.15$$

where A_i, V_i, and μ_i are the amplitude, variance, and mean position, respectively, of mode i of the distribution. Two types of Gaussian curves are used in the model. Peaks in the local density profile that correspond to an adsorbed layer that is in contact with a wall are represented by Gaussian curves with amplitude A_m and variance V_m. Local density maxima that are not adjacent to a pore wall are represented by Gaussian curves with amplitude A_c and variance V_c. The selection of a Gaussian distribution with two distinct types of distribution curves to describe the local density profile is based upon two considerations.

First, it is known, from molecular simulations and from DFT calculations, that an adsorbed fluid is strongly structured by the presence of the adsorbent surface. A confined adsorbed fluid thus exhibits a local density profile with an oscillatory structure that decays toward a bulk-like fluid density (if the pore is sufficiently large) at the pore centerline. The effect of this ordering is represented in the weighted HK model by the spacing of the Gaussian distribution modes. Second, by virtue of the short-ranged dispersion forces near the adsorbent surface, the contact layer of adsorbed fluid is much more highly ordered than interior layers of adsorbate that are not in direct contact with the pore wall. This difference in the ordering of the contact and interior adsorbate layers is

acknowledged by assigning different parameters to describe the shape of the contact and interior peaks of the local density profile. The quartet of shape parameters (A_m, V_m; A_c, V_c) are fitted to a two-parameter correlation of the dimensionless temperature T^* and dimensionless solid-fluid potential well depth E^* using local density profiles obtained from DFT for adsorption on a "nonporous" surface (see next section for a description of the fitting method).

The number of modes n used to represent the local density profile is determined from the physical width of the slit pore according to the pair of formulas

$$n = \text{int}(H/\sigma) - 1 + \Theta(f) \qquad 4.16$$

$$f = H/\sigma - \text{int}(H/\sigma) \qquad 4.17$$

where int(x) is the truncated integer value of x, and Θ is the Heaviside step function: $\Theta(x) = 0$ for $x \leq 0$, and $\Theta(x) = 1$ for $x > 0$. The above equations mathematically express the simple rule that, for pore widths that are non-integer ratios of the molecular diameter σ, an additional mode is added to represent the local density profile. For example, for $H = 2.0\sigma$, a unimodal distribution is used; for $H = 2.5\sigma$, a bimodal distribution; and for $H = 3.1\sigma$, a trimodal distribution.

The *positions* μ_i of the distribution modes are assigned according to the following rules:

For $n = 1$ ($H \leq 2\sigma$), the Gaussian curve is centered in the middle of the slit pore, so that the density profile attains its maximum at position $\mu_1 = H/2$.

For $n = 2$ ($2\sigma < H \leq 3\sigma$), the two distribution modes are centered at $\mu_1 = \sigma$ and $\mu_2 = H - \sigma$, respectively.

For $n = 3$ ($3\sigma < H \leq 4\sigma$), the contact peaks of the distribution are centered at $\mu_1 = \sigma$ and $\mu_2 = H - \sigma$, and the interior peak is centered at $\mu_3 = H/2$.

For $n = 4$ ($4\sigma < H \leq 5\sigma$), the interior peaks are spaced a distance of one adsorbate diameter from the adjacent contact layer peaks; i.e. the positions of the maxima are at $\mu_1 = \sigma$, $\mu_2 = H - \sigma$, $\mu_3 = 2\sigma$, and $\mu_4 = H - 2\sigma$.

For an *odd* number of peaks $n > 4$, the nth peak is placed on the centerline of the pore (i.e. $\mu_n = H/2$). The other peaks are spaced at intervals of one adsorbate diameter from the pore walls at $z = 0$ and $z = H$; i.e. peaks 1 through n-1 placed in pairs at positions $(\mu_k, \mu_{k+1}) = (j\sigma, H - j\sigma)$, where $j = (k+1)/2$.

For an *even* number of peaks $n > 4$, the peaks are placed in pairs at coordinates (σ, $H - \sigma$), (2σ, $H - 2\sigma$), ... ($j\sigma$, $H - j\sigma$), in successive spacings one adsorbate diameter removed from the pore walls at $z = 0$ and $z = H$.

This simple placement algorithm yields density profiles that have peak positions that match those obtained from DFT calculations in pores that contain an odd or even number of density profile maxima. The *amplitudes* A_i of the Gaussian distribution modes are determined according to the following formula:

For $n = 1$, the amplitude of the peak is given as $A_1 = f A_m$, where f is the fractional dimensionless pore width given in equation (18). Thus, for $H = 2.0\sigma$, $A_1 = A_m$, whereas for $H = 1.8\sigma$, $A_1 = 0.8A_m$.

For $n = 2$, the peak amplitudes are calculated as $A_1 = A_2 = (1+f)A_m/2$. For example, for $H = 3.0\sigma$, $A_1 = A_2 = A_m$, whereas for $H = 2.6\sigma$, $A_1 = A_2 = 0.8A_m$.

For $n = 3$, the amplitude of the contact peaks are $A_1 = A_2 = A_m$, and the amplitude of the interior peak $A_3 = f A_c$.

For $n = 4$, the contact peaks have amplitudes $A_1 = A_2 = A_m$, and the interior peaks have amplitudes $A_3 = A_4 = (1+f)A_c/2$.

For an *odd* number of peaks $n > 4$, the contact layer peaks have amplitudes $A_1 = A_2 = A_m$; and the n-th interlayer peak (the one positioned on the pore centerline) has an amplitude $A_n = f A_c$. The other interlayer peaks have amplitudes equal to A_c.

For an *even* number of peaks $n > 4$, the contact peaks have amplitudes $A_1 = A_2 = A_m$; the two innermost interior peaks (i.e. those closest to the pore centerline) have amplitudes given as $A_{n-1} = A_n = (1+f)A_c/2$; and the other interior peaks each have an amplitude of A_c.

This algorithm for assigning the peak amplitudes ensures that, as additional distribution modes are added for larger pore widths, the shape of the weighted local density profile changes smoothly for increasing pore size. In a previous version of the density-weighted HK method, an additional full-size peak was added each time the pore width ratio exceeded a half-fractional molecular diameter (i.e. at $H = 2.5\sigma$, 3.5σ, 4.5σ, and so on) [22]. This previous weighting scheme, however, produced discontinuous jumps in the HK pore filling correlation, whereas the current density-weighting scheme avoids such discontinuities.

Finally, the variances V_i of the Gaussian distribution modes are assigned as follows. For $n \leq 2$, the peak variances are set equal to V_m. For $n > 2$, the contact layer peak variances are $V_1 = V_2 = V_m$, and all interior layer peaks have a variance equal to V_c.

The adsorption isotherm $\Gamma(P,H)$ for the weighted HK method is calculated as

$$\Gamma(P,H) = 0 \qquad \text{for } P < P_c$$

$$\Gamma(P,H) = \int_d^{H-d} \rho(z)dz \Big/ H \qquad \text{for } P > P_c \qquad 4.18$$

where P_c is the filling pressure for pore width H calculated from equations (4.1) and (4.11).

Fitting of Local Density Model Parameters: The unweighted local density model parameter ρ_{av} was fitted to a bivariate logarithmic correlation of the form

$$\rho_{av}(T^*, E^*) = (a_0 + a_1 \ln(T^*))(b_0 + b_1 \ln(E^*)) \qquad 4.19$$

where (a_0, a_1, b_0, b_1) are the set of fitted coefficients (Table 4.2). The Gaussian shape parameters (A_m, V_m; A_c, V_c) used for the density-weighted representation of the local density profile were each fitted to a correlation of the same form as given above. The correlation coefficients were chosen so as to yield the best possible agreement with condensed-phase local density profiles calculated from DFT for adsorption in a slit pore of width $H = 20\sigma$ at the saturation pressure P_0. This pore width is sufficiently large so that adsorbate molecules that are adsorbed at or near one pore wall are far removed from, and essentially do not interact with, the other wall of the slit pore. Thus, adsorption in the $H = 20\sigma$ pore is effectively equivalent to adsorption on a nonporous surface. The local density profiles calculated from DFT for adsorption in the $H = 20\sigma$ pore can therefore be used to develop correlations of the local adsorbate density on isolated planar surfaces.

Table 4.1: Fitted parameters for unweighted and weighted local density models.

Parameter	a_0	a_1	b_0	b_1
ρ_{av}	-1.2	2.02	0.12	3.45
A_m	-0.5	1.08	3.48	7.66
V_m	0.4	0.98	-0.0	0.03
A_c	-0.5	0.37	3.00	7.26
V_c	0.0	0.02	-4.71	4.64

Nineteen density profiles were compiled from DFT over a range of temperatures $0.60 \leq T^* \leq 1.0$ and solid-fluid potential well ratios $0.32 \leq E^* \leq 0.96$. As shown in Table 4.2, this range encompasses the (E^*, T^*) values of most of the probe gases used for PSD analysis of adsorption isotherms measured at 77 K or 273 K. A detailed description of the DFT adsorption model used in this work has been reported in section 2.2 [24]. All of the DFT density profiles were calculated using a grid spacing interval of 0.01σ in the z coordinate for the numerical solution of $\rho(z)$. Indistinguishable results were obtained for grid spacings of 0.005σ, 0.01σ and 0.02σ.

The DFT local density profile in the $H = 20\sigma$ pore at $T^* = 0.70$ and $E^* = 0.80$ is shown in Figure 4.3. To fit the correlation of the unweighted local density as a function of T^* and E^*, the value of ρ_{av} that represents the mean density in the slit pore is determined for each (T^*, E^*) pair. Graphically, this is the height that gives the rectangular region shown in Figure 4.1 the same area as the area under the DFT local density profile. The ρ_{av} values obtained from the DFT results are reported in Figure 4.4. A least-squares optimization was performed to find the set of (a_0, a_1, b_0, b_1) coefficients

Table 4.2: Dimensionless solid-fluid potential and temperature for probe gases on graphite.

Adsorbate	E^*	T^*
Ar	0.526	0.702
C_6H_6	0.252	0.621
CO_2	0.235	0.541
CF_4	0.429	0.954
He	1.441	0.406
H_2	0.801	0.482
Kr	0.389	0.708
CH_4	0.435	0.754
N_2	0.566	0.823
Xe	0.360	0.747

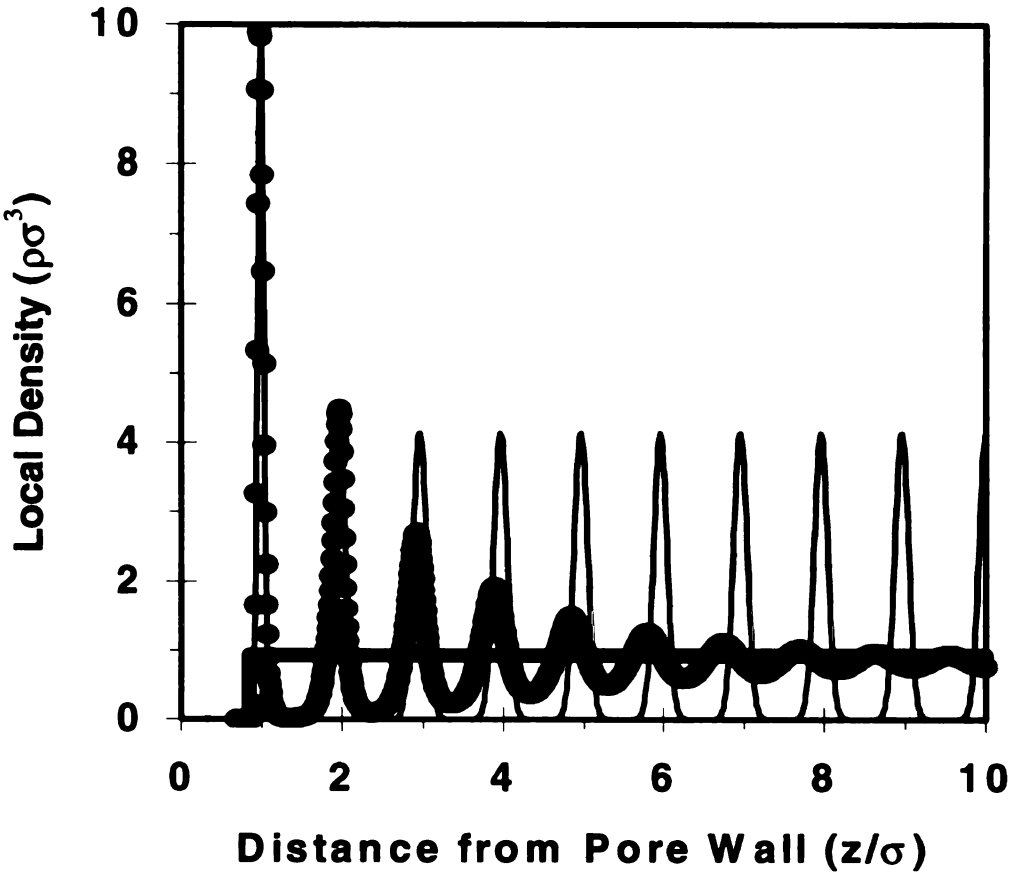

Figure 4.3: Local density profile at the saturation pressure calculated from DFT (points) for a slit pore of width H^*=20 filled with condensate at T^*=0.70 and E^*=0.80. For clarity, only the region from the left-hand wall to the pore centerline is shown; the density profile is symmetric across the centerline of the pore axis. The lines show the fitted profiles at this set of conditions using the unweighted (horizontal line) and weighted density model.

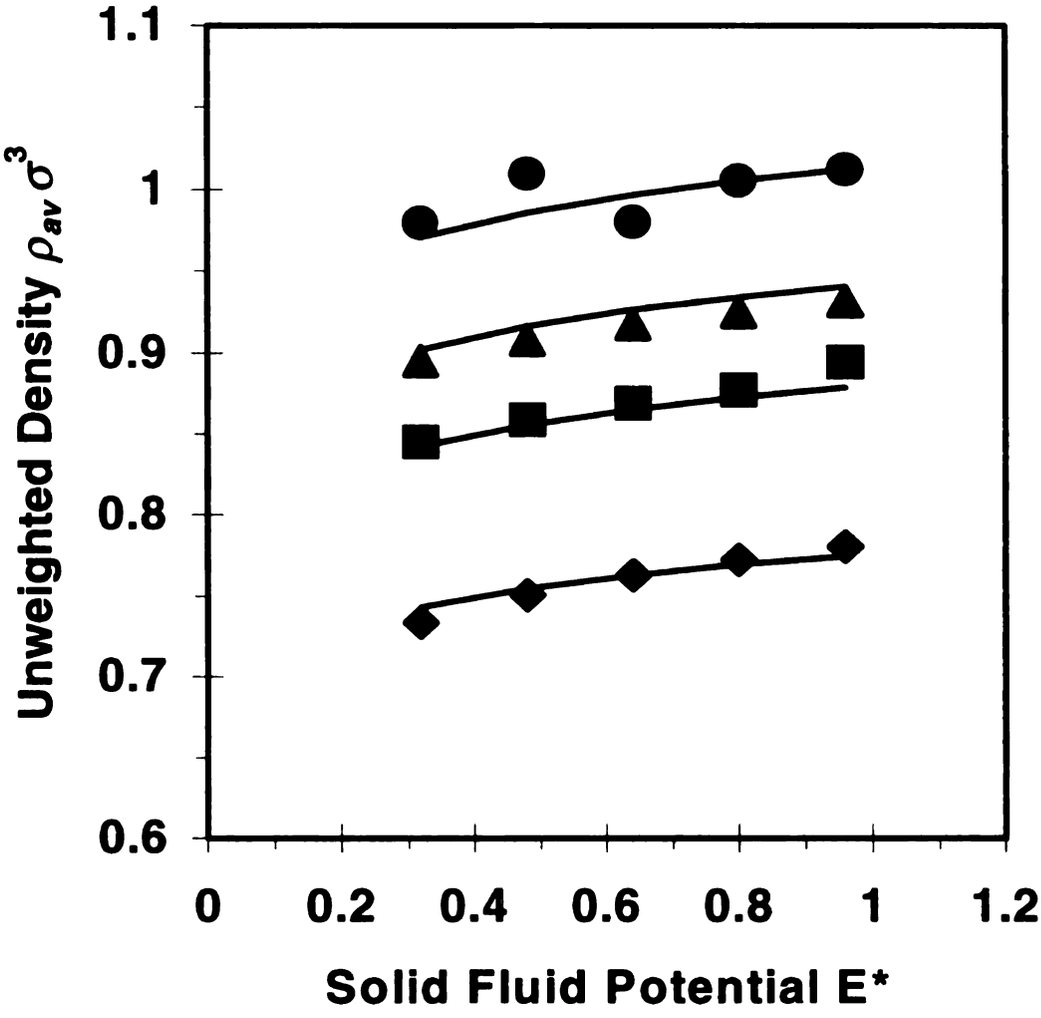

Figure 4.4: Local densities (points) obtained from an unweighted fit of DFT density profiles at T^*=0.60 (circles), 0.70 (triangles), 0.80 (squares), and 1.00 (diamonds) over a range of E^* values. The lines show the fitted bivariate logarithmic correlation of the unweighted local density for the corresponding set of temperatures.

that best reproduces the $\rho_{av}(T^*, E^*)$ correlation. The fitted coefficients are reported in Table 4.1 and the best-fit correlation results are shown as the lines in Figure 4.4.

To fit the Gaussian shape parameters for the density-weighted HK model, the amplitude and variance of the contact layer Gaussian peak (A_m and V_m) were first fitted to match as closely as possible the height and weight of the contact peak obtained in each DFT calculation. The variance V_c of the interior layer (condensate) peak was next chosen so as to reproduce the width of the second layer DFT peak (i.e. the peak in the local density profile adjacent to the contact layer). Finally, the amplitude A_c of the interior layer peak was assigned so that the integrated areas under the DFT and weighted Gaussian density profiles (see Figure 4.3) were the same. The Gaussian parameters (A_m, V_m; A_c, V_c) obtained by fitting the DFT results are shown in Figures 4.5(a-d), and the logarithmic correlation coefficients and correlation results are reported in Table 4.2 and shown in Figure 4.5, respectively. The unweighted and weighted model shape parameters are all well fit using the bivariate logarithmic correlation which has four adjustable coefficients.

4.4 Results

Micropore Local Density Profiles: Using the set of correlation coefficients reported in Table 4.2, local density profiles were computed using the density-weighted sum-of-Gaussians model for a set of micropores ranging in size between $H = 2\sigma$ and 6σ. A comparison of the local density profiles predicted by the weighted density model, and those calculated from DFT at the saturation pressure, is shown in Figure 4.6 for six

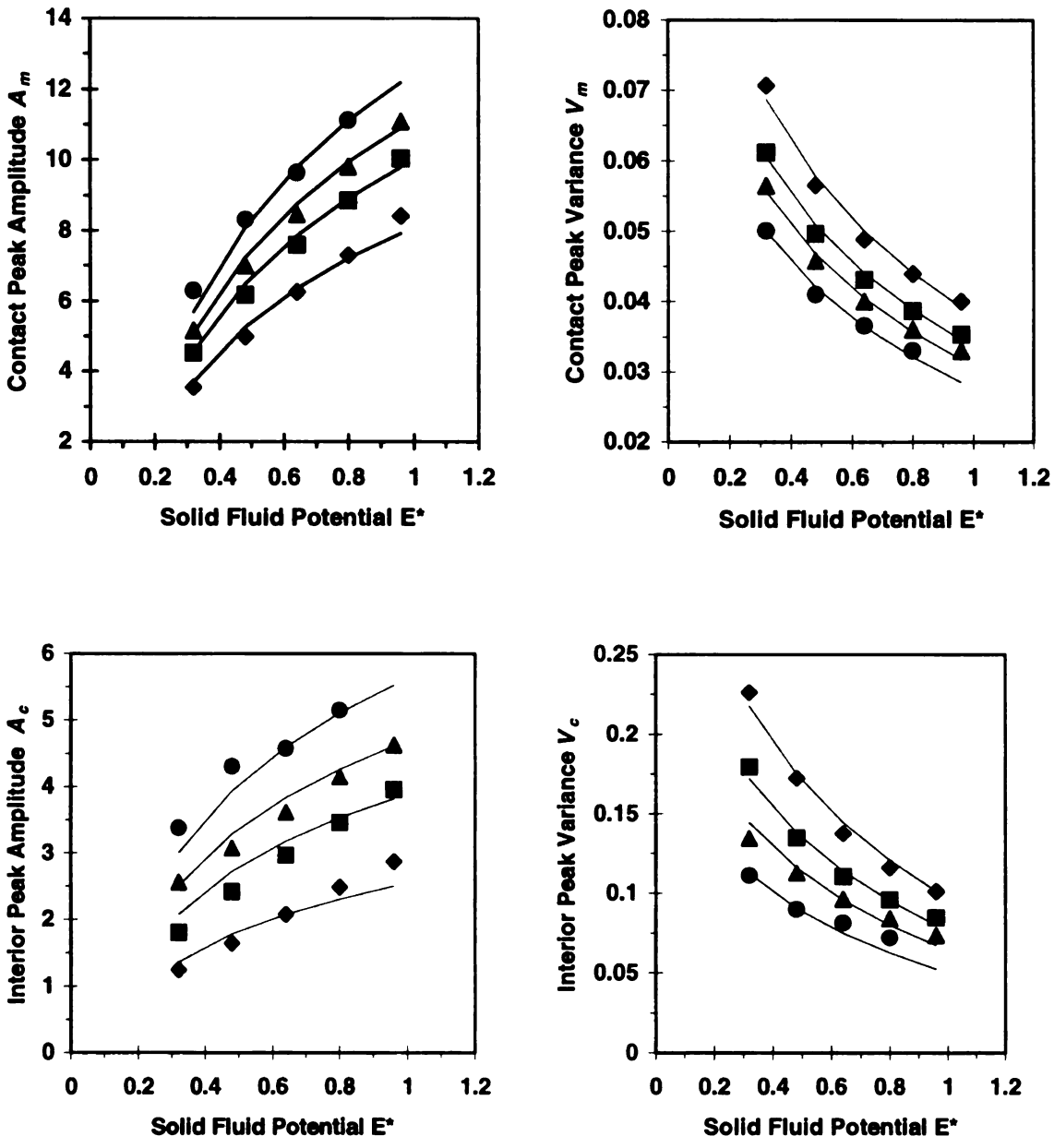

Figure 4.5: Contact layer and interior layer peak heights and variances (points) obtained from a density-weighted fit of DFT density profiles, and fitted two-parameter correlations (lines) of the peak heights and variances. The symbols denote the same temperatures as in Figure 4. (a). Contact peak height. (b). Contact peak variance. (c). Interior peak height. (d). Interior peak variance.

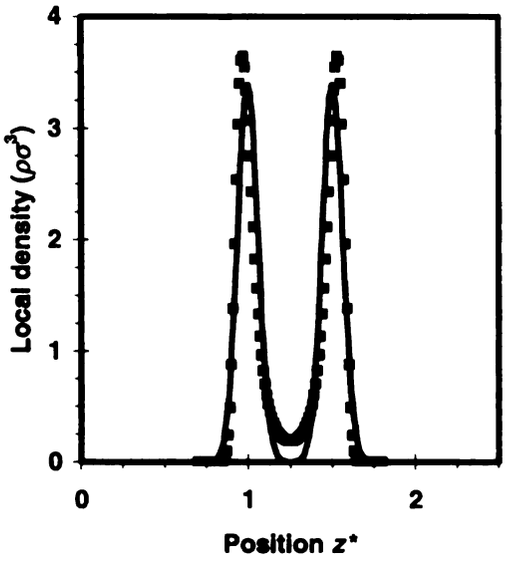

Figure 6a

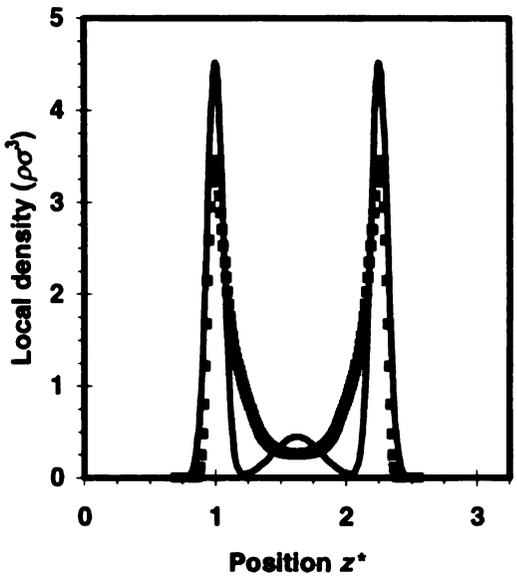

Figure 6b

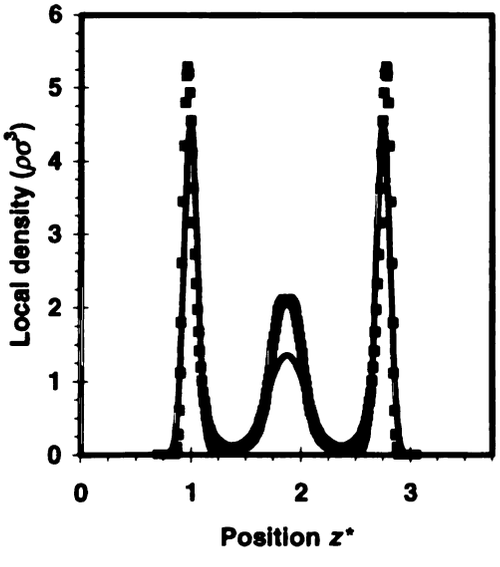

Figure 6c

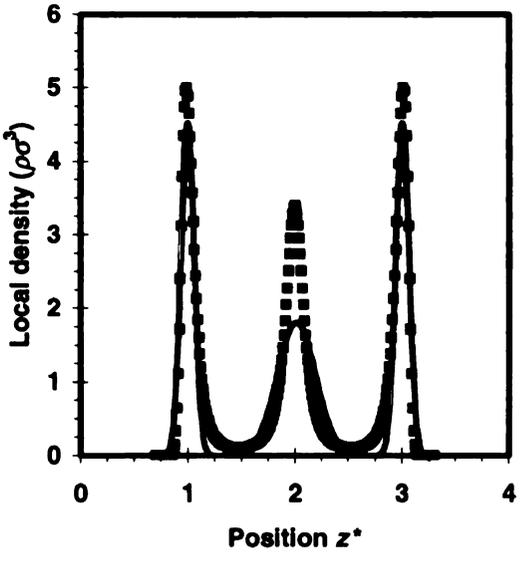

Figure 6d

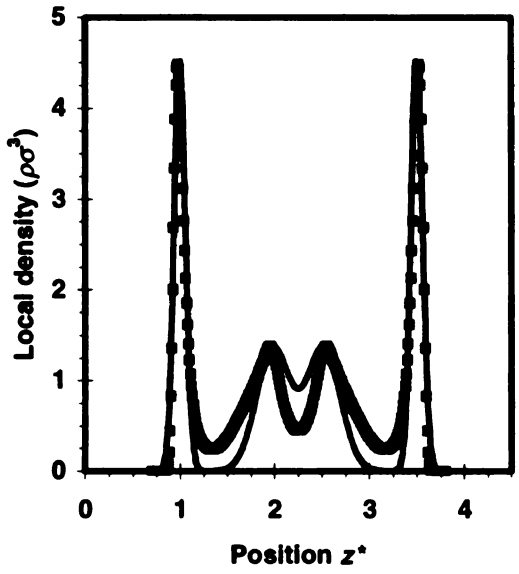

Figure 6e

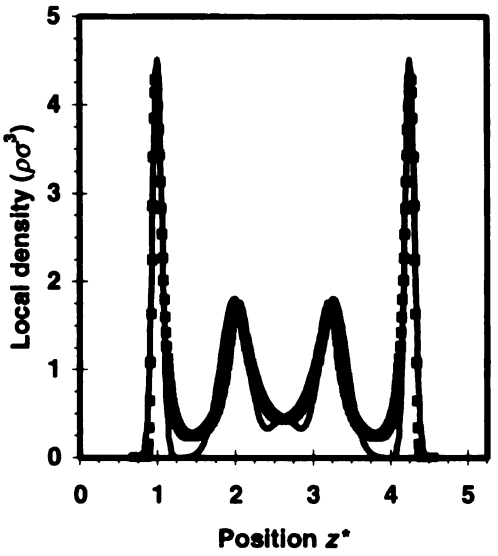

Figure 6f

Figure 4.6: Comparison of local density profiles calculated from DFT (points) and from the density-weighted model (lines) for adsorption in microporous slits at T^*=0.80 and E^*=0.32. (a). H^*=2.5. (b). H^*=3.25. (c). H^*=3.75. (d). H^*=4. (e). H^*=4.5. (f). H^*=5.25.

different pore sizes at T^*=0.80 and E^*=0.32. It can be seen that the DFT local density profiles are reasonably well approximated by the sum-of-Gaussians model over the full range of micropore widths. The best agreement is generally obtained for slit widths that are an integral multiple of the molecular diameter σ. However, the weighted-density model also reproduces the local density profile in pore sizes that are not integral multiples of σ surprisingly well, considering that the density-weighted model algorithm contains only four Gaussian shape parameters.

Comparison of Pore Filling Correlations: Using the unweighted and weighted model representations of the local adsorbate density profile, pore filling correlations were calculated using the HK method to estimate the mean heat of adsorption. The variation in the filling pressures for slit pores between 2σ and 6σ in width is shown for the unweighted HK model for adsorption at different temperatures T^* at fixed E^*=0.80 in Figure 4.7a, and for different wall potential strengths E^* at fixed T^*=0.8 in Figure 4.7b. The same set of results is reported for the weighted HK model in Figures 4.8a and b. As expected, the filling pressure for a given pore size is strongly dependent on the strength of the solid-fluid interaction potential, with a large decrease in filling pressure occurring as the value of E^* increases. The filling pressure is also sensitive, to a lesser extent, to the temperature at which adsorption occurs. As the value of T^* increases, both the filling pressure P and the saturation pressure P_0 increase, but the saturation pressure increases more rapidly with temperature, so the net effect is that the relative filling pressure P/P_0 decreases as T^* increases.

A comparison of the unweighted HK and weighted HK pore filling correlations for identical T^* and E^* values in Figures 4.7 and 4.8 reveals that the density-weighted

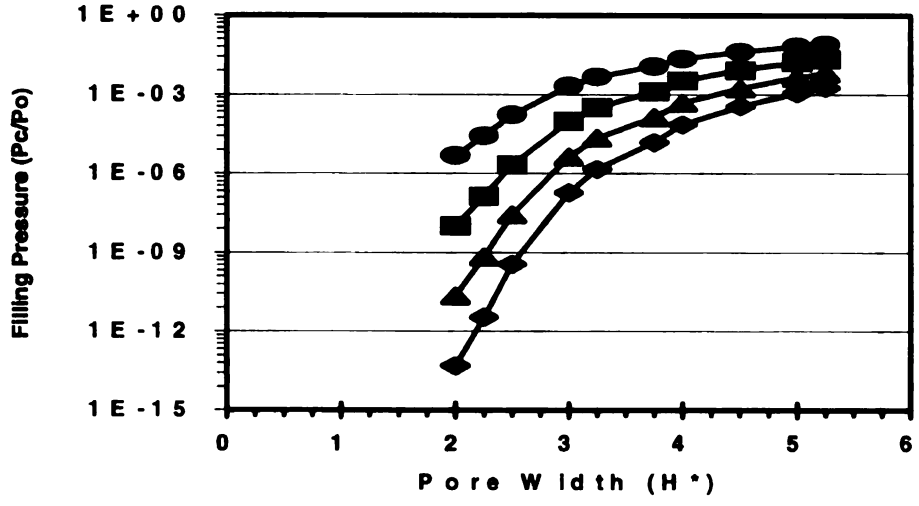

Figure 7a

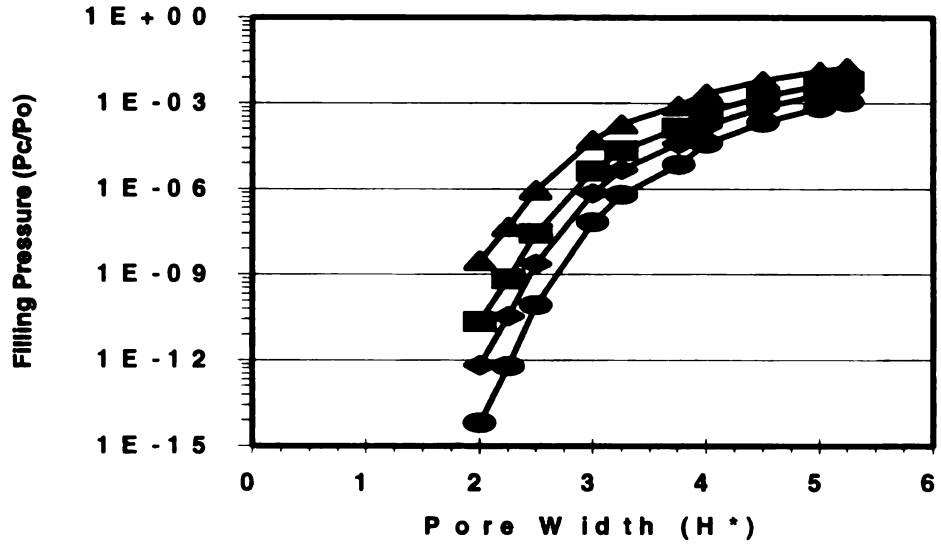

Figure 7b

Figure 4.7: Pore filling correlation for unweighted Horvath-Kawazoe method. (a). Correlation for E^*=0.32 (circles), 0.48 (squares), 0.64 (triangles), and 0.80 (diamonds) at fixed temperature T^*=0.80. (b). Correlation for T^*=0.60 (squares), 0.70 (diamonds), 0.80 (triangles), and 1.00 (circles) at fixed solid-fluid potential E^*=0.80. The lines serve as a guide to the eye.

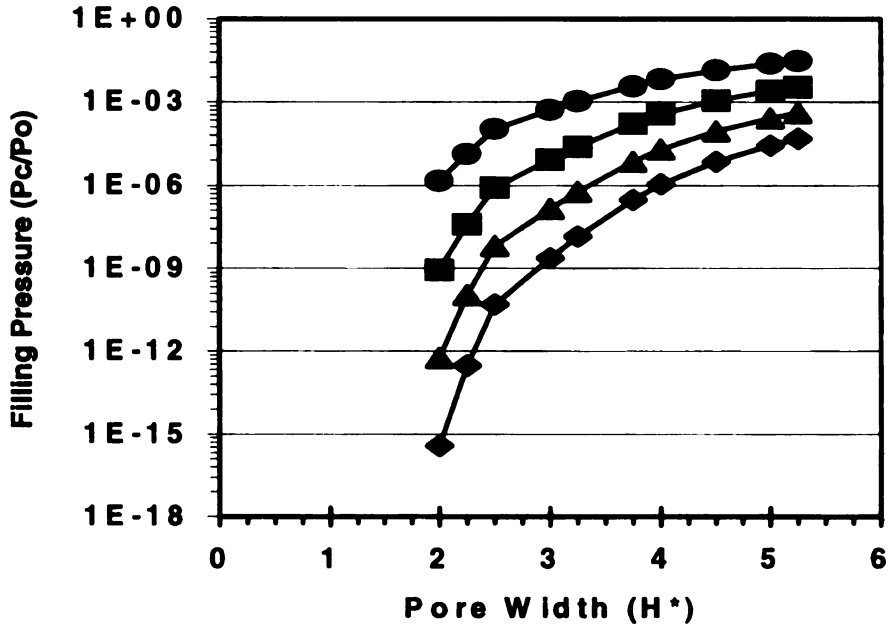

Figure 8a

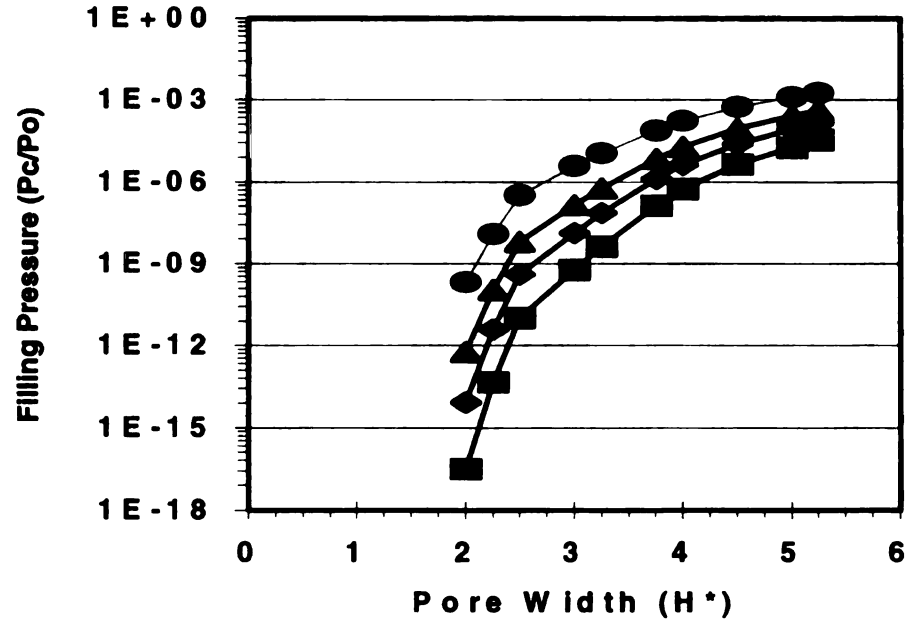

Figure 8b

Figure 4.8: Pore filling correlation for density-weighted Horvath-Kawazoe method. The notations and (T^*, E^*) values in parts (a) and (b) are the same as reported in Figure 4.7.

HK model predicts a lower filling pressure for a given pore width than does the unweighted HK model. This result is to be expected since the density-weighted model was specifically designed to account for the large local adsorbate density in the monolayer region adjacent to the pore wall. A comparison of the unweighted HK, weighted HK, and DFT pore filling correlations is presented for nitrogen adsorption at 77K in Figure 4.9a and for argon adsorption at 77 K in Figure 4.9b. The DFT pore filling correlations at 77 K for nitrogen [23] and argon [24] have been previously reported.

Interestingly, it is found that the unweighted HK adsorption model yields a pore filling correlation that is in relatively good agreement with the DFT correlation for both nitrogen and argon adsorption at 77 K. This finding contradicts previous comparisons of the DFT and HK pore filling models, in which the unweighted HK model overestimated micropore filling pressures relative to DFT. The previous comparisons, however, were carried out using different potentials, and different potential parameters, in the two models to represent the interactions between the adsorbate and the surface atoms. Specifically, the original HK method used the 10-4 potential, whereas DFT results were reported for the 10-4-3 potential. As noted earlier, the 10-4 potential does not include the dispersion interactions of the adsorbate with subsurface solid atoms in the pore walls, and hence predicts a smaller mean heat of adsorption than if the 10-4-3 potential is used. Furthermore, the solid-fluid potential well parameter ε_{sf} calculated using the Kirkwood-Muller formula in the original HK paper is considerably smaller than the ε_{sf} value that has been employed in recent DFT adsorption models. In the present analysis, both the DFT and the HK model results are calculated using the 10-4-3 potential, with the same ε_{ff} and ε_{sf} values, to represent the solid-fluid interaction. The only difference in the solid-fluid

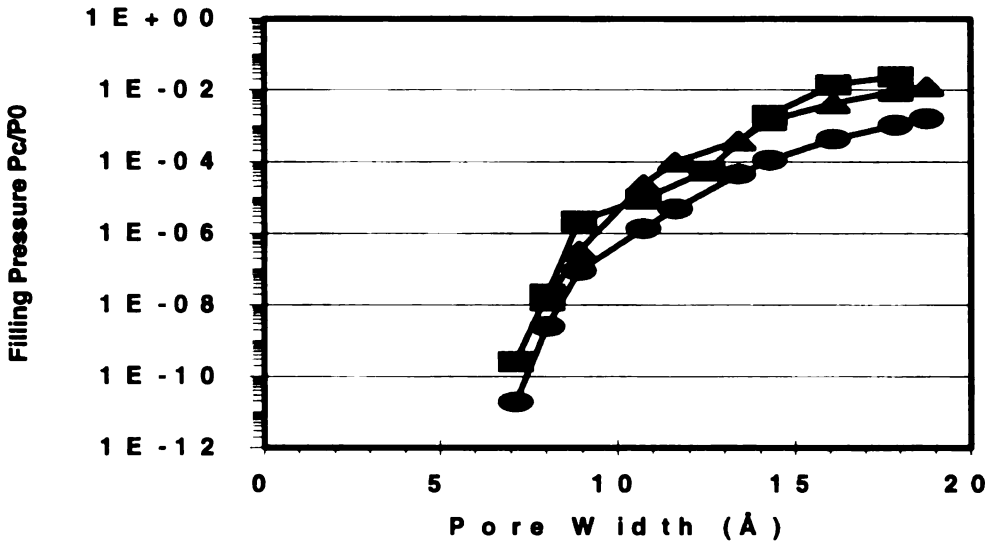

Figure 9a

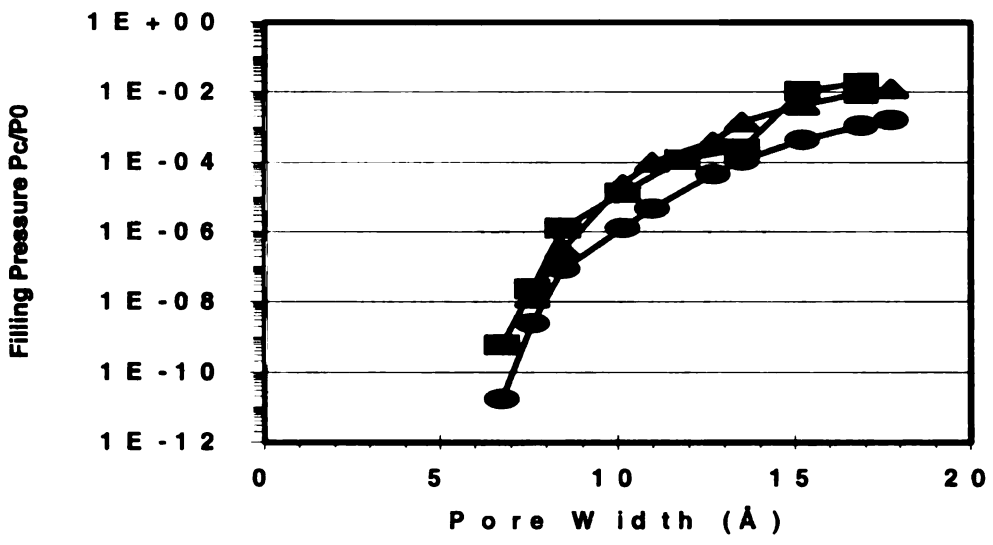

Figure 9b

Figure 4.9: Comparison of pore filling correlations calculated from DFT (squares), the unweighted HK method (triangles), and the density-weighted HK method (circles) for adsorption of (a). nitrogen and (b). argon in carbon slit pores at 77 K. The temperature and solid-fluid potential values used to calculate the pore filling correlations are T^*=0.823, E^*=0.567 for nitrogen and T^*=0.702, E^*=0.526 for argon.

potentials used for DFT and for the HK method in Figure 4.9 is that for DFT, the 10-4-3 potential of equation (9) is used, with $\sigma_{sf} = (\sigma_{ss} + \sigma_{ff})/2 = (3.40\ \text{Å} + \sigma)/2$, and $\Delta = 3.35$ Å; whereas in the unweighted and weighted HK models, the simplified potential of equation (13), with $\sigma_{sf} = \Delta = \sigma$, is employed. This results in a small difference in the solid-fluid potentials for the DFT and HK calculations. Nonetheless, the comparison between the DFT and HK pore filling models in this work is a purer comparison of the adsorption models themselves, rather than of the potentials used in the models

Another somewhat surprising result observed in Figures 4.9a and b is that the density-weighted HK pore filling model is in poorer agreement with the DFT model than the unweighted HK model. Because of the good representation of the local adsorbate density profile obtained using a weighted sum of Gaussians (Figure 4.6), one would expect the density-weighted HK pore filling correlation to agree more closely with the DFT predictions than the unweighted HK correlation. The density-weighted HK model, however, consistently underestimates the pore filling pressure relative to DFT for all micropore widths for both nitrogen and argon adsorption. The unweighted HK correlation, by contrast, overlaps the DFT correlation reasonably well for both of the probe gases.

4.5 Discussion

It should be noted that, although the filling pressure correlation of the unweighted HK model closely matches that of the DFT model, the adsorption isotherms constructed from DFT and from the HK method for a specific pore size are dissimilar, particularly for mesoporous slits. In the HK method, a steplike adsorption mechanism is assumed in

which a pore is completely empty at pressures below its filling pressure, and completely filled with adsorbate at pressures above its filling pressure. Figure 4.10 shows a comparison of the nitrogen adsorption isotherms predicted by the unweighted HK, weighted HK, and DFT models in slit pores of width $H = 3\sigma$ and $H = 5\sigma$ at 77 K. For the case of the weighted HK model isotherm, the phase transition always occurs at a lower pressure than in the counterpart DFT isotherm; whereas for the unweighted HK model, the condensation pressure may lie slightly above or below the DFT filling pressure, as indicated by Figure 4.9. Note that the HK-based model isotherms in Figure 4.10 do not exhibit an increase in adsorbate density above the filling pressure due to compression of the condensed fluid as P/P_0 increases. The more accurate DFT adsorption model accounts for the adsorbate compressibility, and also correctly predicts the formation of a precondensation film or monolayer prior to capillary condensation in slits that are larger than 3.5σ in width. The increased realism of the DFT adsorption model comes, however, at the expense of an increased computational effort needed to assemble the requisite set of isotherms to carry out adsorbent PSD analysis.

Pore Size Distribution Comparison: To illustrate that different results are obtained for the adsorbent PSD based on the choice of adsorption model, the unweighted HK, weighted HK, and DFT pore filling models were each used to interpret the PSD of an Aldrich powdered activated carbon. The adsorption isotherm of the activated carbon for nitrogen adsorption at 77 K is shown in Figure 4.11. Also shown in Figure 4.11 are the best-fit model sorption isotherms obtained for the three pore filling models, using an optimal pore size distribution function $F(H)$ determined numerically for each adsorption model by a sum-of-squares error minimization analysis of the adsorption integral

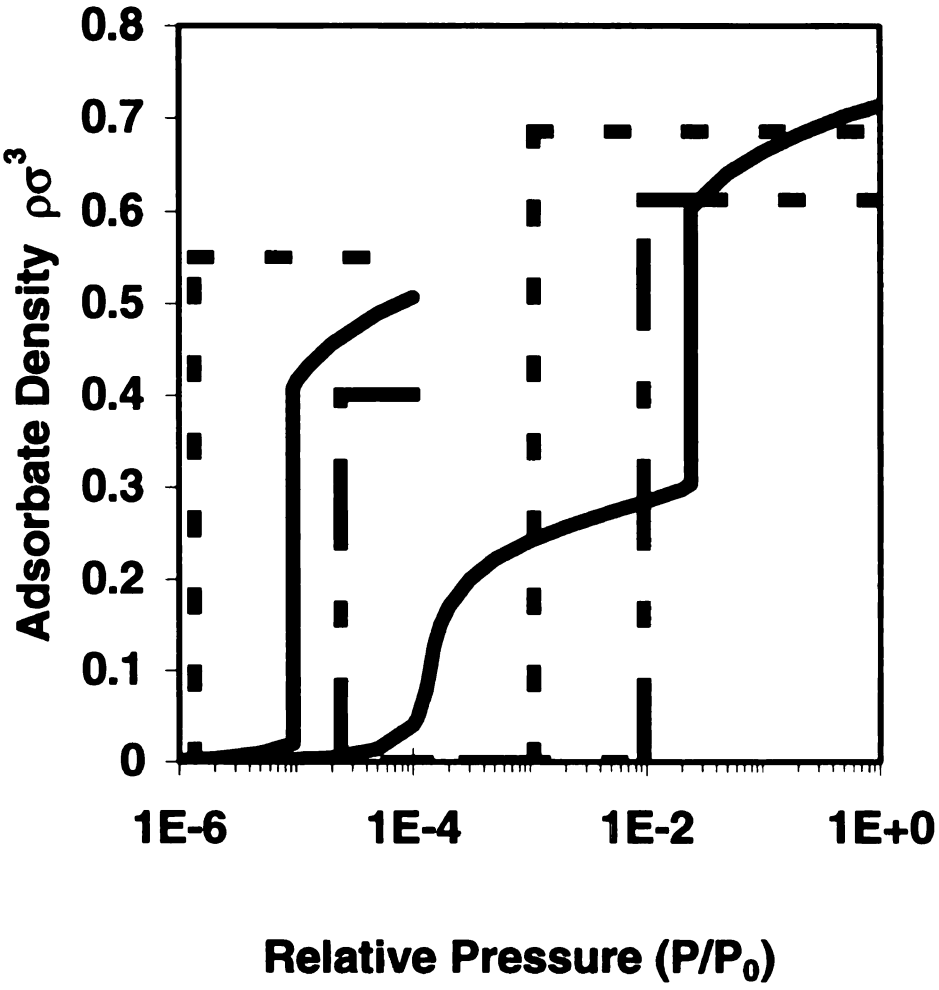

Figure 4.10: Comparison of model isotherms calculated from DFT (solid line), the unweighted HK method (dashed line), and the density-weighted HK method (dotted line) for nitrogen adsorption at 77 K in a slit pore of width 10.7 A (left) and 17.9 A (right).

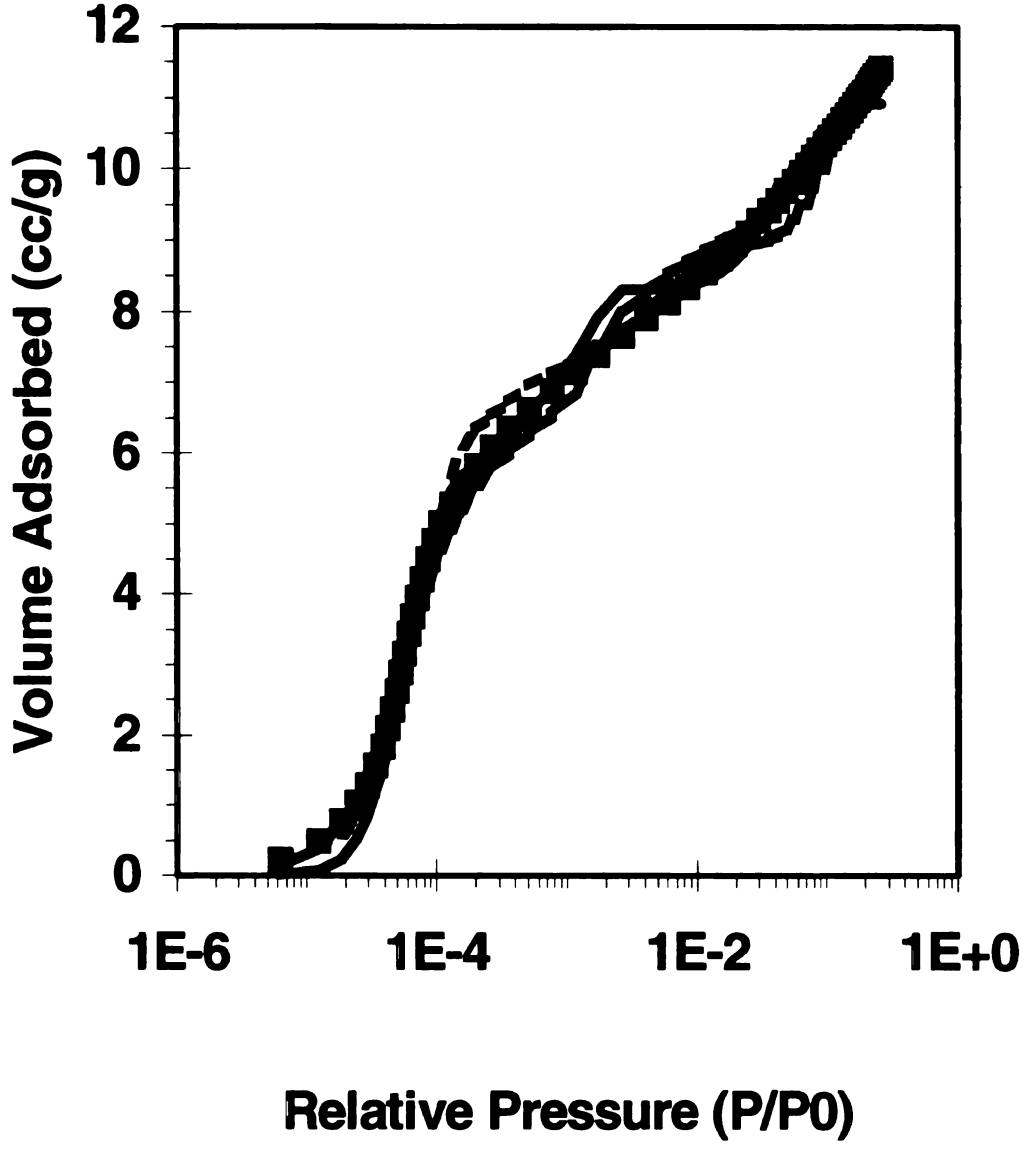

Figure 4.11: Nitrogen adsorption isotherm at 77 K measured on Aldrich powdered activated carbon (points), and fitted isotherms from DFT (solid line), the unweighted HK method (dashed line), and the density-weighted HK method (dotted line). The lines are difficult to distinguish because all three adsorption models give a plausible fit to the experimental adsorption isotherm.

equation (1.1). It can be seen in Figure 4.11 that all three pore filling models give a satisfactory fit to the experimental adsorption isotherm. The best-fit PSDs that yield the fitted model isotherms of Figure 4.11 are shown for each adsorption model in Figure 4.12. The weighted HK model predicts a larger mean pore size for the adsorbent than is obtained from the presumably more accurate DFT model. This is to be expected since the weighted HK model consistently underestimates the filling pressure over all pore size ranges. For the unweighted HK model, the PSD maximum and the mean pore size may coincide reasonably well with the DFT results, or they may lie either above or below the DFT-calculated values, depending on the characteristics of the adsorbent isotherm being interpreted. For the case of the powdered activated carbon of Figure 4.11, a large amount of gas uptake occurs over the relative pressure range P/P_0 between 10^{-5} and 10^{-4}. Over this range of filling pressures, the DFT model predicts that slit pores between 11 and 13 Å are being filled (see Figure 4.9a), while the unweighted HK model predicts condensation in pores between 10 and 12 Å. It is thus not surprising to find that, for this particular isotherm, the unweighted HK model yields a PSD that is shifted to a smaller pore size range relative to the PSD obtained from DFT. For a different experimental isotherm, a different outcome might be observed; for example, for an adsorbent isotherm with a large nitrogen uptake volume between $P/P_0 = 10^{-3}$ and 10^{-2}, the unweighted HK model would predict a larger mean pore size than would the DFT model (Figure 4.9a).

It is somewhat unexpected that the unweighted HK model more closely reproduces the DFT pore filling correlation than the weighted HK model. Given that the local adsorbate density profile is more realistically represented in the weighted HK model, one would expect this model to predict pore filling pressures more accurately than

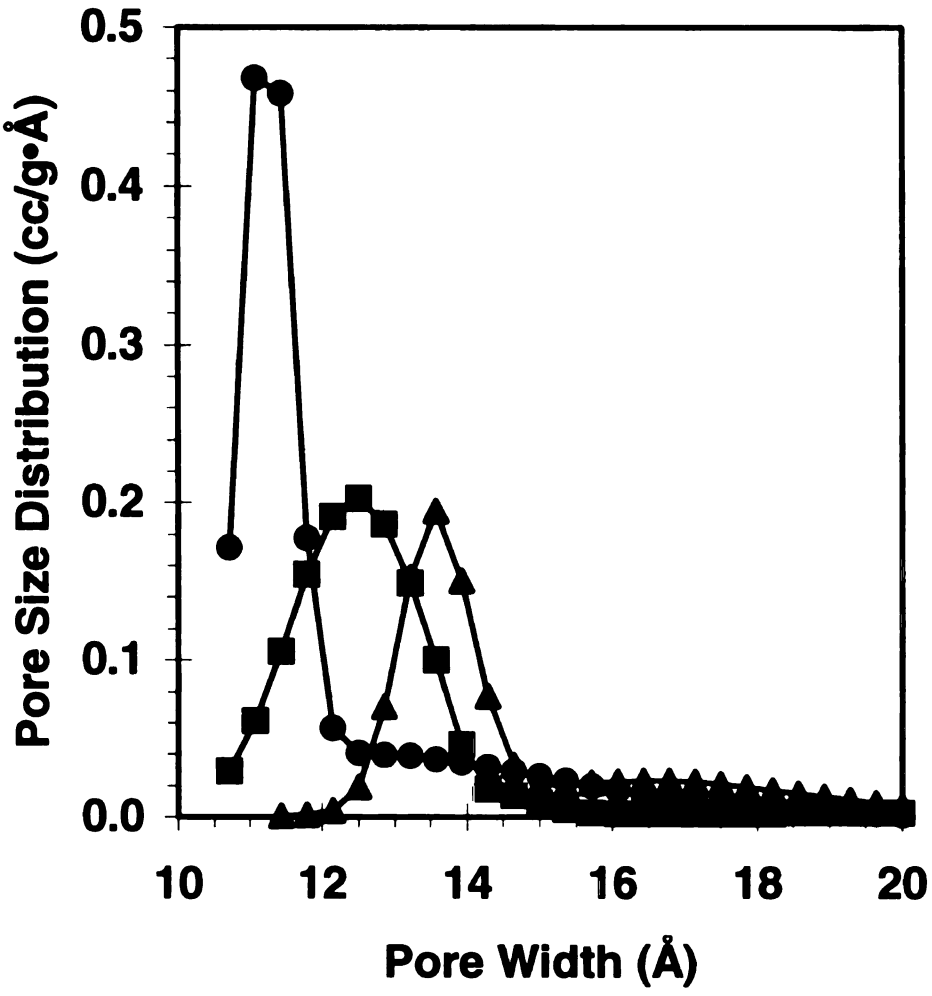

Figure 4.12: Comparison of pore size distributions obtained for Aldrich powdered activated carbon using DFT (solid line), the unweighted HK method (dashed line), and the density-weighted HK method (dotted line).

the unweighted model. However, the weighted HK model consistently underestimates the condensation pressures, even though the adsorbate-adsorbate interactions are altogether neglected in the generalized method. It is apparent that equation (4.11) overestimates the free energy change due to adsorption. One possible explanation of the difference between the DFT and weighted HK model, at least for pores that are larger than 3.7σ in width, is that the mechanisms of capillary condensation are different in the two models. In the DFT model, condensation is preceded by monolayer wetting on each pore wall, whereas in the HK method, the free energy change of adsorption into the contact adsorbate layer adjacent to the pore wall is included in the free energy calculation of equation (4.11). The weighted HK model may therefore underestimate the pore filling pressure because, unlike DFT, it does not recognize monolayer formation and capillary condensation as separate events that occur in mesopores. For pore widths smaller than 3.7σ, pore filling occurs in a single step in both the DFT and HK models, and the difference between the weighted HK and DFT models is more difficult to explain.

Equally surprising is the finding that, when the unweighted HK model and the DFT model are compared using the same gas-solid potential and potential parameter values, the two models yield similar pore filling correlations. Thus, contrary to previous findings, it appears that the original HK method gives a plausible representation of the DFT pore filling correlation, provided that the correct 10-4-3 potential parameters are used in the HK model. Furthermore, the agreement between the DFT and unweighted HK pore filling correlations for both nitrogen and argon adsorption at 77 K suggests that similar results may be obtained for other probe gases. Given the assumption of an unstructured local density profile made in the unweighted HK model, the agreement

between this model and DFT is to some degree fortuitous. It does appear, however, that the simple unweighted integration of the gas-solid potential in equation (4.2) avoids overcounting the energy in the region of the potential minimum where the monolayer forms, and thus gives a more accurate estimate of the pore condensation pressure than does the density-weighted integration.

4.6 Conclusion

The Horvath-Kawazoe method is the simplest adsorption model that is able to predict pore filling pressures with some quantitative accuracy. Previous comparisons of the original HK method with the DFT adsorption model yielded poor agreement between the methods, principally because different gas-solid potentials and different potential parameters were used in the models for calculating the pore filling correlation. In this work, it has been shown that good agreement between the unweighted HK and DFT adsorption models is obtained if the same potential and parameter values are used in both models. A generalized HK adsorption model that involves the use of a weighted density profile in the free energy integration has also been developed. However, the density-weighted HK method predicts pore filling pressures that are too low relative to DFT results. The unweighted HK method does not incorporate important features such as pore wall wetting into the model adsorption isotherm, and therefore it should not be used if an adsorption model from DFT or molecular simulation is available to interpret experimental isotherms for a particular adsorbate-adsorbent system. If DFT model isotherms are unavailable for the probe gas/adsorbent system of interest, however, the generalized HK

method can be conveniently implemented using a spreadsheet to obtain reasonably accurate PSDs for microporous adsorbents with a minimum of computational effort.

4.7 References

1. S. Brunauer, L.S. Deming, W.S. Deming and E. Teller, *J. Amer. Chem. Soc.* **62** 1723 (1940).
2. M.M. Dubinin and L.V. Radushkevich, *Doklady Akad. Nauk. S.S.S.R.* **55** 327 (1947).
3. E.P. Barrett, L.G. Joyner and P.P. Halenda, *J. Amer. Chem. Soc.* **73** 373 (1951).
4. N.A. Seaton, J.R.P.B. Walton and N. Quirke, *Carbon* **27** 853 (1989).
5. V.Y. Gusev, J.A. O'Brien and N.A. Seaton, *Langmuir*, **13** 2815 (1997).
6. G. Horvath and K. Kawazoe, *J. Chem. Eng. Japan* **16** 474 (1983).
7. R.A. Pierotti and H.E. Thomas, *Surface and Colloid Science* **4** 241-245 (1971).
8. J. Frenkel, "Kinetic Theory of Liquids," Clarendon Press, Oxford (1946).
9. G.D. Halsey, *J. Amer. Chem. Soc.* **74** 1082 (1952).
10. T.L. Hill, *J. Chem. Phys.* **17** 668 (1949).
11. D.H. Everett and J.C. Powl, *J. Chem. Soc. Faraday Trans.* 1 **72** 619 (1976).
12. A. Saito and H.C. Foley, *AIChE J.* **37** 429 (1991).
13. L.S. Cheng and R.T. Yang, *Chem. Eng. Sci.* **49** 2599 (1994).
14. C.M. Lastoskie, K.E. Gubbins and N. Quirke, *Langmuir* **9** 2693 (1993).
15. A.V. Neimark and P.I. Ravikovitch, *Studies Surf. Sci. Catalysis* **128** 51 (2000).
16. L. Sarkisov and P.A. Monson, *Studies Surf. Sci. Catalysis* **128** 21 (2000).
17. L.D. Gelb and K.E. Gubbins, *Studies Surf. Sci. Catalysis* **128** 61 (2000).
18. M. Heuchel, E. Buss and R.Q. Snurr, *Langmuir* **13** 6795 (1997).
19. C.M. Lastoskie, N. Quirke and K.E. Gubbins, *Studies Surf. Sci. Catalysis* **104** 745 (1997).

20. W.A. Steele, *Surf. Sci.* **36** 317 (1973).

21. A. Muller, *Proc. Roy. Soc. London* **A154** 624 (1936).

22. C.M. Lastoskie, *Studies Surf. Sci. Catalysis* **128** 475 (2000).

23. C.M. Lastoskie, K.E. Gubbins and N. Quirke, *J. Phys. Chem.* **97** 4786 (1993).

24. R.J. Dombrowski, D.R. Hyduke and C.M. Lastoskie, *Langmuir* **16** 5041 (2000).

Chapter 5.

A Two-Stage Horvath-Kawazoe Adsorption Model for Pore Size Distribution Analysis

5.1 Introduction

Porosity and pore structure are properties of catalysts and adsorbents that may control transport phenomena, selectivity of reactions, and selective physisorption in separation processes [1,2]. Several experimental methods exist for the determination of the pore size distribution (PSD) of porous solids as discussed in Chapter 1. Gas sorption porosimetry is one such method that may be used over the range of mesoporous and microporous materials. The pore size distribution $F(H)$ is obtained from the specific excess adsorption isotherm by solving the adsorption integral equation

The PSD obtained by solving equation 1.1 will depend on the choice of thermodynamic adsorption model $\Gamma(P,H)$ that is used. Pore filling models based upon the Kelvin equation are valid only in pores larger than 7.5 nm [1,3,4]; in smaller pores, continuum thermodynamic models do not accurately represent the properties of the confined fluid. In micropores, the filling pressure decreases sharply on account of the enhanced gas-solid potential in such pores [5]. Adsorption models based upon molecular simulation (MS), density functional theory (DFT), or the Horvath-Kawazoe (HK) method all attempt to account for the effect of the gas-solid interaction potential in predicting model isotherms $\Gamma(P,H)$, for pores of specified size and shape. The HK, DFT and MS thermodynamic models are valid for micropores that have widths approaching molecular dimensions [4]. The reliability of the PSD obtained depends not only on the choice of adsorption model, but also on the form of the gas-solid potential and potential parameters used to represent the molecular interactions. For example, the gas-solid potential in a mesoporous or macroporous activated carbon might best be represented by the 10-4-3 potential [6], whereas a

microporous carbon with thin pore walls (e.g. a ribbon-like microstructure) may have a gas-solid potential that is better described using the 10-4 potential. The PSD results will also depend on the assumed pore geometry. HK pore filling correlations, for example, have been derived for slit-shaped, cylindrical, and spherical pore geometries [7,8,9]. Similarly, MS [2,10,11] and DFT [12] calculations have been carried out on various regular and irregularly shaped pore geometries.

Although MS methods are considered to be the most accurate method of obtaining model isotherms for PSD analysis, a large amount of MS computational time is required to assemble a set of isotherms $\Gamma(P,H)$ in sufficient detail so as to solve the adsorption integral equation. DFT requires less CPU time than MS to generate an equivalent number of isotherms, and it predicts nearly the same filling pressures and adsorbed-fluid densities as MS [4]. Both statistical thermodynamics models (MS and DFT) are robust in the sense that they can be confidently applied to either microporous or mesoporous solids for PSD analysis. For adsorption in micropores at cryogenic temperatures, the DFT and MS adsorption models predict IUPAC Type I adsorption isotherms with continuous filling to maximum capacity at very low relative pressures. For mesopores, the two models predict IUPAC Type IV isotherms, with pore wall wetting followed by a discontinuous phase transition at the condensation pressure. For very large mesopores, the DFT and MS models predict capillary condensation preceded by multilayer film growth suggestive of the IUPAC Type VI isotherm observed in low temperature isotherm measurements [14].

The DFT method of PSD analysis is computationally more efficient than the MS approach, but numerical solution using a computer algorithm is still required in order to obtain the DFT model isotherms. An alternative model of adsorption in microporous solids, one that can be solved using a simple spreadsheet, is the HK pore-filling model. The HK method yields an analytic pore filling correlation that is calculated semi-empirically from an estimated mean

free energy change of adsorption. In the original HK approach, the pores of the adsorbent are assumed to be completely filled with adsorbate or completely empty, depending on whether a given pore is above or below its respective filling pressure. The HK model further assumes that filling occurs in a single step and that no pore wall wetting or compression of the condensed phase occurs as the bulk gas pressure increases. Because of these assumptions, model isotherms constructed per the original HK method do not exhibit the wetting and film growth features that are obtained for DFT- and MS-derived isotherms. In spite of such approximations, it has been recently shown that the HK method reproduces the DFT pore filling pressure correlation with surprising accuracy when the two models are compared using the same gas-solid potential and dispersion parameters[15].

Various modifications of the original HK method have been proposed. These involve corrections to either the shape of the pore [8,9] or the method of calculating the mean adsorption free energy change [3,14,15]. A few other analytic adsorption models have been suggested that derive a relationship between the pore filling pressure and the Gibbs energy of adsorption [16,17]. As with the variations of the HK method, however, these adsorption models do not account for the multiple filling events that occur in mesopores. To improve the realism and the range of applicability of the HK method, it would be useful to modify the original HK model so that the significant effect of pore wall wetting is accounted for in some manner. A new adsorption model based upon this concept, referred to as the two-stage HK pore-filling model, is presented in this paper. The two-stage HK model is described in Section 5.2, and a comparison of the PSD predictions of this model with results obtained for the predecessor "single-stage" HK method are presented in Section 5.4. Original DFT calculations are reported in Section 5.4 for comparison with HK results. A summary of findings and recommendations for PSD analysis is reported in Section 5.5.

5.2 Description of Two-Stage Horvath-Kawazoe Method

5.2.1 Review of the Original HK Model:

The premise of the HK method is that the pressure at which pore filling occurs may be obtained from the mean free energy change of adsorption from the bulk gas phase to the adsorbed phase through the equation 4.1. Due to the fact that equation 4.1 and consequently equation 4.7 both have analytical results, the generation of model isotherms requires far less time to generate than the iterative solution found using DFT. The pore filling correlation described by equation 4.7 is applicable to pore widths $H > 2\sigma_{sf}$, and it predicts that the pore filling pressure decreases monotonically with decreasing pore width. In the original HK formulation, the density of fluid adsorbed in a pore is set equal to the liquid adsorbate density ρ_l if the bulk gas pressure is greater than the filling pressure given by equation (4.7). Otherwise, the pore is assumed to be empty. The model isotherms $\Gamma(P,H)$ generated in the original HK method are thus a set of Heaviside step functions

$$\Gamma(P,H) = \rho_l \Theta[P - P_{HK}(H)] \qquad 5.1$$

where $\Theta[x] = 0$ for $x < 0$, and $\Theta[x] = 1$ for $x \geq 0$. Consequently, in the HK method, the gas uptake that occurs at bulk gas pressure P in an experimental isotherm measurement can be uniquely assigned to condensation in pores of only a single width.

As indicated by equation (4.7), the HK model in its original form assigns a contribution to the potential from interactions between adsorbate molecules. However, there are some conceptual difficulties with this treatment. The mathematical form of equation (4.7) implies that adsorbate molecules occupy the same space as the adsorbent atoms [3,15]. Clearly this is physically unrealistic. There are also errors in the original HK method associated with the magnitude and sign of the term representing the adsorbate-adsorbate interactions in equation (7). As noted in a recent paper [15], the Kirkwood-Muller equation for the A_{ff} dispersion coefficient, given as equation (4.6) in the original HK paper, is too small by a factor of two; Muller [18] reports the correct form of this equation. Also, for the HK method to be consistent with its conceptual underpinnings in the Frenkel-Halsey-Hill theory, the term in

equation (4.7) that represents the adsorbate-adsorbate interaction should be subtracted from, rather than added to, the term for the adsorbate-adsorbent interaction.

In practical applications of equation (4.7), the adsorbate-adsorbent interaction energy is often an order of magnitude larger than the adsorbate-adsorbate interaction. In such cases, the aforementioned errors regarding the magnitude and sign of the A_{ff} term are not significant. The original HK paper, for example, presents a model for nitrogen adsorption in carbon slit pores at 77 K; in this model, 93% of the total potential energy is attributed to nitrogen-carbon interactions, and only 7% to nitrogen-nitrogen interactions. Given the uncertainties regarding the correct form of the adsorbate pair interaction in equation (4.7), it may therefore be sensible to disregard these interactions altogether, and calculate the pore filling pressure solely from the gas-solid potential which accounts for the bulk of the free energy change.

One of the principal shortcomings of the original HK method is that it is unable to accurately portray the full sequence of filling events that occur within mesopores. The shape of the HK model isotherm given by equation (5.1) is similar to that of the Type I isotherm, which is characteristic of adsorption in a microporous solid. The original HK method does not generate realistic model isotherms for mesoporous adsorbents, which have Type IV isotherms in which pore wall wetting is followed by capillary condensation. To develop a robust HK method, suitable for PSD analysis of either microporous or mesoporous materials, one might consider extending the HK model to incorporate film wetting and growth in mesopores. In this extended HK method, the mesopore isotherm features two or more filling steps, rather than just a single step as in the original HK method. The first step corresponds to formation of the monolayer on the pore walls; the final step represents capillary condensation in the center of the pore.

In large mesopores, stepwise (Type VI) film growth is known to occur at low temperatures. In principle, each growth step could be modeled as a separate filling event in the new HK

formulation. From a practical standpoint, however, the development of the multilayer is a secondary structural feature of the mesopore isotherm. Of greater importance, in the context of the PSD analysis, is that the initial pore wall wetting and the final capillary condensation events be modeled as accurately as possible. Therefore, a two-stage HK pore-filling model, with monolayer formation followed by condensation, has been developed for the PSD interpretation of mesoporous solids. The new HK model integrates seamlessly with the original HK method for microporous adsorbents, and so the improved model can be used to interpret the PSDs of materials that have a combination of microporosity and mesoporosity. A description of the two-stage HK model follows.

5.2.2 Description of the Two-Stage HK Pore Filling Model

The same methodology of the original HK model is applied to the two-stage HK model, with the addition of new features that describe the wetting and growth of a monolayer film. The two-stage HK model is generalized so that it may be applied for any adsorbate/adsorbent pair at any subcritical temperature. The adsorbate-adsorbate and adsorbate-adsorbent interactions in the new HK model are modeled using the Lennard-Jones potential with respective well-depth parameters ε_{ff} and ε_{sf}. The adsorbate and adsorbent molecular diameters are assumed to be identical, i.e. $\sigma_{ff} = \sigma_{ss} = \sigma_{sf} = \sigma$.

The two-stage HK model isotherms are of the general form illustrated in Figure 5.1. The filling transition pressures and the adsorbed fluid densities are calculated according to the following procedure.

(1). The pressure P_c at which capillary condensation occurs in the two-stage HK model is calculated in the same manner as in the original HK method:

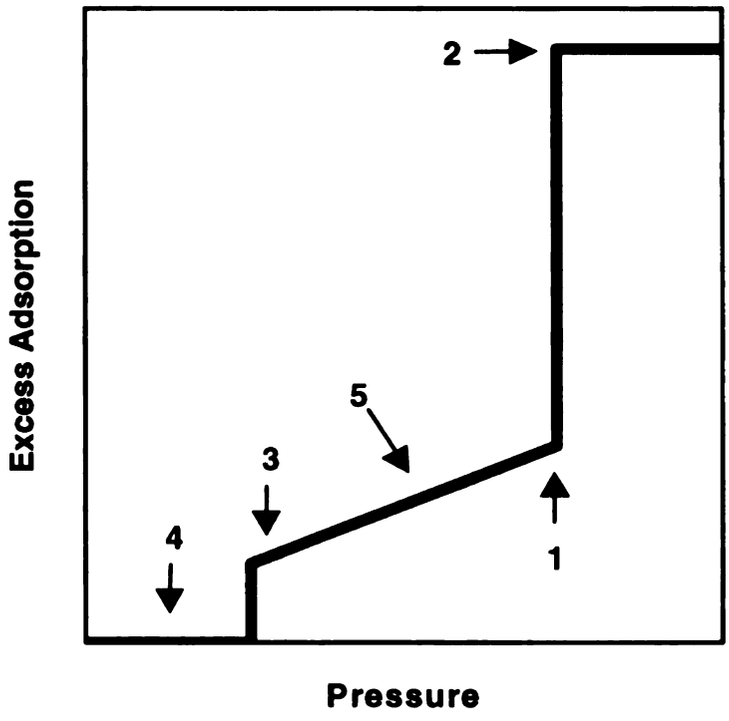

Figure 5.1: Schematic of two-stage Horvath-Kawazoe pore filling method showing the principal features of the model mesopore isotherm: (1) capillary condensation pressure; (2) condensed fluid interval; (3) film wetting pressure; (4) empty pore interval; and (5) film growth interval.

$$kT\ln(P_c/P_0)=\bar{\phi}_c(H)=\frac{\int_{d_0}^{H/2}\Phi(H,z)dz}{\int_{d_0}^{H/2}dz}=\frac{\int_{d_0}^{H/2}\Phi(H,z)dz}{H/2-d_0} \qquad 5.2$$

$$\Phi(H,z)=\phi_{sf}(z)+\phi_{sf}(H-z) \qquad 5.3$$

where the gas-solid potential ϕ_{sf} is symmetric about the pore centerline at $H/2$. Equation (5.2) is the same as that given by equations (4.2) and (4.3), except that the lower integration endpoint has been changed to d_0, the distance from the surface at which the gas-solid potential has a zero value. The implicit assumption is that the accessible pore volume is the region in which the gas-solid potential has a negative value. In this paper, results are reported for two gas-solid potentials, the 10-4-3 potential and the 10-4 potential

$$\phi_{10-4-3}(z)=2\pi\varepsilon_{sf}\rho_s^*\left[\frac{2}{5}\left(\frac{\sigma}{z}\right)^{10}-\left(\frac{\sigma}{z}\right)^{4}-\frac{\sigma^3}{3(z+0.61\sigma)^3}\right] \qquad 5.4$$

$$\phi_{10-4}(z)=2\pi\varepsilon_{sf}\rho_s^*\left[\frac{2}{5}\left(\frac{\sigma}{z}\right)^{10}-\left(\frac{\sigma}{z}\right)^{4}\right] \qquad 5.5$$

For both potentials $d_0 \cong 0.85\sigma$. The dimensionless adsorbent density $\rho_s^* = \rho_s\sigma^3$ is set equal to the density of graphite, for which $\rho_s^* = 5.2$.

(2). For bulk gas pressure $P > P_c$, the adsorbed fluid density $\Gamma(P,H)$ is assumed to be constant, with a value ρ_f calculated from the dimensionless temperature $T^* = kT/\varepsilon_{ff}$ and the dimensionless gas-solid potential well depth $E^* = \varepsilon_{sf}/\varepsilon_{ff}$ as

$$\rho_f(T^*,E^*)=\rho_0(1-c_0\ln(T^*))^*(1+c_1\ln(E^*)) \qquad 5.6$$

where $\rho_0 = 0.834$, $c_0 = 0.600$ and $c_1 = 0.0375$. This correlation was fitted to DFT results obtained over a range of (T^*, E^*) values for the mean density at the bulk fluid saturation pressure of a Lennard-Jones fluid adsorbed in slit pores of width H = 20σ [15]. The condensate density is a strong function of temperature and a weak function of the gas-solid well depth.

(3). The pressure P_m at which a monolayer film adsorbs is given as

$$kT\ln(P_m/P_0)=\bar{\phi}_m(H)=\frac{\int_{d_0}^{d_0+\sigma}\Phi(H,z)dz}{\int_{d_0}^{d_0+\sigma}dz}=\frac{\int_{d_0}^{d_0+\sigma}\Phi(H,z)dz}{\sigma} \qquad 5.7$$

Equation (5.7) is applicable to slit pores of width greater than $H_m = 2(d_0 + \sigma)$. For the 10-4 or 10-4-3 potential, this corresponds to a cutoff pore width $H_m = 3.70\sigma$. Thus, for pore widths $H > H_m$, the model isotherm has two filling transitions, one for monolayer wetting and one for capillary condensation; whereas for pore widths $H \leq H_m$, a single transition occurs at the filling pressure given by equation (5.2). Consequently, for pore widths $H \leq H_m$ in the two-stage HK model, the model isotherm does not have the shape shown in Figure 5.1, but rather is a Heaviside step function similar to that described in equation (5.1) for the single-step HK pore filling model.

Equation (5.7) implicitly assumes that the mean free energy change $\bar{\phi}_m$ for monolayer adsorption may be calculated from a weighted average of the gas-solid potential, in the region of the pore volume extending one molecular diameter from the zero-point coordinate of the gas-solid potential. The definition of equation (5.7) is such that as the pore width approaches the limiting value H_m, the wetting pressure given by equation (5.7) maps seamlessly into the filling pressure correlation given by equation (5.2). Also, in the large pore limit $H \rightarrow +\infty$, the monolayer wetting pressure P_m asymptotically approaches a limiting value that corresponds to the wetting pressure on a planar nonporous surface. Equation (5.7) is therefore both mathematically well defined and physically consistent with the wetting behavior observed in DFT model calculations.

(4). For bulk gas pressure $P \leq P_m$ (or $P \leq P_c$ in the case of pores smaller than H_m), the pore is assumed to be completely empty: $\Gamma(P,H) = 0$.

(5). For bulk gas pressures $P_m < P \leq P_c$, the adsorbed fluid density is assumed to have a logarithmic dependence on the pressure as given by the following equation:

$$\Gamma(P,H) = \rho_f(T^*,E^*)\frac{2\sigma}{H} + S(T^*,E^*,H)\ln\left(\frac{P}{P_c}\right) \qquad 5.8$$

where the coefficient $S = (\partial\Gamma/\partial\ln(P/P_c))\big|_{T^*,E^*,H}$ is given by the correlation

$$S(T^*,E^*,H) = S_0\left(1-\frac{a_0}{T^*}\right)\left(1-\frac{a_1}{E^*}\right)\left(\frac{b_0\sigma - 2(d_0+\sigma)}{H-2(d_0+\sigma)}\right)^{b_1} \qquad 5.9$$

where S_0 = 0.0222, a_0 = 0.536, a_1 = 1.32, b_0 = 20 and b_1 = 0.6. The first term on the right hand side of equation (5.8) is the adsorbed fluid density at the saturation pressure, multiplied by the fraction of the pore volume occupied by the monolayer film. It is assumed that at the onset of capillary condensation, the adsorbed fluid on each pore wall has a thickness equal to σ. Also, the wetted film is assumed to have the same molar volume as the condensed fluid phase.

The second term on the right hand side of equation (5.8) is a correction that accounts for film growth over the interval between the onset of wetting and the condensation transition to the completely filled state. The (T^*,E^*) dependence of equation (5.9) was obtained by fitting DFT results at twenty different (T^*, E^*) values, as shown in Figure 5.2, so as to reproduce the average slope of the isotherm for a pore of width $H = 20\sigma$ between the first and second phase transitions (see Figure 5.3 for an illustration). The pore width dependence of equation (5.9) was then correlated to the average slope of the DFT isotherm between the first and second filling events for the range of pore widths $3.70\sigma < H \leq 20\sigma$, as shown in Figure 5.4 for fixed T^* = 0.70 and E^* = 0.80. The form of equation (5.9) is chosen so that as the pore size decreases toward H_m, the slope S goes to infinity. This is physically consistent with a transition from two-step to single-step pore filling at the critical pore width H_m, an important feature of the two-stage HK adsorption model.

5.3 Results

Selection of the Potential Parameters: As noted in the introduction, one of the principal reasons why the original HK method and the DFT method predict different pore

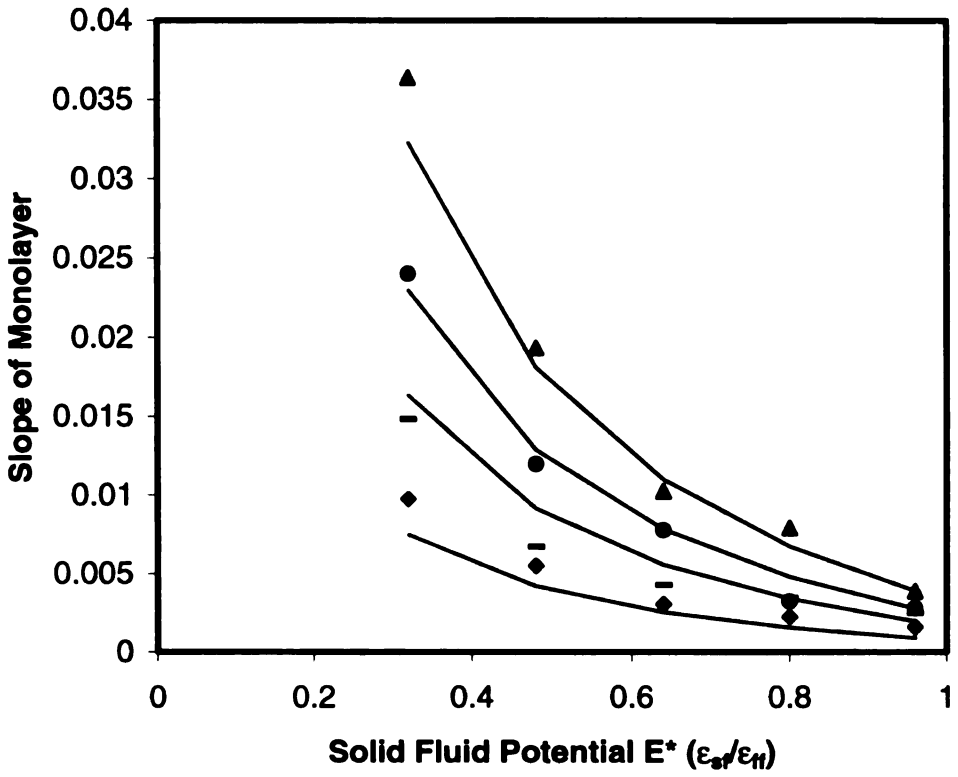

Figure 5.2: Fitted correlation of the slope of the isotherm of a slit pore of width $H = 20\sigma$ over the interval corresponding to growth of the wetted film. Symbols denote results from DFT for $T^* = 1.0$ (triangles), 0.8 (circles), 0.7 (squares), and 0.6 (diamonds). Lines show the correlation fit to the DFT data.

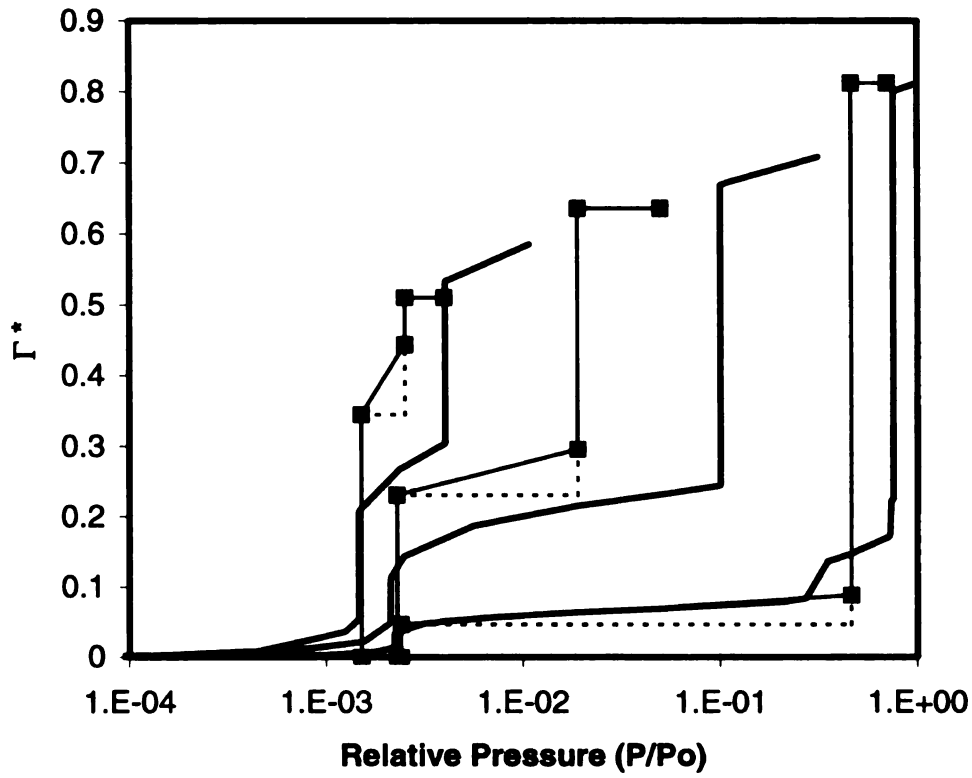

Figure 5.3 A comparison of DFT model isotherms and two-stage HK model isotherms the slope of the monolayer region is given by the dotted lines

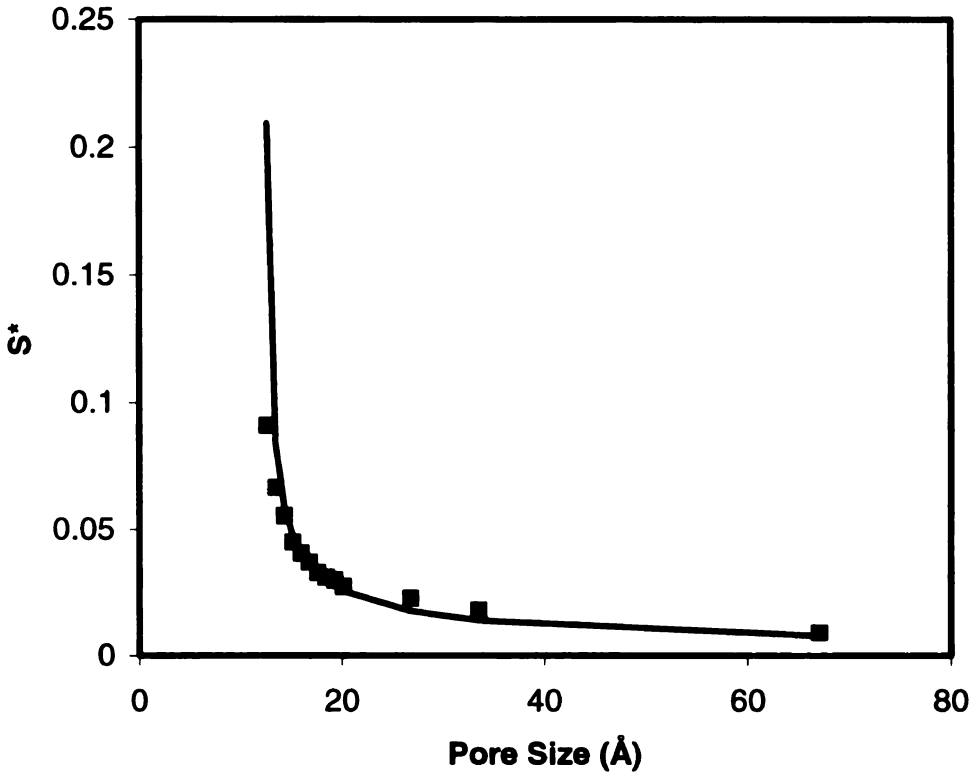

Figure 5.4: Fitted correlation of the slope of the isotherm for slit pores of different width over the interval corresponding to growth of the wetted film. The symbols denote DFT results for $T^* = 0.7$ and $E^* = 0.8$; the line shows the correlation fit at the same conditions.

filling correlations is that a different procedure is used to fit the potential parameters of each model. In this work the DFT parameters of the adsorbate-adsorbate interaction potential are fitted to the physical properties of the saturated liquid adsorbate at its normal boiling point temperature. The parameters of the gas-solid potential, meanwhile, are selected so that the DFT model isotherm of a large pore (e.g. $H = 20\sigma$) is in good agreement with the low-pressure (monolayer) portion of the experimental isotherm of a nonporous reference adsorbent. Ideally, the reference material that is chosen has a chemical composition and surface structure similar to the porous adsorbents for which PSDs are to be determined.

In the original HK approach, the potential parameters for the adsorbate-adsorbate and adsorbate-adsorbent interactions are obtained from the polarizability and magnetic susceptibility of the adsorbate and adsorbent using the Kirkwood-Muller formulas. Because different methods are used to fit the potential parameters of the DFT and HK adsorption models, divergent potential parameter values are obtained for the two methods. For example, the DFT fitting procedure gives ε_{sf}/k = 53.2 K for nitrogen adsorption at 77 K on a graphitized nonporous carbon [4]. By contrast, for the HK method a nitrogen-carbon well depth of varies with the size of the pore as shown in equation (4.7) using physical data from the original HK paper [7]. Because the HK well depth determined by the Muller equations is only 40% of the DFT-fitted value, the original HK model predicts nitrogen condensation pressures in small carbon mesopores that are 1 to 3 orders of magnitude too large.

It has been noted elsewhere that the Kirkwood-Muller parameter fitting approach may introduce large errors into the adsorption model [19]. Also, for gas-solid systems that have not previously been studied, the physical property data needed to apply the Kirkwood-Muller formulas may not be readily available from the published literature. Given these considerations, a new, experimentally facile procedure is proposed for fitting the potential

parameters of the two-stage HK model. As in the original HK method, the adsorbate molecular diameter σ is specified as an unfitted parameter. However, the potential well depths ε_{ff} and ε_{sf} are fitted using a procedure akin to that used to fit the gas-solid well depth in the DFT model, as shown schematically in Figure 5.5 and explained further in section 2.2.

In order to fit the potential well depth, one must have a reference material that is chemically similar to the material being analyzed and may be regarded as nonporous. The potential function that best describes a nonporous sample the 10-4-3 Steele potential, as it is capable of accounting for the influence of multiple layers of sorbent, which is physically analogous to such a system. A nonporous surface is expected to have a potential that is similar to that of a slit pore whose walls are separated by a distance large enough that the superposition of the potentials is comparable to that of a single wall. An experimental isotherm contains two forms of information, the relative pressure (P/P_o) and the amount adsorbed (mmol/g). A nonporous adsorbent will typically have an isotherm that exhibits a step like behavior, these steps can be attributed to layer formation. The region of an isotherm before the second layer transition is the most relevant section for fitting the solid fluid parameters. The monolayer density ρ_m within a pore can be described by the following using the multiple filling model as given by equation 5.8.

For pores that are significantly large (≥67 Å) the monolayer density is a weak function of the pore size H. The density in a pore may be related to the volume adsorbed V though the following equation.

$$V = \frac{HS\rho_m}{\sigma^3 A_v} \qquad 5.10$$

Where H is the pore size, S is the surface area, A_v is Avagodro's number. The monolayer filling pressure is also a function of the pore size, dimensionless temperature and energy. The value of the surface areas, S, may be the BET surface area, however this has been shown to under predict the actual value, therefore the method of using the film thickness as

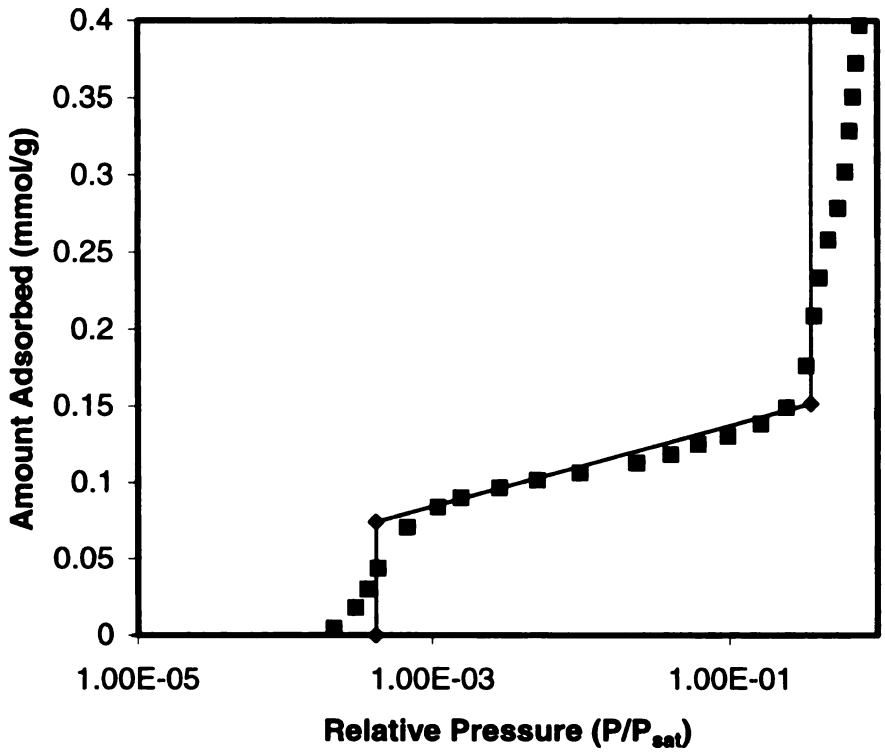

Figure 5.5 Comparison of a fitted two-stage HK model isotherm (solid line) and a reference isotherm Argon adsorption on sterling activated carbon square symbols.

described by [13]Lastoskie should be utilized. Following the method of de Boer *et al.*[18], the specific surface area is obtained by fitting a line through a plot of the argon uptake versus the theoretical film thickness figure 2.2. A specific surface area of 11.3 m^2/g was measured for the Sterling carbon; this value was then used to convert the multiple filling model-calculated specific excess argon adsorption in the 67 Å-slit pore from a pore volume basis to an adsorbent mass basis, as described in previous work [21].

Utilizing the 10-4-3 Steele potential and substituting into equations 5.7 and 5.8, one finds that the monolayer filling pressure is a function of the ratio of E * / T*. After the proper selection of the E*/T* ratio, the monolayer filling pressure has been determined, and the values of E* or T* can be fitted, while maintaining the ratio determined earlier, to match the volume adsorbed, at the relative pressure just below the formation of a second layer, as seen in Figure 5.5.

The selection of the potential is determined by the physical characteristics of the material being studied. If pores are assumed to have only one layer of atoms as a forming a wall, then the 10-4 potential should be used, however if two or more layers of adsorbent or adsorbent and adsorbate are expected the 10-4-3 potential should be used. As illustrated in Figure 5.6 the potential for the two or more layers is approximately the same as for a semi-infinite plane. The 10-4 potential and the 10-4-3 potentials should bracket all the possible potentials due to the structural inhomogeneities for a slit pore.

Utilizing the 10-4 and 10-4-3 potentials of the slit pore for both argon and nitrogen at 77K four series of fourteen isotherms, whose size ranged between two to twenty molecular diameters, were generated using DFT. The potential parameters for argon were chosen to match those found in the literature [5] with the exception of the fluid-fluid molecular diameters being chosen to equal the molecular diameter of the adsorbent (3.35Å). The error

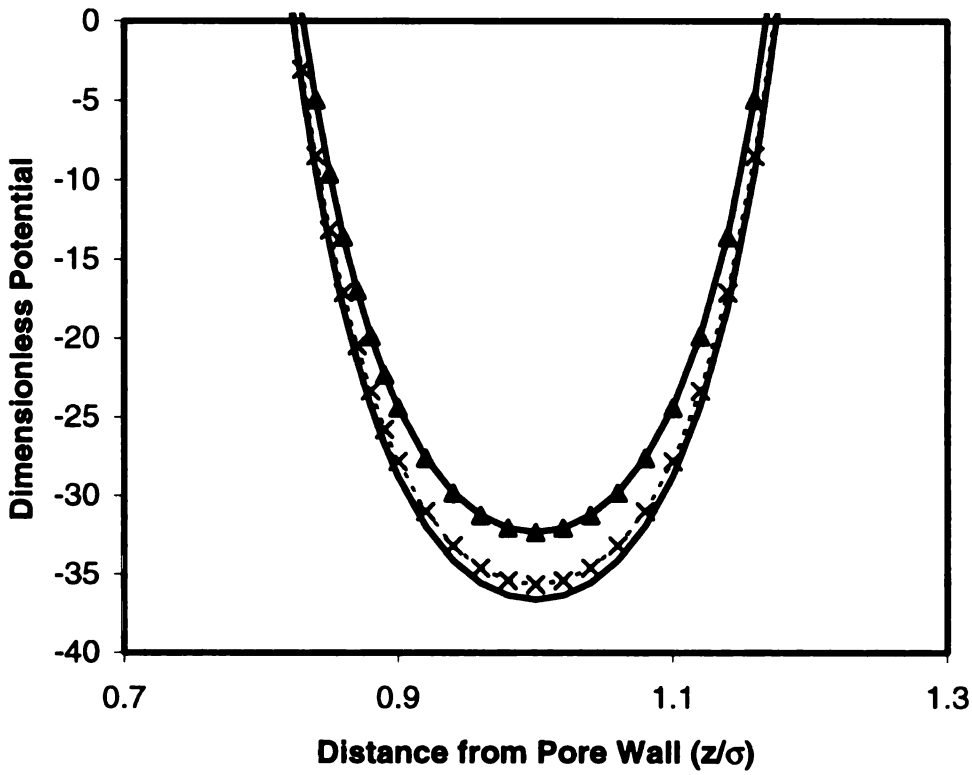

Figure 5.6 Spatially varying potential in a 2 molecular diameter slit pore at 77K for single planes of graphite (triangles), for a double layer of graphite planes(crosses), and for a semi-infinite slab of graphite (solid line)

associated with the change in the fluid molecular diameter was found to be insignificant for the argon. (isotherm not shown) The potential parameters for the nitrogen were refit using the method described by Lastoskie et al.[21] for the generalized 10-4-3 potential. The net effect was an increase in the potential well depth to 58.46/k, when the nitrogen molecule was assumed to have a diameter equal to that of a carbon atom. The 10-4 potential isotherms displayed similar trends to the isotherms generated using the 10-4-3 potentials [5] for the same conditions, with the notable exception that the filling occurred at slightly higher relative pressures as seen by comparing Figures 5.7a-d. The higher filling pressures are expected as the 10-4 potential has a higher net energy well depth. In all cases the DFT isotherms show a single layer or single filling for slit pores smaller than 3.7σ and multiple filling steps for larger pores. All DFT isotherms also display adsorption before and after the relative filling pressure, representing the compression of the adsorbed layer or layers. The two-stage HK model mimics the filling behavior of the DFT isotherms for both the single and semi-infinite layers of adsorbent for both monolayer and multilayer condensation. The two-stage HK model correctly displays the filling of a monolayer and its density relative to the final density at the saturation pressure, while correctly displaying the limiting value between single and multiple filling isotherms. Additionally, the model isotherms as seen in figures 5.8a-d correctly predict that the monolayer filling pressures approach an asymptotic limit similar to the behavior of the DFT isotherms.

The filling pressures can be broken into two categories the monolayer filling pressure and the condensation filling pressure for the two-stage model. In most cases the two-stage HK model, like the original HK model with an improved potential function, under predicts the multilayer filling pressure compared to DFT.(see figure 5.9a-d) With the same potential function and potential parameters the multiple filling model generally over predicts the monolayer filling pressure, this apparent disparity indicates that the potential is

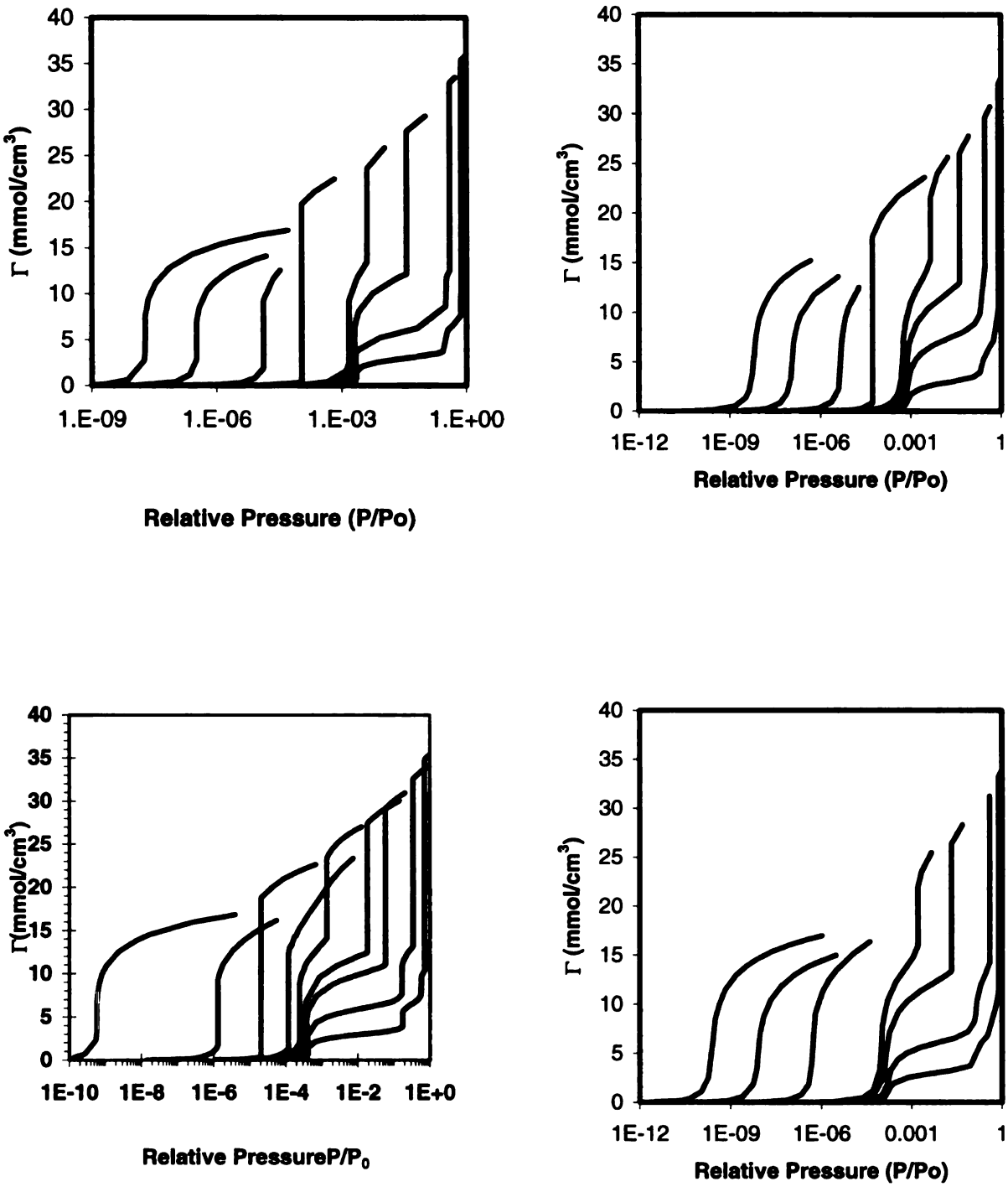

Figure 5.7 a-d. DFT model isotherms for a) argon 10-4 potential pore sizes 6.7, 7.5, 8.3, 10.1, 13.4, 33.5, and 67A b) nitrogen 10-4 potential pore sizes 6.7, 7.5, 8.3, 10.1, 13.4, 26.8, and 67A c) argon 10-4-3 potential pore sizes 6.7, 7.5, 8.3, 10.1, 13.4, 33.5, and 67A d) nitrogen 10-4-3 potential pore sizes 6.7, 7.5, 8.3, 10.1, 13.4, 26.8, and 67A

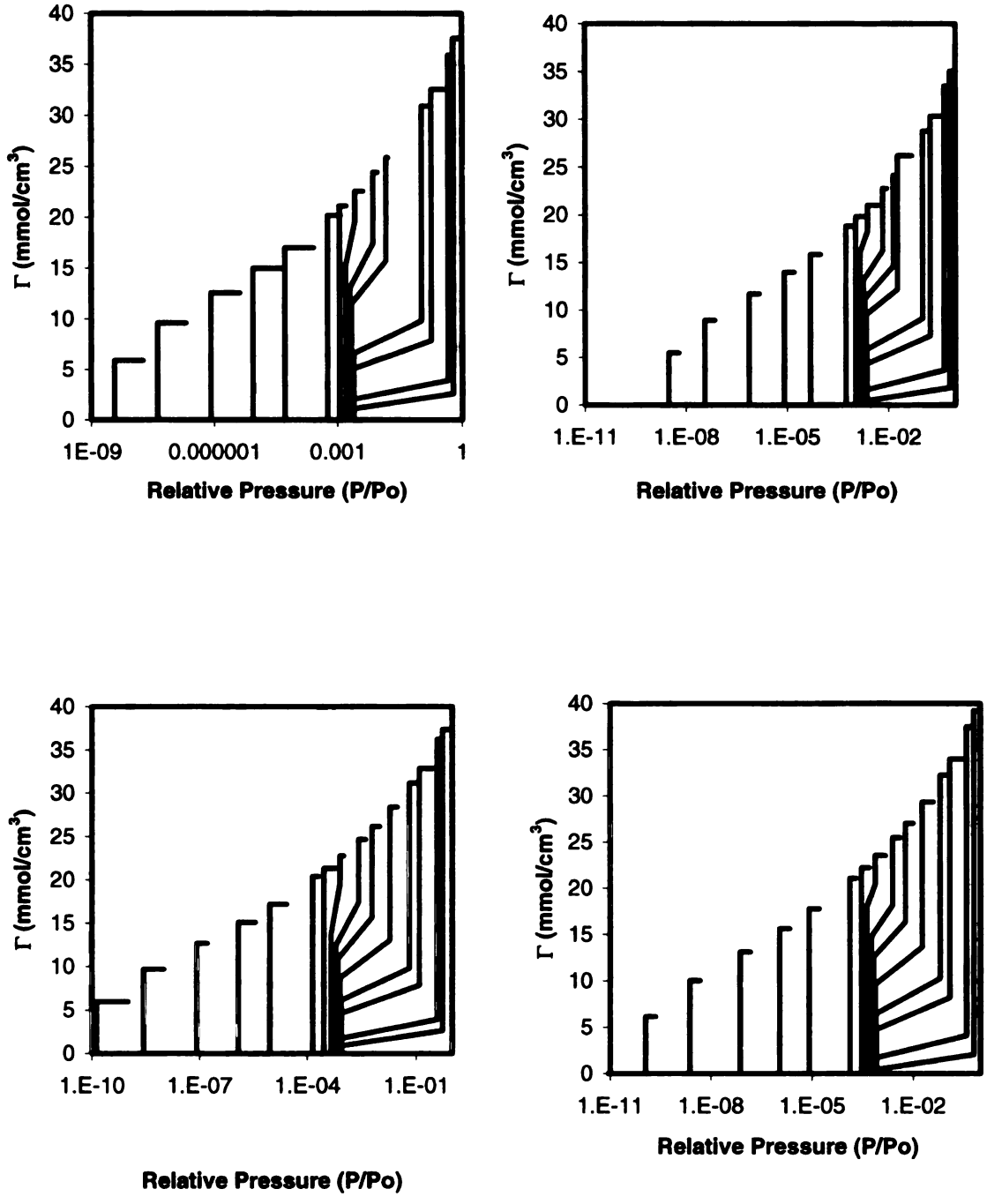

Figure 5.8 a-d. Two-stage HK model isotherms for poresizes 6.7, 7.5, 8.4, 9.2, 10.1, 10.9, 11.7, 12.6, 13.4, 15.1, 16.8, 20.1, 26.8, 33.5, and 67A for a) argon with a 10-4 potential b) nitrogen 10-4 potential c) argon with a 10-4-3 potential d) nitrogen with a 10-4-3 potential

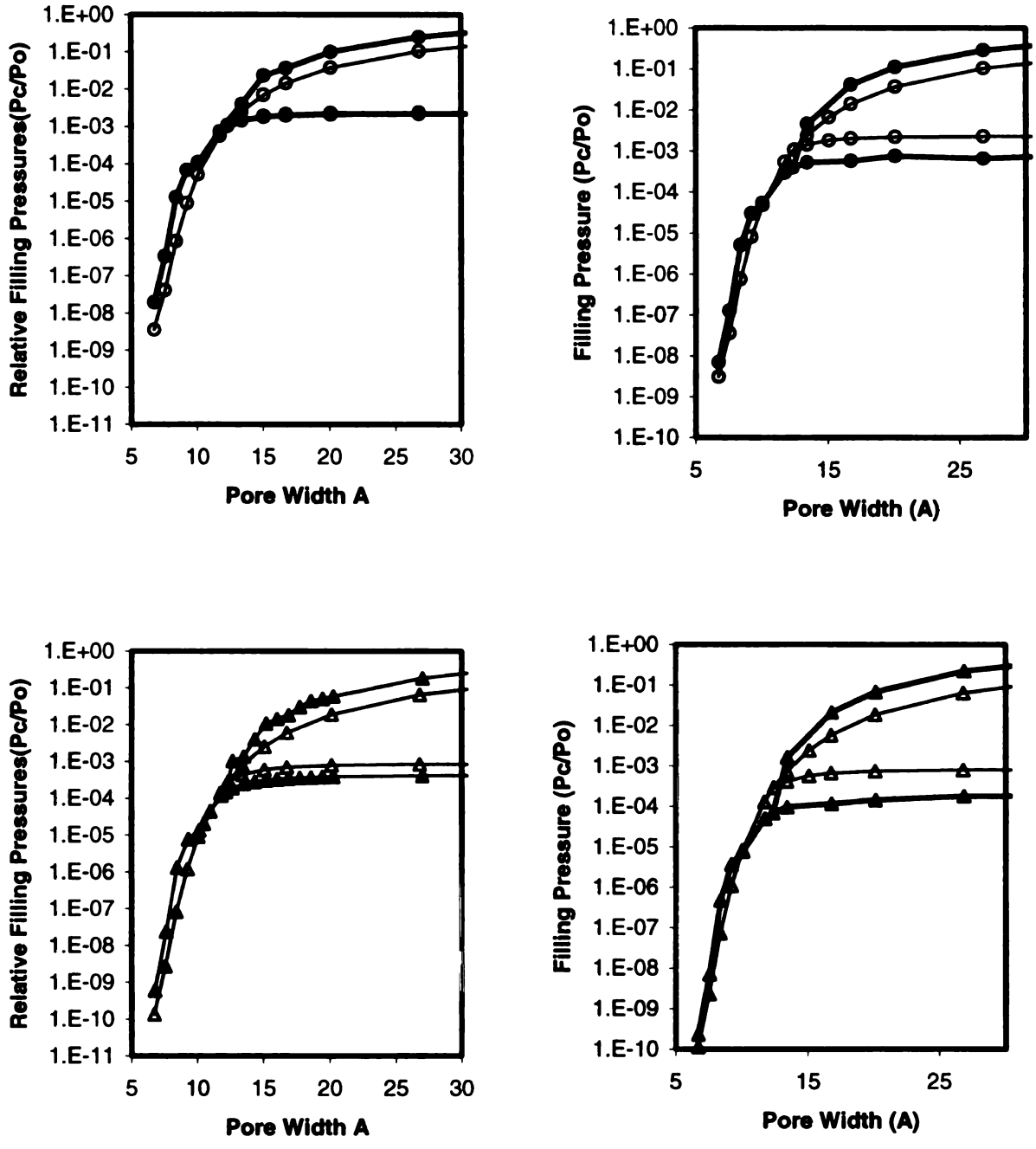

Figure 5.9 a-d Filling pressure correlations of DFT solid symbol and two stage HK methods open symbols for a) argon 10-4 potential b) nitrogen 10-4 potential c) argon 10-4-3 potential d) nitrogen 10-4-3 potential all at 77K

simultaneously too strong and too weak. While it is tempting to attribute this behavior to the density profile within a pore, Dombrowski *et al* [15] and Lastoskie [21] have shown that the density weighted average of the potential would increase the average potential, improving the monolayer fit at the expense of the multilayer fit.

The solutions to the inversion the adsorption integral equation 1.1 have been found for a powdered activated carbon for each potential and adsorbate system. The isotherm fits to the experimental data are reported in figures 5.10a-d. A simple inspection reveals that all the isotherm fits are plausible. The multiple filling model closest fit isotherms display a consistent irregularity near the limit of the monolayer filling pressure, which are not displayed by the DFT model isotherm fit. The characteristic malformation of the isotherms is due to the monotonic increase in the final density and zero slope after the single filling transition of the isotherms smaller than 3.7σ, where as the DFT model isotherms do not display a consistent increase in the density following pore filling. The simplistic representation of a single filling of the generalized version of the HK method also does not display any characteristic abnormalities, however none are expected with such a model. The resulting PSDs obtained from each of the three methods are displayed in figure 5.11a-d clearly indicate that the multiple filling model provides better agreement to the DFT calculations than the generalized HK method. For pores that are smaller than 12.4 Å the multiple filling model and the generalized HK methods are identical, therefore the true comparison lies in the prediction of larger pores. The generalized and multiple filling HK model isotherms for specific pore sizes become less accurate for smaller pores than for large pores, upon which the model is based. As demonstrated by Dombrowski et al [13] the local density of the adsorbed phase is higher than the interior local density, and a model which is based upon a large pore, would tend to weigh the interior density higher than the monolayer density. Although there is a systematic error produced by using this one size fits all pores

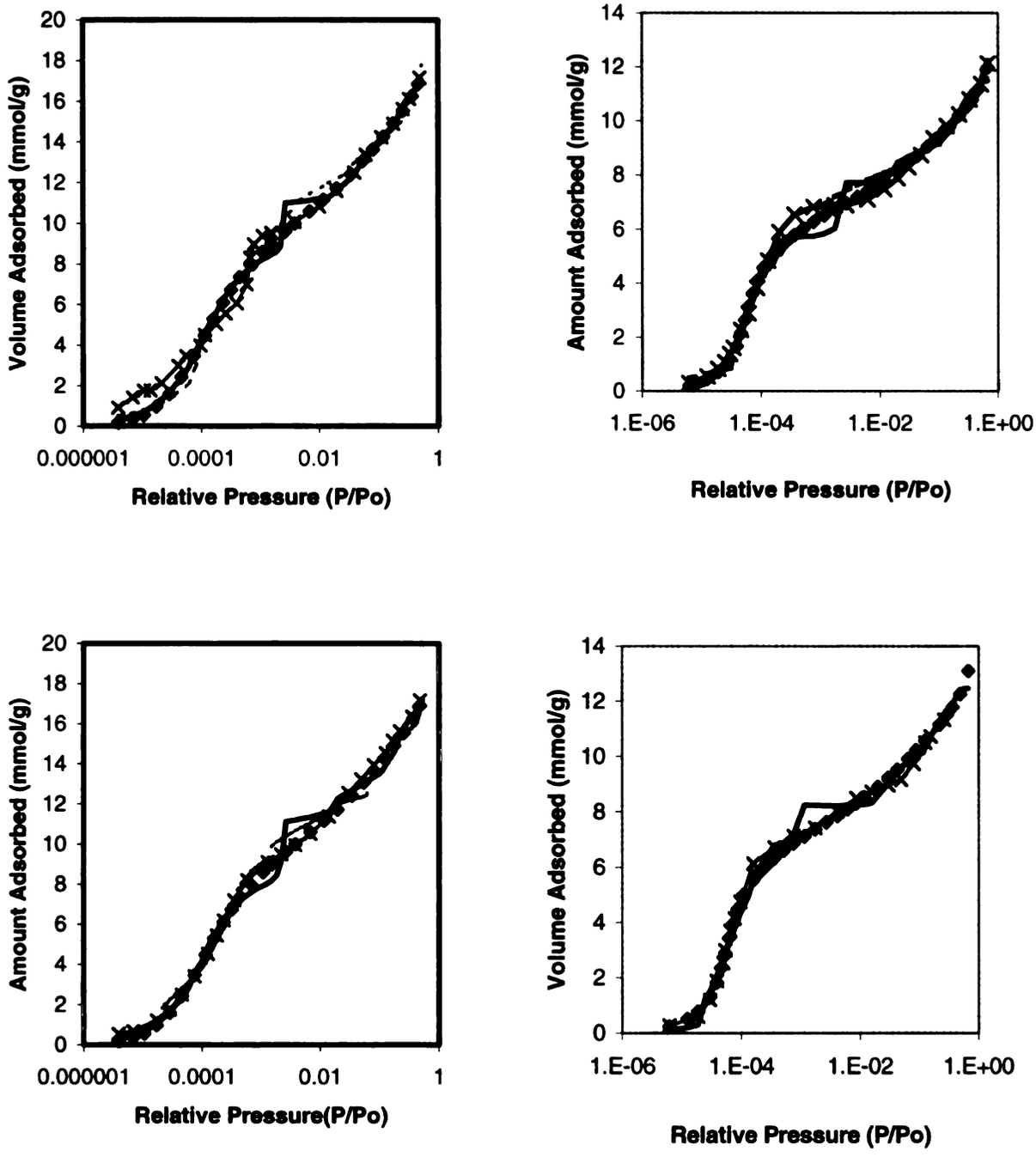

Figure 5.10 a-d Isotherm fits to experimental data(diamonds) on powdered activated carbon at 77K, DFT (dotted line), generalized HK (crosses), two stage HK(solid line). The data overlap indicates that each of the models fit well. For a) argon 10-4 potential b) nitrogen 10-4 potential c) argon 10-4-3 potential d) nitrogen 10-4-3 potential.

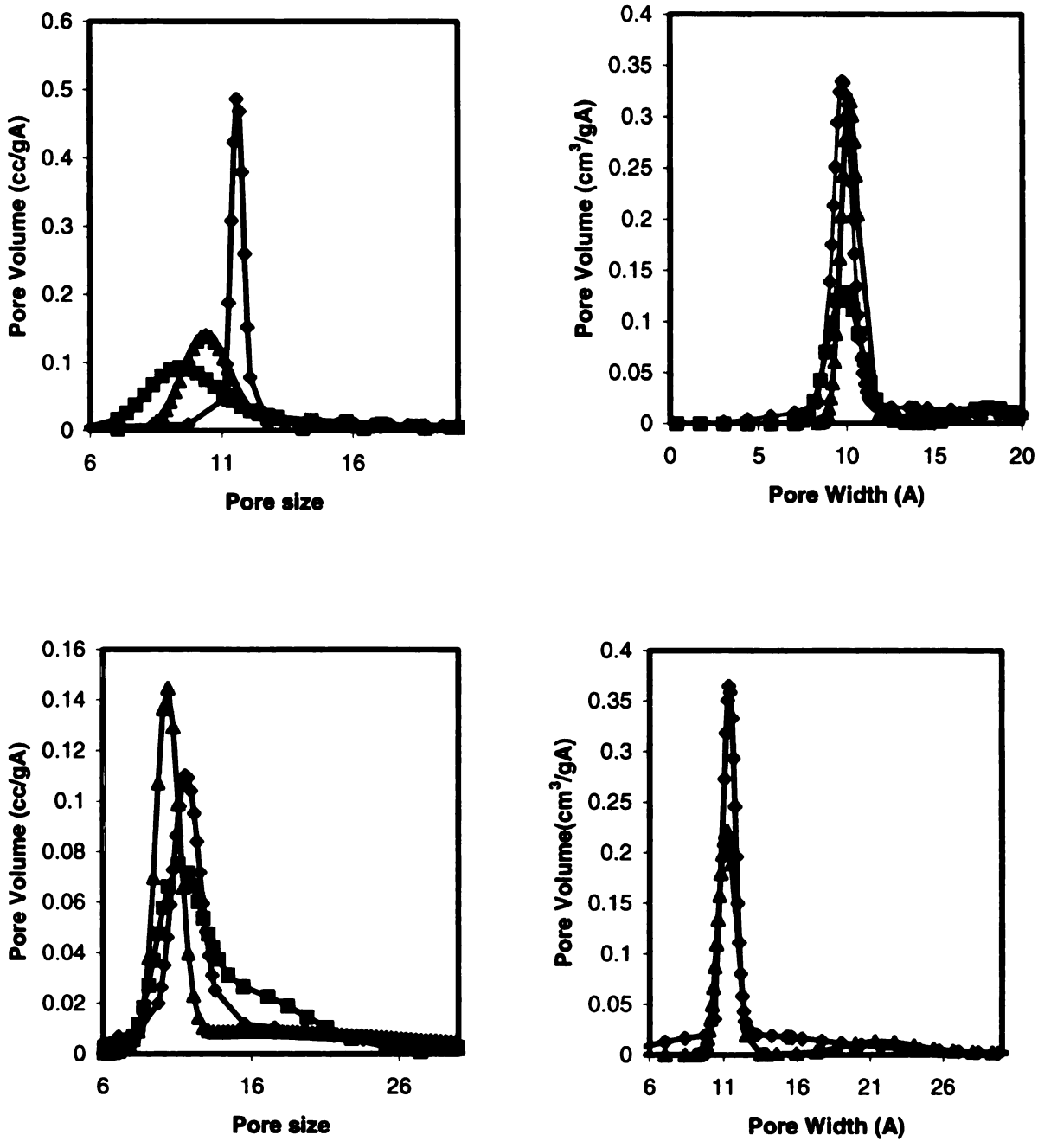

Figure 5.11 a-d Pore size distributions calculated from isotherm fits in figure 5.10. The DFT fit(squares) is presumed most accurate, the two stage HK method (triangles) is closer to the DFT than the generalized HK method(diamonds).

Table 5.1 The maximum pore size (Hmax), average pore size (H) and the pore volume Vp.

Model	Hmax	H	Vp
10.4.3 Ar DFT	11.055	21.8588	0.5512
10.4.3 Ar 2HK	10.438	17.5402	0.7298
10.4.3 Ar HK	11.725	17.4206	0.6106
10.4.3 N2 DFT	11.2895	20.3730	0.536
10.4.3 N2 2HK	11.225	18.8422	0.6287
10.4.3 N2 HK	12.7635	21.3935	0.5292
10.4 Ar DFT	9.38	15.9592	0.7397
10.4 Ar 2HK	10.552	17.4906	0.7251
10.4 Ar HK	11.5575	15.9529	0.709
10.4 N2 DFT	9.74	18.4298	0.5927
10.4 N2 2HK	10.0835	16.8587	0.7706
10.4 N2 HK	9.715	15.1630	0.877

local density profile it contains a significant improvement, through its ability to relate the local density to the temperature and solid fluid interaction energy. The result of the low density predicted in the smaller pores is an increase in the volume of such pores predicted by the inversion of the adsorption integral (equation 1.1). The increased volume of the smaller pores results in the average pore sizes being shifted to smaller values than those predicted by DFT. Table 5.1 illustrates the pore sizes associated with either method compared DFT. As stated earlier it is anticipated that the average pore size will be skewed towards smaller values for both methods, while the pore volumes are anticipated to be higher, than that predicted by DFT for small pores. In cases where DFT predicts micropores the generalized and multiple filling models should be interchangeable, however, for systems that contain some of the smaller mesopores the multiple filling model should behave more similarly to the DFT than the generalized version. Pores that are larger than about 40 Å begin to see a diminishing return from the addition of the multiple filling steps. As the pore size increases to larger mesoporous sizes the relative contribution from the monolayer rapidly decreases, and the second filling transition becomes the dominant trait of the isotherm. In the case where DFT predicts PSD whose peak is larger than 11 Å the multiple filling HK model is in

closer agreement than the generalized HK model. While the generalized model is closer to the DFT when the pore size is anticipated to be small. For comparison a fictitious DFT isotherm was generated for a mesoporous size distribution as shown in Figures 5.12a-b, the two-stage HK method predicts a mesopore maximum in the PSD that is within 2.1% of the maximum predicted by DFT, whereas the original HK predicts a maximum with an error of 10.7%. The over prediction of the monolayer filling pressure in the two-stage HK model results in the erroneous prediction of micropores and an under prediction of small mesopores to balance the volume of the falsely predicted micropores. The over estimation of the filling pressure in the original HK method results in the under prediction of the pore size culminating in an incorrect PSD in the micropore regime.

The tendency of the original HK method to over predict the size of small pores coupled with the under prediction of the size of mesopores reduces the applicability of the model. Simply altering the potential function overcomes these difficulties and displays the true robustness of the HK method. Through the incorporation of multiple filling steps and altering the potential function, the two-stage HK model can yield results that are comparable to DFT, while offering analytical results that may be processed using a simple spreadsheet program.

5.4 Conclusions

The generalized and two-stage HK models are relatively efficient tools to measure PSD and are recommended for use when DFT isotherms are not available. DFT does provide a more realistic version of the isotherms for individual pore sizes, however it is time consuming to fit the Lennard-Jones parameters and to generate a series of isotherms required consuming to fit the Lennard-Jones parameters and to generate a series of isotherms required to invert the adsorption integral. The two-stage HK model is advantageous in the simplicity that the Lennard-Jones potential parameters and their respective isotherms may be generated

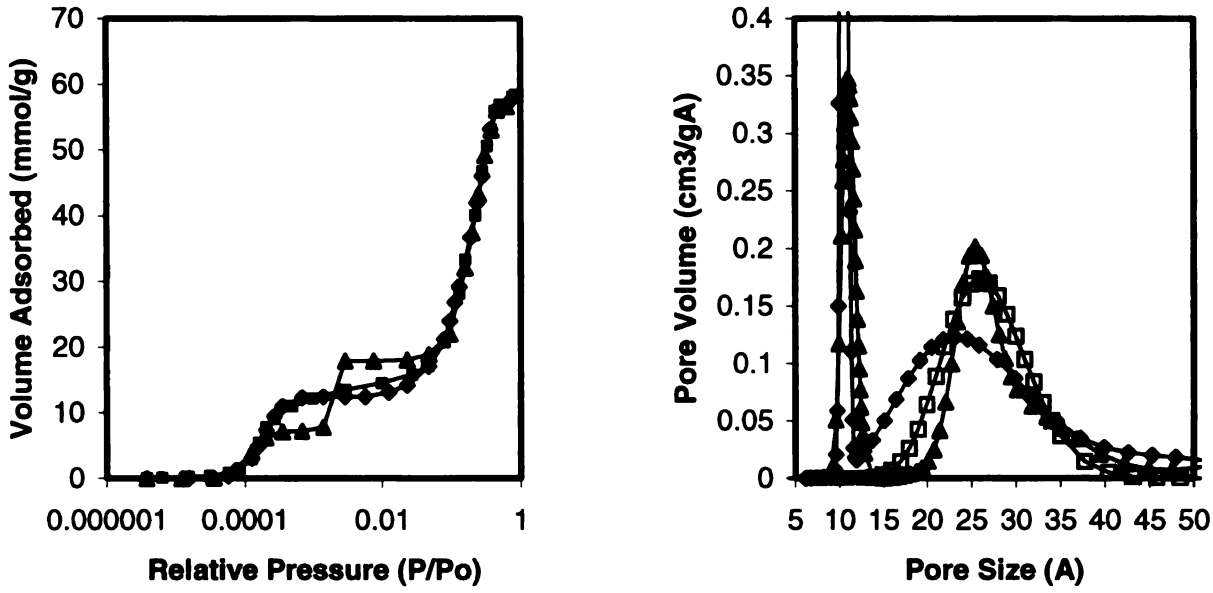

Figure 5.12 a and b. Fictitious isotherm fit and comparison of the PSD predictions. Figure a the DFT (squares) isotherm corresponds to the selected DFT PSD in figure b. The two-stage HK method(triangles) is in close agreement in the mesoporous regime. The original HK method (diamonds) is in closer agreement with the isotherm but worse agreement with the PSD.

in minutes with a spreadsheet program as opposed to the days required for the DFT counterparts. The two-stage HK method is superior to the generalized HK version for pores whose size is between 12.4 and 50 A. It is important to note that there has not been an efficient method suggested for fitting the Lennard-Jones potential parameters to any experimental results for the single-stage HK method, whereas a simple method is presented for the two-stage model. The effects of the wrong potential parameters can propagate and result in inaccurate PSDs, therefore the two-stage model is suggested despite the characteristic flaw that occurs near the maximum attainable monolayer filling pressure.

5.5 References

1. Storck, S., H. Bretinger, and W. Maier, "Characterization of micro- and mesoporous solids by physisorption methods and pore-size analysis." Applied Catalysis A., 174, 137 (1998).

2. Maddox M. W., S. L. Sowers, and K.E. Gubbins. "Molecular Simulation of Binary Mixture Adsorption in Buckytubes and MCM-41." Adsorption, 2, 23, (1996).

3. Rege, S. U. and R. T. Yang. "Corrected Horvath Kawazoe Equations for Pore-size Distribution." AICHE J. 46, 734 (2000).

4. Lastoskie C., K. E. Gubbins, and N. Quirke. "Poresize Heterogeneity and the Carbon Slit Pore: A Density Functional Theory Model." Langmuir. 9, 2693 (1993).

5. Dombrowski R. J., D. R. Hyduke, and C. M. Lastoskie. "Pore size Analysis of Activated Carbons from Argon and Nitrogen Porosimetry Using Density Functional Theory." Langmuir, 16, 5041, (2000).

6. Steele, W. A. "The Physical Interaction of Gases With Crystalline Solids." Surface Science. 36, 317, (1973)

7. Horvath, G., K. Kawazoe. "Method For The Calculation Of Effective Pore Size Distribution In Molecular Sieve Carbon." Journal of Chemical Engineering Japan. 16, 470, (1983).

8. Satio A., H. C. Foley. " Curvature and Parametric Sensitivity in Models for Adsorption in Micropores." AICHE Journal. 37, 429, (1991).

9. Cheng, L. S., and R. T. Yang. "Improved Horvath-Kawazoe Equations Including Spherical Pore Models For Calculating Micropore Size Distribution." Chemical Engineering Science. 49, 2599, (1994).

10. Gelb, L. D. and K. E. Gubbins. "Characterization of Controlled Pore Glasses: Molecular Simulations of Adsorption." Studies in Surface Science and Catalysis. 128, 61, (2000).

11. Maddox, M. W. and K. E. Gubbins. "Molecular Simulation of Fluid Adsorption in Buckytubes." Langmuir. 11, 3988, (1995).

12. Lastoskie, C. M., N. Quirke, and K. E. Gubbins. "Structure of Porous Adsorbents: Analysis Using Density Functional Theory and Molecular Simulation." Studies in Surface Science and Catalysis, 104, 745, (1997).

13. Lastoskie, C., K.E. Gubbins, and N. Quirke. "Pore Size Distribution Analysis of Microporous Carbons: A Density Functional Theory Approach." The Journal of Physical Chemistry. 97, 4786, (1993).

14. Gregg, S. J., S. W. Sing. *Adsorption, Surface Area and Porosity*. New York : Academic Press,(ch 2.)1982.

15. Dombrowski R. J., D. R. Hyduke, and C. M. Lastoskie. "Horvath-Kawazoe Method Revisited." Journal of Colloid and Surface Chemistry A. Submitted 2000.

16. Nilson, R. H., Giffiths, S. K. "condensation pressures in small pores: An analytical model based on density functional theory." Journal of Chemical Physics, 111, 4281, (1999).

17. M. Jaroniec, K. P. Gadkaree, J. Choma, Relation between adsorption potential distribution and pore volume distribution for microporous carbons, Colloids and Surfaces A: 118 (1996) 203-210.

18. Muller A. *Proc. Roy. Soc. London* **A154** 624 (1936).

19. Sadus R. J. *Molecular simulation of fluids : theory, algorithms, and object-orientation* New York : Elsevier, (Ch. 4) 1999.

20. de Boer, J.H.; Linsen, B.G.; Osinga, T.J. *J. Catal.* **1965**, *4*, 643.

21. Lastoskie C. M. "A Modified Horvath-Kawazoe Method For Micropore Size Analysis." Studies in Surface Science and Catalysis, 128, 475, (2000).

Chapter 6.

Conclusions and Future Directions

6.1 Summary of Results

Several amorphous porous carbons were analyzed using argon and nitrogen as probe gases at 77K, the pore size distributions (PSD) were found to agree well when analyzed with DFT model slit pores. The DFT model is designed to predict the equilibrium between a bulk gas and a liquid like adsorbed phase. The triple point of argon is 83.8K therefore the dense adsorbed phase must be either super-cooled liquid or a solid. In this work it was found that excellent agreement between the PSD predicted by the two probes was attained when the potential parameters of argon were fit as a super-cooled liquid in a slit pore at 77K. The specific pore volume, mean pore width and the mode pore size on average were within 8% of one another for the two probes. The DFT method presumes that the probe gas is a monoatomic gas with no permanent quadrupole moment, and the surface is defect free and chemically homogeneous. These assumptions are known to be simplifications of the actual system. However, the argon probe more closely fits these criteria than nitrogen, which has a quadrupole moment, is diatomic and known to interact more strongly with surface defects and functional groups. Therefore it is recommended that argon be used as a probe gas in lieu of nitrogen when surface functional groups are known to be present.

Characterization of microporous materials requires that the method of generating the model isotherms accounts for the enhanced adsorption due to the superposition of the potential of opposing pore walls. Therefore the correct potential between the adsorbent and adsorbate is essential for determining the proper pore size distribution. MS, DFT and

the HK methods all use the Lennard-Jones potential, whose parameters may be determined by either the physical properties of the system or via fitting to the experimental conditions. Potential parameters found by fitting have been proven to be more accurate than those obtained from the bulk properties. The current state of the art fitting methods require the use of a nonporous reference adsorbent that is chemically similar to the system being probed. Through the use of the adsorption integral equation 1.1, a nonporous surface is considered to be a Dirac delta function PSD, and the monolayer filling pressure can be matched to a an isotherm of a nonporous material. The potential parameter may also be determined by fitting a known distribution of micropores to an experimental isotherm. This method has the advantage of increased sensitivity to potential due to the superposition of the wall potential. Additionally the micropores tend to adsorb at pressures lower than flat surfaces, which allows one to determine the potential when the monolayer filling pressure is to high to measure without the use of special high pressure equipment. In addition to the fore mentioned advantages SWNTs have a high surface area therefore tend to yield accurate results with a small sample size. One of the limitations faced when studying nanotubes with small diameters is the rate of diffusion into the tubes, due to their small size attaining an equilibrium isotherm may require protracted times to obtain and isotherm. Therefore it becomes necessary to either fracture the tubes or shorten their lengths to decrease the time required to diffuse through the tubes. An alternate method to shorten the diffusion time would be to raise the temperature at which the experiment is conducted, unfortunately this requires the construction of a cryostat to maintain the temperature within a strict tolerance. As shown

in Chapter 3 despite the diffusion limitations the SWNTs show promise as an alternate reference adsorbent.

Determining the proper potential parameters is essential for determining the PSD of micro and mesoporous carbons. Although the DFT and MS are exact for idealized systems, they are iterative techniques that are computationally very expensive. The HK method may be modified to yield PSD results that are comparable to DFT while requiring less than one hundredth of the time. When the potential function of the HK method is altered to the 10-4-3 potential or the 10-4 potential with fitted parameters the filling-pressures of the DFT method and HK method coincide with one another for the unweighted HK method. It may be demonstrated that the PSD predicted by the HK method with improved potential function yields PSD modes that are within 15% of the values predicted by DFT for microporous carbons.

A novel modification to the HK method was also proposed to account for the multiple filling events that are shown to occur in DFT and MS isotherms. Through the addition of a monolayer filling pressure the two-stage HK isotherm more closely represents the mesopores in a carbon when compared to the DFT predicted PSD. It has been demonstrated that the two-stage HK method can predict the mesopore mode with an error of 2% compared to the DFT mode while the original HK method predicts a mode that is in 12% error. The addition of a monolayer filling pressure enables one to fit the Lennard-Jones potential parameters when a nonporous reference isotherm is provided.

6.2 Topics for Future Investigation

The techniques used in this dissertation were limited by several constraints that may be investigated by future researchers. The models used to determine the PSD were

limited to simplistic representations of adsorbent adsorbate systems, many common adsorbents contain some degree of chemical as well as structural heterogeneity. Also further development of the factors that influence the equilibrium sorption isotherms require investigation. Some relevant extensions of this work include:

6.2.1 Further Improvements to the HK model

The HK model simplistically relates the free energy of adsorption to the heat of adsorption, while neglecting the effects of entropy. It is known that the entropy of a system typically decreases with the order and density of a system. DFT and MS have shown that the adsorbed fluid is typically ordered and on average 1000 times as dense as the bulk gas. Therefore although the magnitude of the entropic effects are less than those of the enthalpic effects they are none the less important. The ordering of the adsorbed phase would indicate that the proper average heat of adsorption in a pore should be weighted with respect to density, however when entropic effects and adsorbate-adsorbate interactions are neglected, the density-weighted HK performs poorly. As demonstrated in Chapter 4 the density profile within a pore can be represented by a series of Gaussian distributions. Integration of the area of these distributions would correctly identify the density for a pore of any size, which would be an improvement to the one size fits all density suggested, which would reduce the pore volume that is attributable to micropores. In addition to the improper saturation density selection in micropores the density has been shown to increase after the filling event. The addition of increased adsorption after filling would ameliorate and in some cases remove the discontinuous fits of the two-stage HK model near the monolayer filling pressure. The current work investigated the HK method and improved models for systems that could be modeled with slit pores, however

there may be adsorbents that are best modeled with cylindrical or spherical pores. It is recommended that the two-stage method be expanded to alternate pore geometries. Therefore, further investigation topics include: the study of entropic effects, the effect of adsorbate-adsorbate interactions, seeking the correct micropore density, study of compression of adsorbed layers, and study of other pore geometries.

6.2.2 Investigation of Adsorption at Alternate Temperatures

Sorption isotherms must be measured at a single temperature. Current methods to keep the temperature static involve the use of a temperature bath where a material is at its normal boiling point or sublimation point. The use of a phase change cryostat constrains the temperatures that may be studied to the few readily available cryogenic fluids. However, it has been shown that for very small pores diffusion may require protracted times to reach equilibrium. To determine if an isotherm is in apparent or true equilibrium the temperature may be increased to determine the effect. When adsorption is exothermic the amount adsorbed should decrease and the filling pressure should increase with increasing temperature. The limitations of studying SWNTs at liquid nitrogen and liquid argon temperatures did not allow for sufficient temperature change to determine if the isotherms had reached equilibrium. The construction and use of a cryostat that controls the temperature with a tolerance of ± 0.01 K is recommended for studies pertaining to the equilibrium sorption in small pores as well as alternate adsorbents.

6.2.3 Study of Alternate Probe Gases

The porosimetry of amorphous materials can be conducted with a variety of commonly used probes. The current work investigated the use of argon, nitrogen and to some extent carbon dioxide. While these gases are representative of most probes they do not meet all

the criteria for studying all materials. The study of nearly spherical molecules best matches the assumption of a single centered Lennard-Jones molecule used in the DFT and HK calculations. A molecule that is nearly described by these criteria is methane, which does not have a permanent multipole moment. With the construction of a cryostat the study of methane is recommended at relative temperatures comparable to either nitrogen or argon at 77K. Previous studies have shown that methane adsorption on graphite at 77K yields results that conflict with argon and nitrogen porosimetry.

6.2.4 Study of Irregular Adsorbents

As discussed in the introductory chapter molecular simulations have progressed to the point where it is now becoming possible to conduct simulations of irregular porous materials. It has been demonstrated that soil organic matter is composed of macromolecules that have characteristics that are similar to polymers. Although, simulations of pure polymeric systems of larger than forty carbon units have been unable to reach equilibrium with current methods, recent advances in computing technology and combinations of displacement moves have vastly improved the state of the art. Sorption to soil organic matter continues to be one of the principle mechanisms of contaminant retention by soils, therefore it makes an interesting and relevant topic of study. Quench time models have shown that quasi-equilibrium states are suitable for adsorptive studies and are capable of producing realistic irregular micropores. Current attempts to model the behavior of an adsorbate such as carbon tetrachloride in a dense polymer model of soil have met with limited success. It is recommended that hybrid Monte Carlo simulations be attempted where the polymer adsorbent is not treated as a fixed lattice.

The study of such a system could incorporate several forms of heterogeneity such as the structural variances due to irregular pores as well as chemical heterogeneity.